1974

A study of exothermic chemical reaction in a porous catalyst wedge

Joseph Michael Schardl Jr.

Department: Chemical and Biochemical Engineering

A STUDY OF EXOTHERMIC CHEMICAL REACTION IN A POROUS CATALYST WEDGE

by

JOSEPH MICHAEL SCHARDL, JR., 1944-

A DISSERTATION

Presented to the Faculty of the Graduate School of the

UNIVERSITY OF MISSOURI - ROLLA

In Partial Fulfillment of the Requirements for the Degree

DOCTOR OF PHILOSOPHY

in

CHEMICAL ENGINEERING

1974

Advisor

ABSTRACT

Temperature and composition were measured at various locations in a system where ethylene is hydrogenated to ethane on a 1/4 inch porous catalyst wedge made of nickel supported on alumina. When the wedge of catalyst was bathed in hydrogen, experimental results indicated a high temperature rise from the feed temperature to the catalyst which is implied by the diffusion controlled regime for solid catalyzed, highly exothermic reactions. This high activity was reversibly reduced by bathing the catalyst wedge in nitrogen for extended time periods (greater than 24 hours). This nitrogen soaking changed the experimental conditions from those of diffusion controlled kinetics to those typically exhibited by systems in the kinetic regime.

The experimental system was simulated numerically for a variety of boundary conditions using reasonable assumptions and physical property data for this reaction system. Heat and mass transfer coefficients were allowed to vary along the wedge according to boundary layer theory results. For the internal wedge temperatures predicted by the model to agree within 1% of those measured experimentally, it was necessary to consider finite heat transfer at the stagnation point which is contrary to the classical boundary layer theory commonly applied to flat plate and wedge flows. It was also necessary to allow modest (~6% or less) heat loss from the back edge of the wedge.

ACKNOWLEDGEMENTS

I would like to acknowledge with great appreciation the special efforts of Dr. Orrin K. Crosser, who aided and directed me through the extended duration of this work. His personal and technical advice will always be remembered and appreciated.

I would also like to thank the following individuals and organizations whose help and aid made this study possible:

Jerry Zweerink for making up several glass reaction vessels used throughout this study.

Leon Otte for his moral support throughout, but especially during, the preparation of the thesis.

The Department of Chemical Engineering, the American Oil Company, the Esso Research Foundation, and the Shell Oil Company whose financial assistance made this investigation possible.

Chris Boggs without whose efforts this manuscript would never have been completed.

My daughters Jody and Jennifer whose willing acceptance of the fact that "Daddy has to go to work again tonight" made it easier to complete this work and finally my wife Joan whose understanding and encouragement has persevered through all the years.

Thanks again

Joseph M. Schardl, Jr.

TABLE OF CONTENTS

	Page
ABSTRACT	ii
ACKNOWLEDGEMENT	iii
LIST OF ILLUSTRATIONS	vii
LIST OF TABLES	viii
I. LITERATURE REVIEW	1
II. EXPERIMENTAL APPARATUS AND PROCEDURES	6
A. THE GAS FEED SYSTEM	6
B. THE SINGLE PELLET WEDGE REACTION VESSEL	8
C. THE THERMAL MONITORING SYSTEM	13
D. THE GAS ANALYSIS SYSTEM	13
E. EXPERIMENTAL PROCEDURE	15
III. EXPERIMENTAL RESULTS	17
A. HYDROGEN PRETREATMENT	17
B. NITROGEN PRETREATMENT	23
C. SUMMARY	25
IV. NUMERICAL STUDIES OF THE SYSTEM MODEL	26
V. DISCUSSION OF RESULTS AND COMPARISON WITH THE NUMERICAL STUDIES	36
A. HYDROGEN PRETREATMENT	36
B. NITROGEN PRETREATMENT	42
C. NITROGEN DILUTED FEED	44
VI. CONCLUSIONS	46

TABLE OF CONTENTS, CONTINUED

	Page
TABLE OF NOMENCLATURE	48
BIBLIOGRAPHY	53
APPENDICES	57
A. THEORETICAL DEVELOPMENT OF THE MATERIAL AND ENERGY BALANCE APPLICABLE IN THE CATALYST WEDGE INTERIOR	58
B. A COMPARISON OF THE NUMERICAL AND ANALYTICAL SOLUTIONS FOR AN ISOTHERMAL FIRST ORDER REACTION IN A CATALYST WEDGE WITH THE SURFACE-SATURATION BOUNDARY CONDITION	67
C. SOLUTION FOR THE CASE OF NON-ISOTHERMAL FIRST ORDER REACTION IN A CATALYST WEDGE WITH SURFACE SATURATION OF BOTH CONCENTRATION AND TEMPERATURE	78
D. DEVELOPMENT OF BOUNDARY CONDITIONS TO INCORPORATE BOUNDARY LAYER CONSIDERATIONS INTO THE MODEL SOLUTION	84
E. SOLUTION FOR THE CASE OF NON-ISOTHERMAL FIRST ORDER REACTION IN A CATALYST WEDGE WITH CONSTANT HEAT AND MASS TRANSFER COEFFICIENTS AT THE BOUNDARY	96
F. SOLUTION FOR THE CASE OF NON-ISOTHERMAL FIRST ORDER REACTION IN A CATALYST WEDGE WITH VARIABLE HEAT AND MASS TRANSFER COEFFICIENTS AT THE BOUNDARY (INFINITE HEAT AND MASS TRANSFER COEFFICIENTS AT THE STAGNATION POINT AND PERFECT INSULATION AT THE BACK EDGE)	102
G. SOLUTION FOR THE CASE OF NON-ISOTHERMAL FIRST ORDER REACTION IN A CATALYST WEDGE WITH VARIABLE HEAT AND MASS TRANSFER COEFFICIENTS AT THE BOUNDARY (FINITE HEAT AND MASS TRANSFER AT THE STAGNATION POINT AND PERFECT INSULATION AT THE BACK EDGE)	107

TABLE OF CONTENTS, CONTINUED

		Page
H.	SOLUTION FOR THE CASE OF NON-ISOTHERMAL FIRST ORDER REACTION IN A CATALYST WEDGE WITH VARIABLE HEAT AND MASS TRANSFER COEFFICIENTS AT THE BOUNDARY (FINITE HEAT AND MASS TRANSFER AT THE STAGNATION POINT WITH HEAT LOSS AT THE BACK EDGE)	118
I.	EXPERIMENTAL DATA	124
J.	SAMPLE CALCULATIONS	127
VITA		137

LIST OF ILLUSTRATIONS

Figure		Page
II-1	EXPERIMENTAL FLOW SYSTEM	7
II-2	LOCATION OF THERMOCOUPLES IN THE EXPERIMENTAL WEDGE	10
II-3	LOCATION OF THERMOCOUPLES WITH RESPECT TO THE COMPUTED GRID	12
V-1	COMPARISON OF THE COMPUTED SURFACE TEMPERATURE PROFILES WITH THE MEASURED SURFACE TEMPERATURE PROFILES FOR RUNS AT VARIOUS FEED RATES WITH THE WEDGE SOAKED IN HYDROGEN	40
V-2	COMPARISON OF THE COMPUTED SURFACE TEMPERATURE PROFILE WITH THE MEASURED SURFACE TEMPERATURE PROFILE FOR RUN 1-10 WITH NITROGEN DILUTED FEED	45

LIST OF TABLES

Table		Page
III-1	EFFECT OF TOTAL FEED RATE ON THE HYDROGENATION OF ETHYLENE (A) TO ETHANE (C) FOR THE HYDROGEN (B) SOAKED WEDGE	18
III-2	EFFECT OF INLET FEED COMPOSITION ON THE CONVERSION OF ETHYLENE TO ETHANE FOR THE HYDROGEN SOAKED WEDGE	20
III-3	EFFECT OF INLET FEED TEMPERATURE ON THE CONVERSION OF ETHYLENE TO ETHANE FOR THE HYDROGEN SOAKED WEDGE	22
III-4	EFFECT OF CHANGES IN ETHYLENE CONCENTRATION AND INLET GAS TEMPERATURE ON THE KINETICS IN THE CATALYST WEDGE AFTER NITROGEN SOAKING	24
V-1	COMPARISON OF THE CALCULATED ETHYLENE CONVERSION WITH THAT WHICH WAS MEASURED IN EXPERIMENTAL RUNS	38

I. LITERATURE REVIEW

In 1939 Zeldowitsch (1) in the U.S.S.R. and Theile (2) in the U.S. both published concerning the effect of pore diffusion in a catalyst particle on a catalytic chemical reaction. Since these initial pioneering works there have been numerous studies on the subject of mass and heat transfer in porous catalysts and all of its ramifications.

Early studies centered around the diffusional retardation of the catalyst and ignored the thermal effects involved due to the heat release upon reaction.

In the middle 1950's Prater (3) and Wheeler (4) pointed out that the condition of isothermal operation during catalytic reaction may not exist within the particle. These efforts brought forth a rash of theoretical articles (e.g., see (5), (6), and (7) among others) which treated the non-isothermal effects. These efforts can be put into two categories:

(i) There is no external boundary layer resistance to heat and mass transfer and surface temperature and concentration are constant over the entire catalyst surface.

(ii) There is a resistance, but it is constant, and heat and mass transfer coefficients are constant over the entire catalyst surface.

A third and more realistic condition is:

(iii) There is a developed boundary layer over the catalyst which implies that neither the surface temperature and concentration nor the transport coefficients are constant, but are a function of the position on the surface.

With the theoretical background for cases (i) and (ii), measurements were made of the temperature difference between the surface and the center of a spherical particle by Cunningham et. al. (8), of the bulk fluid and center of a cylinder by Miller (9) and Jiracek et. al. (10), and the temperature was measured at four points in the interior of a cylinder by Irving and Butt (11).

Cunningham et. al. constructed their apparatus in such a way as to approximate operation under condition (i). Juracek et. al. assumed (i) applied but gave no justification. Miller extended his work to consider condition (ii) but had no means of checking his surface temperature. Irving and Butt assumed a model of constant surface temperature and inferred this value from their intraparticle temperature measurements, but they did not consider the boundary layer effects, nor that the total reaction must be equal to the total surface fluxes.

Recently Bischoff (12) and Copelowitz and Aris (13) considered the effects of non-uniform but prescribed surface gradients in temperature and composition on the effectiveness factors for porous spherical catalyst particles. Both assumed these surface gradients to be linear in the angular

variable. Petersen et. al. (14) studied surface reaction on a non-porous catalytic sphere. This allows the non-linear reaction rate to present itself in the boundary conditions with the differential equations describing the internal temperature and composition being homogeneous (Laplace's Equation).

Mihail (15) considered the influence of developing boundary layer mass transfer on a first order reaction over an isothermal porous flat plate catalyst of infinite thickness. His development assumes

$$D \frac{d^2 c_A(x,z)}{dz^2} = k c_A$$

where z is the depth of penetration and x the coordinate along the flat plate parallel to the flow. The boundary conditions are:

$$z = 0 \qquad c_A = c_{A_s}(x) \qquad \text{and } z \to \infty \; \frac{dc_A}{dz} = 0$$

With the solution

$$c_A(x,z) = c_{A_s}(x) \exp(-\Phi_z)$$

where Φ_z is the local Thiele modulus, $\Phi_z = z\sqrt{k}/D$. Mihail then suggests that the expression to be used for $c_{A_s}(x)$ could be one of those derived by Chambre (16), Chambre and Acrivos (17), Rosner (18) or the one derived from his present work. All of these expressions were derived using

the flat plate boundary solution for the mass transfer coefficient at a non-porous reaction surface. This flat plate theory includes the assumptions of an infinite mass transfer coefficient at the leading edge.

This assumption might be acceptable in the case of hypersonic flows encountered in space studies, but not in the chemical industry where the flow conditions commonly are much slower, for Reynolds numbers less than 350 (19).

Thus, it can be seen that reaction rate expressions inferred from bulk flow temperature and composition measurements may be incorrect because of the temperature and composition distributions which may occur along the fluid film as well as in the porous solid catalyst. Only Cunningham et. al. and Irving and Butt have experimentally accounted for film effects on temperature, and no one has determined the experimental extremes of temperature which can occur along the surface of a catalyst particle as indicated in condition (iii). Consequently the effect of assymmetry upon the distribution of the reaction in the solid has not been studied and only two experiments are available to interpret the wealth of theoretical results which have been and are still being published.

Therefore, the experimental system which has been chosen is that of a catalyst wedge upon which a laminar boundary layer will develop with no complications of separation as encountered in the spherical and cylindrical geometry, thus lending itself to description by the standard

boundary layer equations. The reaction being used is the hydrogenation of ethylene. This experimental system permits the study of the reaction on a catalyst wedge instrumented with fine wire thermocouples to measure temperature distributions, supplemented with measurements of bulk fluid temperature and composition. An appropriate numerical model for this system can be developed to solve for the temperature, composition and reaction rate distribution in the catalyst wedge. These results should help define experimentally the range of applicability of theoretical studies describing the effects of film and pore heat and mass transfer on solid catalyzed gas phase reactions.

II. EXPERIMENTAL APPARATUS AND PROCEDURES

The experimental system can be divided into four main categories. The gas feed system, the single pellet wedge reactor and reaction vessel, the thermal monitoring system, and the gas analysis system are shown in Figure II-1.

A. The Gas Feed System

The gases (hydrogen, ethylene and nitrogen) were fed from commercial gas cylinders to the reactor section using two-stage constant pressure regulators and reducing valves. The specifications on gas purity as given by the supplier (Matheson Company, Inc.) were:

Nitrogen purity $\geq$ 99.7%

Hydrogen purity $\geq$ 99.95% with less than 20 ppm oxygen

Ethylene purity $\geq$ 99.5%

The hydrogen passed through an Engelhard Model D-10-50 Deoxo Gas Purifier which converted traces of oxygen to water. The ethylene was passed through a heated Engelhard Model C-3-2500 Deoxo Gas Purifier which removed oxygen and any sulfur compounds. Hydrogen and ethylene were passed through drying tubes containing anhydrous calcium sulfate from the W. A. Hammond Drierite Co. This was done to remove moisture produced in the purifiers. All gases then passed through separate capillary flow meters which were calibrated using a 1/10 Cubic Foot Precision Wet-Test Gas Meter. This

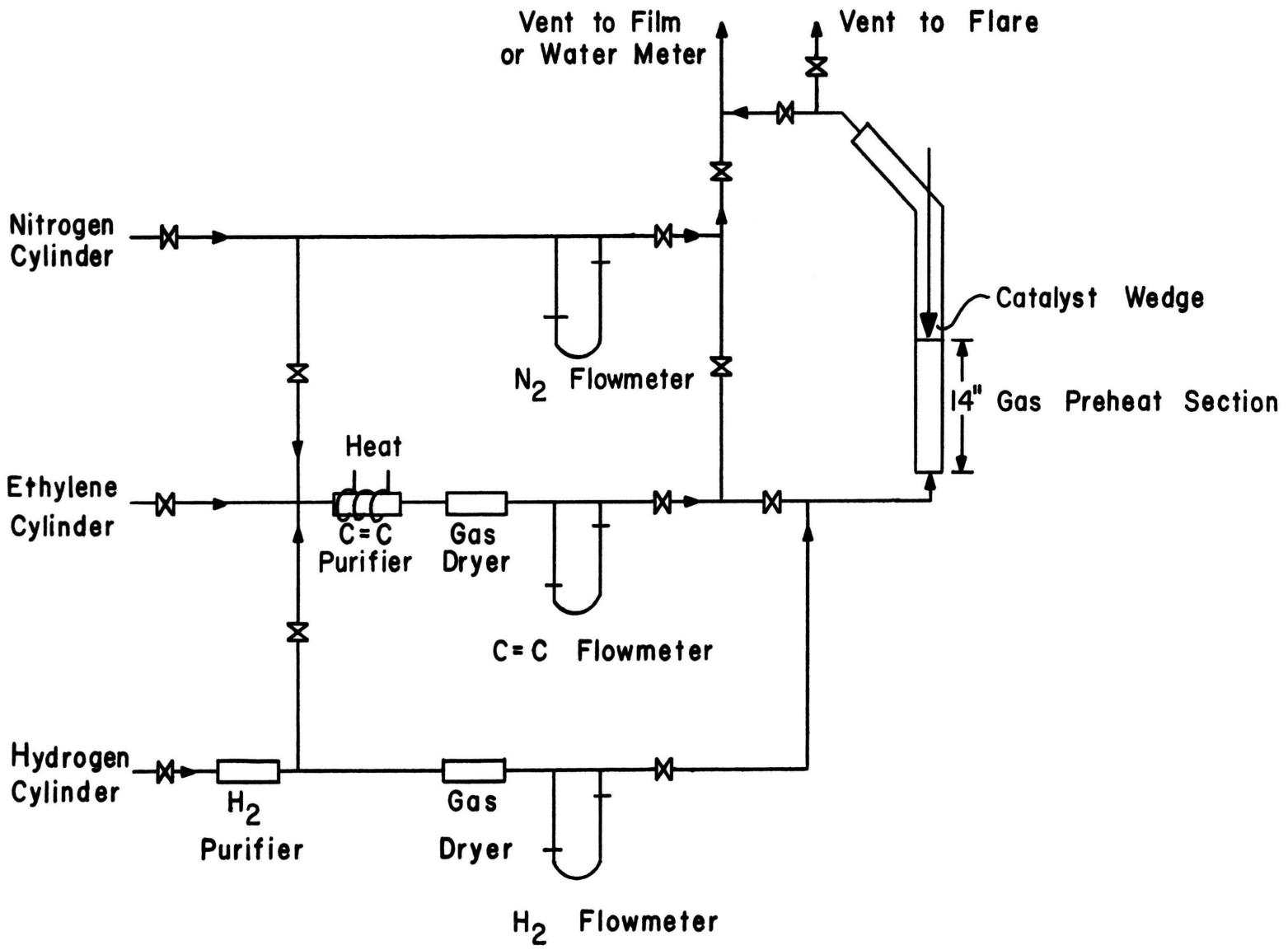

Figure II-1 Experimental Flow System

meter had subdivisions each representing 1/1000 of a cubic foot with a maximum capacity of 20 cfh and a normal accuracy of 0.5%.

The fluid used in the manometers of the capillary flow meters was hexadecane (M.W. 266.45) because of its low vapor pressure at room temperature (1mm of Hg at 105°C).

Because of the low flowrates used (nominally 0.5 to 2.0 cfh) it was necessary to use another flow regulator to maintain a constant flow rate of ethylene. This consisted of a Fisher and Porter Company Constant Flow Purgerator, Model 313505WG, and a Fisher and Porter Company Flow Regulator, Model 53RB2110, Series A2.

The gases were then passed from a common feed line to the reactor preheater section where they were heated and mixed.

B. The Single Pellet Wedge Reaction Vessel

The catalyst pellet consisted of nickel supported on alumina and was held in place in the reaction vessel by an 14 inch section of 1/4" 304 stainless steel tubing which was fastened to the back of the catalyst edge. The stainless steel tubing served as a housing for eight pairs of thermocouple leads and a section of 1/16" stainless steel tubing used to take samples from the rear of the wedge surface.

The catalyst wedge was made of Girdler G-65 Nickel Hydrogenation Catalyst (Sample order number 4633-S) from

Girdler Catalysts, Catalysts Division of Chemetron Corporation. The following data was provided by Girdler (20,21) on this particular catalyst type.

Nominal Nickel Content: 25%

Internal Surface Area: 54 m^2/g

Effective Thermal Conductivity: approximately 0.0001 Cal/Cm °C at 100°C

Average Bulk Density: 65#/ft^3

Porosity of the catalyst is indicated below:

	Hg Porosimeter	
CCl_4 PV*, cc/g	PV, cc/g	Pore Diameter Range, Microns
0.09 at 800 A° 0.05 at 140 A°	0.08	0.5-0.035

*Pore volume as associated with pores of the indicated threshhold diameter and smaller.

The catalyst was received as 1/2" by 1/2" tablets and the catalyst wedge was constructed by first butting two catalyst tablets together using a light cement. The wedge was then shaped using a fine metal file and finished with emery cloth. Dust from the filing operation was brushed off to minimize undesirable fines on the wedge surface. The two halves were then separated and the fine wire (50 gauge, 0.001" diameter) chromel-alumel thermocouples were installed in the experimental catalyst wedge as shown in Figure II-2. A small piece of cellophane tape was used to support the leads and a spot of Saureinsen insulating cement to lend

Figure II-2

Location Of Thermocouples In
The Experimental Wedge

support at the back edge. The two wedge halves were then rejoined and sealed at both ends and on the back edge with insulating cement to minimize heat and mass transfer from these portions. The thermocouples were all placed in the center so that any axial conduction in the wedge should affect all the measurements equally. Figure II-3 shows the location of the experimental thermocouple tips with respect to the numerical computation grid.

The instrumented wedge was then placed in the reactor and slowly heated to 700°F with hydrogen gas for about 24 hours to activate the catalyst (22).

The 14 inch long preheat section was packed with 1/16" diameter glass beads. The preheat section was connected to the reaction section by a glass joint to allow entry to the reactor. The reaction section was 8" in length with the catalyst wedge located in the first inch of the section to minimize the velocity boundary layer development on the vessel walls, thus preventing interaction with the boundary layer developing on the catalyst wedge. The preheat section and the reaction section were both constructed of 30mm pyrex glass tubing. The gases entered at the bottom of the preheat section and exited through a 1/2" brass tee at the top of the reaction vessel.

The preheat and reaction sections were enclosed in semi-cylindrical electric heating units supplied by Lindberg Hevi-Duty, a Division of Sola Basic Industries. These units were Model 50032, Type 77-KSP, 12 inches in length and

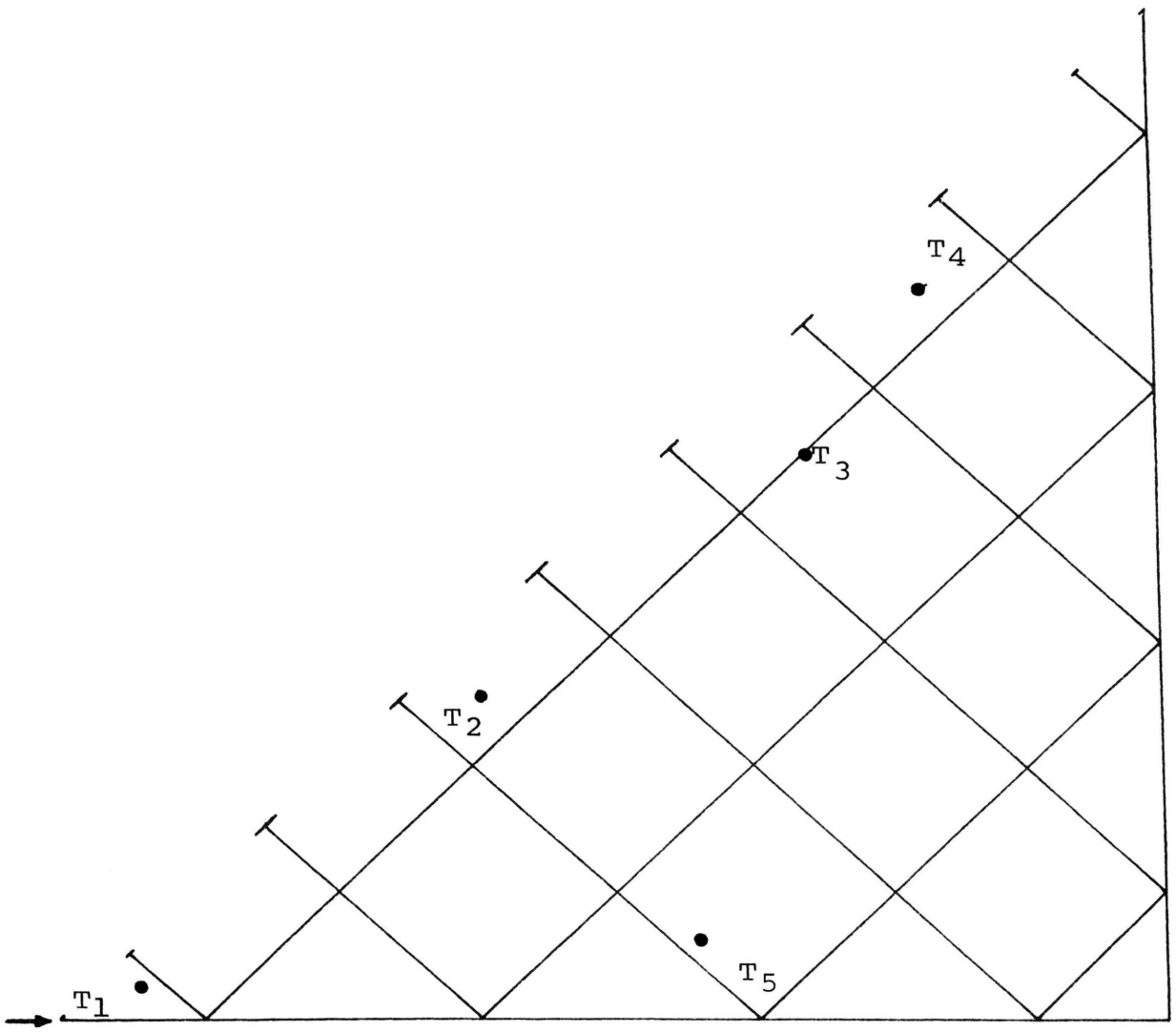

Figure II-3

Location Of Thermocouples With
Respect To The Computation Grid

capable of delivering 480 watts each. These two units were connected in series and controlled by a Barber-Colman Series 620 Power Controller (Silicon Controlled Rectifier). The power to the rectifier was controlled using a Barber-Colman Model 357A Digiset Null Balance Controller (23,24). These units were used to control the temperature of the bulk entering gas.

C. The Thermal Monitoring System

The temperatures were monitored using chromel-alumel thermocouples, connected to an 8 position rotary thermocouple selector switch supplied by Omega Engineering Inc. The millivolt signals produced were measured using a Model 7554 Leeds and Northrup Type K-4 Potentiometer and Model 9834 Leeds and Northrup Electronic D-C Null Detector. On the 16 mv range, values are stated to be in error by not more than $\pm$ (0.005% + 0.5 μv). Further information pertaining to these instruments may be obtained from references (25) and (26).

Thermocouples were calibrated in nitrogen against the average temperature reading of all thermocouples at various controller settings. Corrections from the average were less than 1°F at 320°F.

D. The Gas Analysis System

Samples of the exit gas were taken for the purpose of determining the bulk conversion by the catalyst wedge. The gas was also sampled at the rear edge of the catalyst wedge to establish an upper bound on the surface ethylene

concentration and a lower bound on the surface ethane concentration. Samples were analyzed during each run for ethylene and ethane using a Lab-Line Chromalyzer-100 gas chromatograph. Complete details of this unit are available elsewhere (27).

The chromatograph was fitted with a 4 foot, 3/16" O.D. copper tubing column. The packing used was Porapak Type Q, 100-120 mesh from Waters Assoc., Inc. The column was purged with helium for two hours at 230°C as recommended to remove any residual chemical in the beads, thus eliminating spreading of the peaks, change in retention time and loss of resolution.

The chromatograph was operated at room temperature with helium carrier gas flowing at a rate of 30 cc/min. The helium flow rate was determined using a rising soap film bubble meter connected to the exit of the sample side of the chromatograph.

The signal from the chromatograph was attenuated and then sent to a Beckman Model 1005 Ten-Inch Laboratory Potentiometric Recorder which was outfitted with a Model 236 - Disc Chart Integrator. The full scale response was less than 0.5 seconds. A chart speed of 0.5 in/min was used during all runs. For more information see references (28) and (29).

The chromatograph was calibrated using three standard ethylene-ethane mixtures supplied by the Matheson Company, Inc. The instrument was calibrated for various sample volumes between 0.01 and 0.40 cc and attentuations varying by a factor of 8. The results showed the conversion of ethylene to ethane varied by no more than $\pm$ 0.15% at 21.0% conversion. Thus it was deemed unnecessary to correct the chromatograph for various sample sizes and attenuations.

Gas samples were introduced into the chromatograph through a silicone septum using a Hamilton 0.00-0.50 cc Gas Tight Syringe equipped with a Chaney Adaption.

E. Experimental Procedure

Reactant flow rate, composition, and the bulk gas temperature were set and the system was allowed to attain steady state (about 1 hour). Steady state was assumed when changes in successive readings of all temperatures and exit compositions were not detectable over a 15 minute time interval. The thermocouple readings were then taken and samples from the back edge of the wedge and bulk exit gas were taken. Generally at least two samples of each were obtained to assure that the steady state had been reached and that the chromatogram could be quantitatively reproduced.

After collecting the data, the reactor conditions were changed and steady state established at new conditions. Inlet compositions were inferred from the calibrations of the hydrogen and ethylene flow meters which were recalibrated each day. Agreement with chromatographic measurements of the exit compositions was generally within 1% with four tests within 2%.

III. EXPERIMENTAL RESULTS

Ethylene conversions obtained in the wedge reactor, and the resulting internal temperature profiles were measured as a function of the inlet feed flow rate and inlet feed temperature for several ethylene-hydrogen feed compositions. The catalyst wedge was pretreated with hydrogen for the first set of tests and in nitrogen for the second set.

A. Hydrogen Pretreatment

In Table III-1 and those succeeding, V_i denotes the volumetric feed rate of species i in standard cubic feet per hour (SCFH). V_T is the total feed rate, i.e. the sum of all V_i's, also expressed in standard cubic feet per hour (SCFH). X_i denotes the mole fraction of species i in the feed stream (IN) and in the exit stream (OUT). Y_i denotes the measured percent conversion of species i in the outlet stream (BULK) and at the back edge of the wedge (BL). Y_i' is the percent conversion of species i based on the total moles of inlet feed. ΔT_1 is the difference between the temperature at position T_1 and the bulk gas temperature (T_∞).

Table III-1 shows the effect of total feed rate on the conversion of ethylene to ethane for the wedge saturated in hydrogen. As the inlet feed rate is increased in Runs 1-15, 1-19, and 1-22, the exit mole fraction of ethane and the percent conversion of ethylene to ethane decrease. The

TABLE III-1

EFFECT OF TOTAL FEED RATE ON THE HYDROGENATION
OF ETHYLENE (A) TO ETHANE (C) FOR THE HYDROGEN (B) SOAKED WEDGE

Composition and Conversion Data

Run Number	$V_{A_{IN}}$ (SCFH)	$V_{B_{IN}}$ (SCFH)	$V_{T_{IN}}$ (SCFH)	$X_{A_{IN}}$	$X_{B_{IN}}$	$X_{A_{OUT}}$	$X_{B_{OUT}}$	$X_{C_{OUT}}$	$Y_{A_{BULK}}$	$Y_{A_{BL}}$	Y'_A
1-15	1.420	14.86	16.28	0.0872	0.9128	0.0782	0.9119	0.0099	11.22	53.91	0.9783
1-17	1.395	14.41	15.81	0.0883	0.9117	0.0786	0.9108	0.0106	11.87	54.42	1.0489
1-19	0.775	8.08	8.86	0.0875	0.9125	0.0736	0.0111	0.0153	17.19	53.53	1.5040
1-22	0.426	4.74	5.17	0.0825	0.9175	0.0642	0.9159	0.0199	23.69	52.48	1.9531

Temperature Measurement Data (°F)

Run Number	ΔT_1	T_∞	T_1	T_2	T_3	T_4	T_5
1-15	211.8	80.7	292.5	287.8	279.5	277.3	277.3
1-17	213.6	81.5	295.1	289.8	201.1	279.5	279.7
1-19	201.1	81.3	282.4	274.1	267.4	265.7	266.5
1-22	173.1	92.4	265.5	258.7	252.7	251.8	252.4

reaction is substantially increased causing the temperatures to rise as the total feed rate is increased at constant inlet compositions. Runs 1-15 and 1-17 illustrate the reproducibility of all measurements.

Table III-2 gives the effect of inlet feed composition on the conversion of ethylene to ethane for several feed rates. At a given total feed rate when the inlet ethylene composition was increased, the outlet ethane mole fraction increases as does the conversion of ethylene per mole of inlet feed. Temperature measurements consistently indicate that as the reactant feed composition is increased, at any level of total feed rate, the temperature at all measured positions increases.

Table III-3 shows the effect of inlet feed temperature on the conversion of ethylene to ethane for the hydrogen soaked wedge. At this level of inlet feed composition, an increase in inlet gas temperature increases only slightly the conversion of ethylene (about 0.83% ethylene converted per 10°F increase in temperature).

In all of these runs the temperatures within the catalyst are substantially higher than the bulk gas temperature and the surface temperatures are monotonically decreasing from T_1 through T_4 with increasing distance from the point of the wedge. With the location of T_1 as shown in Figure II-3 only 0.0094 inches from the wedge surface and

TABLE III-2

EFFECT OF INLET FEED COMPOSITION ON THE CONVERSION OF ETHYLENE TO ETHANE FOR THE HYDROGEN SOAKED WEDGE

Composition and Conversion Data

Run Number	$V_{A_{IN}}$ (SCFH)	$V_{B_{IN}}$ (SCFH)	$V_{T_{IN}}$ (SCFH)	$X_{A_{IN}}$	$X_{B_{IN}}$	$X_{A_{OUT}}$	$X_{B_{OUT}}$	$X_{C_{OUT}}$	$Y_{A_{BULK}}$	$Y_{A_{BL}}$	Y_A'
1-8	0.66	14.35	15.01	0.0440	0.9560	0.0406	0.9559	0.0036	8.08	41.38	0.3557
1-24	0.725	14.10	14.825	0.0489	0.9511	0.0443	0.9509	0.0048	9.82	47.28	0.480
1-17	1.395	14.41	15.805	0.0883	0.9117	0.0786	0.9108	0.0106	11.87	54.42	1.0489
1-2	0.152	8.10	8.252	0.0184	0.9816	0.0164	0.9815	0.0021	11.35	-	0.2096
1-3	0.512	8.76	9.262	0.0553	0.9447	0.0474	0.9443	0.0084	15.00	48.95	0.8291
1-19	0.775	8.08	8.855	0.0875	0.9125	0.0736	0.9111	0.0153	17.19	53.53	1.5040
1-21	0.263	4.45	4.713	0.0558	0.9442	0.0432	0.9435	0.0133	23.56	49.78	1.3145
1-22	0.426	4.74	5.166	0.0825	0.9175	0.0642	0.9159	0.0199	23.69	52.48	1.9531
1-4	0.512	4.58	5.092	0.1005	0.8995	0.0775	0.8970	0.0256	24.87	54.10	2.4961

TABLE III-2 continued

Temperature Measurement Data (°F)

Number	ΔT_1	T_∞	T_1	T_2	T_3	T_4	T_5
1-8	74.4	79.2	153.6	152.6	148.6	147.9	148.8
1-24	88.7	78.2	166.9	164.8	160.5	159.6	160.5
1-17	213.6	81.5	295.1	289.8	281.1	279.5	279.7
1-2	28.0	75.2	103.2	102.6	101.3	100.6	101.1
1-3	139.0	78.0	217.0	211.5	205.4	204.0	205.3
1-19	201.1	81.3	282.4	274.1	267.4	265.7	266.5
1-21	109.8	92.5	202.3	198.1	194.2	193.4	194.4
1-22	173.1	92.4	265.5	258.7	252.7	251.8	252.4
1-4	245.1	96.1	341.2	330.5	322.9	321.0	321.5

TABLE III-3

EFFECT OF INLET FEED TEMPERATURE ON THE CONVERSION OF ETHYLENE TO ETHANE FOR THE HYDROGEN SOAKED WEDGE

Composition and Conversion Data

Run Number	$V_{A_{IN}}$ (SCFH)	$V_{B_{IN}}$ (SCFH)	$V_{T_{IN}}$ (SCFH)	$X_{A_{IN}}$	$X_{B_{IN}}$	$X_{A_{OUT}}$	$X_{B_{OUT}}$	$X_{C_{OUT}}$	$Y_{A_{BULK}}$	$Y_{A_{BL}}$	Y'_A
1-8	0.66	14.35	15.01	0.0440	0.9560	0.0406	0.9559	0.0036	8.08	41.38	0.3557
1-9	0.63	14.00	14.63	0.0431	0.9569	0.0383	0.9569	0.0050	11.51	46.88	0.4955

Temperature Measurement (°F)

Run Number	ΔT_1	T_∞	T_1	T_2	T_3	T_4	T_5
1-8	74.4	79.2	153.6	152.6	148.6	147.9	148.8
1-9	95.0	120.8	215.8	212.8	208.8	207.9	208.4

0.0219 inches from the front, the T_1 measurement greater than 200°F above T_∞ contradicts the assumption $T_o = T_\infty$, which is commonly used in the flat plate boundary layer theory (15, 16, 17, 18).

B. Nitrogen Pretreatment

When the catalyst was soaked in nitrogen for at least 24 hours, the kinetics changed from the "ignited" or diffusion controlled conditions shown above to an induced "kinetic" region.

The existence of a surface temperature maximum between the stagnation point and the back edge of the catalyst wedge after soaking in nitrogen is seen from Table III-4 in experimental runs 1-11 to 1-13. The wedge had been soaked in nitrogen for nearly five (5) days. The hydrogen flowrate was maintained quite high (15.3 to 16.3 SCFH).

The ethylene feed rate was 0.63 SCFH in Run 1-11 with a resulting surface temperature maximum between front and back. However, the bulk outlet conversion was less than 1% with the boundary layer showing 1.24% conversion of ethylene to ethane and a ΔT_1 of only 1.3°F. As the ethylene feed rate was increased from 0.63 SCFH in run 1-11 to 1.57 SCFH in run 1-12 the maximum temperature was still observed. There was still less than 1% total conversion, with a slight decrease in the measured ethylene conversion in the boundary layer from 1.24% to 1.13%. In keeping with the increased total conversion, there was an increase in the measured ΔT_1 to 3.2°F.

TABLE III-4

EFFECT OF CHANGES IN ETHYLENE CONCENTRATION AND INLET GAS TEMPERATURE ON THE KINETICS IN THE CATALYST WEDGE AFTER NITROGEN SOAKING

Run Number	$V_{A_{IN}}$ (SCFH)	$V_{B_{IN}}$ (SCFH)	$V_{T_{IN}}$ (SCFH)	$X_{A_{IN}}$	$X_{B_{IN}}$	$Y_{A_{BL}}$	$Y_{A_{BULK}}$
1-11	0.63	15.38	16.01	0.0394	0.9606	1.24	<1.0
1-12	1.57	16.30	17.87	0.0879	0.9121	1.13	<1.0
1-13	1.58	15.30	16.88	0.0936	0.9064	1.62	<1.0
1-14	1.425	14.95	16.375	0.0870	0.9150	53.92	11.79

Temperature Measurement Data (°F)

Run Number	ΔT_1	T_∞	T_1	T_2	T_3	T_4	T_5
1-11	1.3	78.2	79.5	79.9	79.8	79.6	80.2
1-12	3.2	78.4	81.6	82.4	82.4	81.9	83.3
1-13	15.3	99.1	114.3	116.0	116.6	115.9	115.2
1-14	216.9	107.1	315.5	310.9	302.4	300.2	299.3

For Run 1-13, the feed rates and feed compositions were maintained relatively constant but the bulk gas feed temperature was increased. This increase in the inlet feed temperature probably caused some of the nitrogen to desorb, thus increasing the rate of reaction. Run 1-13 still showed the surface temperature maximum with a further increase in the difference between the temperature T_1 and the bulk gas feed temperature (ΔT_1 = 15.3°F)

Finally, the inlet gas temperature was increased from 99.1°F to 107.1°F. Immediately the front temperature (T_1) began rising, reaching 300°F in about 5 minutes. After steady state was obtained the reaction mechanism had obviously changed from the induced kinetic reaction regime with total conversions of less than 1% and ΔT_1 about 15°F or less, to the diffusion controlled regime with total ethylene conversions of 10% or more and $\Delta T_1 > 200$°F.

C. Summary

These experimental results show the high temperature rise implied by the diffusion controlled regime for solid catalysed, highly exothermic reactions, and indicate the great difficulty in obtaining reaction within the kinetic regime on active catalysts. They also demonstrate how activity can be reduced, reversibly, by adsorbing inert nitrogen onto the catalyst surface.

IV. NUMERICAL STUDIES OF THE SYSTEM MODEL

The system model was derived and then solved with the aid of the U.M.R. IBM 360 Model 2 Digital Computer.

The rectangular (90°) wedge used in the experimental system was modelled using the appropriate differential equations (see Appendix A for the derivation) and solved for internal temperature and composition distributions for a variety of boundary conditions (see Appendices B through H) with reasonable assumptions and physical property data for the catalyst and the ethylene-hydrogen reaction system.

The material and energy balances applicable to the wedge interior which were derived in Appendix A are as follows:

Mass Balance:

$$\frac{\partial \Psi_A}{\partial \tau} = \alpha^2 \left(\frac{\partial^2 \Psi_A}{\partial \xi^2} + \frac{\partial^2 \Psi_A}{\partial \zeta^2}\right) - \exp\left[\beta\left(1-1/\Phi\right)\right]\Psi_A \qquad (1)$$

and the Energy Balance

$$\Pi \frac{\partial \Phi}{\partial \tau} = \left(\frac{\partial^2 \Phi}{\partial \xi^2} + \frac{\partial^2 \Phi}{\partial \zeta^2}\right) + \lambda \exp\left[\beta\left(1-1/\Phi\right)\right]\Psi_A \qquad (2)$$

where the symbols are defined as follows:

Dimensionless Mole Fraction: $\Psi_A = X_A/X_{A_\infty}$

Dimensionless Time: $\tau = \theta k_\infty$

Dimensionless Length: $\xi = x/L$

Dimensionless Length: $\zeta = y/L$

Activation Energy Parameter: $\beta = E/RT_\infty$

Dimensionless Temperature: $\Phi = T/T_\infty$

Theile Modulus: $1/\alpha^2 = D/k_\infty L^2$

Heat of Reaction Parameter: $\Pi = DcC_p/k_H$

Energy Balance Parameter: $\lambda = -\Delta H_A Dc_{A\infty}/k_H T_\infty$

Reaction Rate Constant at Bulk Conditions: $k_\infty = A\exp(-\beta)$.

The first numerical solution to these equations in Appendix B ignored boundary layer resistance and heat effects in order to compare the numerical procedure with the analytical solution available for this case. Figures B-1 and B-2 respectively show agreement between the analytical and numerical solution of 2% or less at all calculated points.

Next, the non-isothermal case with infinite heat and mass transfer at the surface (Figures C-1 and C-2), was solved following a method developed by Prater (3) in which the temperature and concentration are directly related by

$$\Phi - 1.0 = \lambda\ (1.0 - \psi_A) \qquad (3)$$

for any constant surface conditions. This relation could be substituted for the energy balance, thus still requiring the solution of only one partial differential equation.

These two cases have assumed that the temperature and concentration on the surface were constant. This has also been the case elsewhere with the boundary conditions assumed to be a constant (6,7,8,9), or a prescribed function of

length or radial position (12,30,31). This type of assumption as previously mentioned by Bischoff (12) "...greatly simplifies the mathematics."

It is of interest to note that in the solutions of Appendix B and Appendix C, where there is symmetry of the boundary conditions, that there is also a zero gradient of Ψ_A in the middle of the half-wedge shown in Figure B-1 for the isothermal case and in Figures C-1 and C-2 for both Ψ_A and Φ with the saturated boundary conditions on Ψ_A and Φ.

Next, classical boundary layer transport was imposed on the wedge, and these boundary conditions, derived in Appendix D, are:

$$\frac{\partial \Psi_A(\xi,0)}{\partial \zeta} = \text{DCMTC} \; (\Psi_A - 1.0) \tag{4}$$

$$\frac{\partial \Phi(\xi,0)}{\partial \zeta} = \text{DCHTC} \; (\Phi - 1.0) \tag{5}$$

where

$$\text{DCMTC} = k_x^{\cdot} L/Dc \tag{6}$$

and

$$\text{DCHTC} = h^{\cdot} L/k_H \tag{7}$$

This type of development usually contains the conditions that the heat and mass transfer coefficients at the stagnation point are infinite. For the flux at this point to

be finite the conditions

$$\Psi_{Ao} = 1.0 \tag{8}$$

and

$$\Phi_{o} = 1.0 \tag{9}$$

must be imposed.

The first problem solved using these boundary conditions assumed finite but constant heat and mass transfer coefficients along the surface as given in Appendix E. (This case was solved for the one dimensional cylinder by Miller (9) in which he required the convective heat and mass transfer to be equal to the flux at the solid surface.) This is general and sufficient, but it should be noted that each of these quantities should also be equal to the total heat and mass species generated by chemical reaction throughout the catalyst particle at steady-state.

The solutions of Appendix E show that with large values for the dimensionless heat and mass transfer parameters (Figure E-1) the character of the solution approaches that of Appendix C, Figures C-1 and 2, with the saturated conditions (i.e., DCHTC and DCMTC are infinite). That is, the composition and temperature distributions are symmetrical about the center of the half-wedge even for finite values of DCHTC (2.86) and DCMTC (2.86).

Figures E-2 and E-3 show further decreases in the dimensionless heat transfer parameter or specifically in the heat transfer coefficient if k_H and L are assumed constant, and the resultant increases in surface temperature at each calculation position. There is essentially no effect of changing the heat transfer coefficient on the dimensionless concentrations in Figures E-1 and E-2 with DCHTC equal to 2.86 and 1.86 respectively. However, when DCHTC is reduced to 0.86 in Figure E-3 there is a sufficient change in the temperature distribution to show a significant decrease in the dimensionless concentration at all positions.

Variation of the heat and mass transfer coefficients with distance along the wedge surface was introduced next. The relationships used for these coefficients are:

$$k_x^{\cdot} = \frac{cU(x)\,\pi'}{Sc}\left(\frac{(m+1)}{2}\,\frac{\nu}{U(x)x}\right)^{1/2} \tag{10}$$

and

$$h^{\cdot} = \frac{C_p U(x)\,\pi'\rho}{Pr}\left(\frac{(m+1)}{2}\,\frac{\nu}{U(x)x}\right)^{1/2} \tag{11}$$

where

$U(x)$ = Velocity profile at the edge of boundary layer given by $U_\infty x^m$

U_∞ = Free stream velocity

π = Similarity solution to equations (D-3) and (D-4)

π' = First derivative of similarity solution to equations (D-3) and (D-4)

c = Total molar density

Sc = Schmidt number (ν / D_{ij})

D_{ij} = Gaseous diffusion coefficient

$m = \sigma/2-\sigma$

σ = Included wedge angle in radians

ρ = Total mass density

ν = Kinematic viscosity (μ / ρ)

μ = Absolute viscosity

Pr = Prandtl number ($\mu C_p / k_G$)

C_p = Specific heat

k_G = Gas thermal conductivity

These were derived by Elzy and Myers (32). A brief presentation of Elzy and Myers' (33) formulation is given in Appendix D. Solution of equations (1) and (2) in the steady state form, with boundary conditions (4), (5), (8), (9) and $k_x^{\cdot}$ and $h^{\cdot}$ being given by (10) and (11) is given in Appendix F.

Figures F-1 and F-2 indicate as expected, that as the mass transfer parameter, specifically the mass transfer coefficient if D, C, and L are held constant, is increased from 1.43 to 2.43 the surface mole fraction increases and this increase is distributed through the remainder of the catalyst wedge by diffusion.

Trends in the initial experimental results did not agree with the results predicted by the system model even incorporating classical boundary layer theory.

From the experimental results it was obvious that the temperatures and probably the concentrations near the stagnation point were not equal to those in the bulk gas phase. In some cases the measured temperature at position one was greater than 200°F above the bulk gas temperature implying a tip ethylene concentration of about one-half that of the bulk gas concentration. (This was estimated with the relationship given in Appendix J.) Generally the experimental surface temperature distributions did not show a maximum on the surface as predicted by the model, but were monotonically decreasing from front to back.

Each case studied numerically in Appendices G and H was defined by setting the numerical values for the dimensionless coefficients α^2, β, λ, and defining DCHTC and DCMTC as functions of length along the wedge. The general approach to the numerical solution began by setting the non-infinite value for the transport coefficients at the wedge tip, and using their boundary layer dependence on distance along the wedge surface. This is sufficient to define the solutions uniquely. A temperature profile was assumed and iterations were performed upon the concentration profile until the sum of all the reaction terms inside the wedge agreed with the surface mass flux (Equation D-30 Appendix D). Then the assumed temperature profile was adjusted by requiring that all the heat of reaction in the wedge be equal

to the surface heat flux (Equation D-42 Appendix D). When successive iterations of both temperature and concentration profiles agreed with their respective surface fluxes within 1%, the iteration was concluded.

Figures G-1 and G-2 show that changing the heat transfer parameter at low reaction conditions results in substantial increase in the dimensionless temperature profile, and a decrease in the concentration profiles. Figures G-3 and G-4 show that changing this parameter at high reaction rates causes the same effects with considerably greater magnitude. Figures G-5 and G-6 show that if the heat transfer parameter is held constant while the reaction rate is increased by a factor of two, that the temperatures also show substantial increases with concommitant decreases in concentrations. These calculations also indicate that most (70-90%) of the reaction is uniformly distributed along the wedge surface, i.e., essentially a surface reaction with little generation in the wedge interior.

As can be seen from these figures in Appendix G, the condition of finite heat and mass transport coefficients does allow the stagnation temperature T_o to rise above T_∞ as experimentally observed. All these profiles still show a maximum in temperature and a minimum in concentration along the surface between the front and back of the wedge. This behavior was observed with a nitrogen soaked wedge and nitrogen diluted feed, but was distinctly not found for ignited reaction obtained with a hydrogen soaked wedge.

For these hydrogen soaked results it was necessary to allow modest (6% or less) heat loss from the back of the wedge in order to match the shape of measured temperature distribution. Appendix H shows the results of these calculations.

Figures H-1 and H-2 give a comparison of the dimensionless temperature and mole fraction profiles when the amount of heat loss is increased. As expected, the temperature gradient becomes a steeper monotonic decreasing function from the stagnation point to the back edge of the wedge. Figures H-3 and H-4 show a similar situation for considerably higher values of Theile modulus ($1/\alpha$).

In summary, it is expected that the numerical studies reported in Appendices B through H apply to the following physical conditions.

(1) The solutions of Appendix B are applicable in case of high turbulence, with essentially no mass transfer resistance and only negligible or no heat generation effects.

(2) The solution of Appendix C is applicable also in the case of high turbulence but can be used for systems with heat generation along with the material conversion.

When it is necessary or desired to consider the boundary layer the following general solution types can be categorized for various system restrictions.

(3) The solution of Appendix E is applicable to cases with high reactant velocities, catalysts of low reactivity,

or catalyst-reactant systems in the kinetic regime where the resistance to heat and mass transfer is assumed constant over the surface, except at the stagnation point.

(4) The solution of Appendix F would be applicable for systems with high reactant velocities, catalysts of low reactivity, or other conditions under which the reaction is very slow (in the kinetic regime) where it is desired to consider the variation of heat and mass transfer coefficients along the catalyst surface.

(5) The solution of Appendix G would be applicable for the same class of systems as in (4) except that the flow velocities could be high or low instead of strictly high as in case (4).

(6) The solution of Appendix H is a further generalization of case (5), where here the flow velocities could be either high or low, reaction rates high or low with allowance for heat loss from the back edge of the wedge.

V. DISCUSSION OF RESULTS AND COMPARISON WITH THE NUMERICAL STUDIES

Of interest is the comparison of the nature of the experimentally determined wedge temperature distributions with those predicted by the numerical models.

A. Hydrogen Pretreatment

The hydrogen soaked experimental runs could be placed in the general classification of diffusion controlled. This is substantiated by the experimental measurements of temperature differences between the catalyst wedge and the bulk gas as great as 200°F or more along with total ethylene conversions of 10 to 25 percent. Furthermore, the gas phase was sampled quite close to the wedge surface (about 1/16") at the back edge of the wedge where the measured conversion was of the order of the average conversion calculated on the surface. These boundary layer measurements for the diffusion controlled runs show from 40 to 60 percent conversion of ethylene to ethane over the catalyst surface implying that the average dimensionless mole fraction of ethylene should be about 0.6 to 0.4 in the boundary layer near the catalyst surface. This is comparable to the values of Ψ_A as given in Figures G-4 and G-7 in which the computed total reaction rate is similar to that observed experimentally. These values are also similar to the average dimensionless surface mole fraction of 0.641 computed in Appendix J assuming uniform surface conditions.

The kinetic equation for the rate of hydrogenation of ethylene on this catalyst was chosen from Fulton (34,35). Others (8) have reported considerable variations in rate constants for this reaction even though the calculated rates vary far less. For this catalyst, agreement with the experimentally measured temperatures required increasing the pre-exponential constant (A of Aexp(-E/RT)) by a factor of ten, from 32.4 sec^{-1} to 356 sec^{-1}. Fulton's catalyst was also manufactured by Harshaw, but the catalyst used in this study was newer, with "higher activity".

This increase in the value of A would reflect a catalyst with more active sites per unit weight or area, but with the same reaction mechanism. The activation energy was therefore held constant at 1960 cal/gm-mole and A was changed to give a total calculated conversion consistent with the experimental conversion.

The models presented in Appendices E, F, and G assumed perfect insulation at the back edge of the wedge. Although these models give computed reaction and heat generation rates which are consistent with the conversion of ethylene across the reactor, the computed temperature distributions do not agree with those experimentally measured. With heat loss from the back of the wedge (see Appendix H), the ethylene conversion changed by only about 1 percent as seen in Table V-1, but the character of the calculated surface temperature distribution became consistent with the experimental measurements.

TABLE V-1

COMPARISON OF THE CALCULATED ETHYLENE CONVERSION WITH THAT WHICH WAS MEASURED IN EXPERIMENTAL RUNS

Case	Considered	Parameter Comparison T_∞ (°R)	X_{A_∞}	U_∞ (cm/sec)	Conversion of Ethylene (gm-moles/hr) x 10^2
(1)	Wedge Perfectly Insulated at the Back Edge (Figure G-11)	540	0.1000	40	0.876
(2)	Heat Loss from the Back Edge of the Wedge (Figure H-1)	540	0.1000	40	0.864
(3)	Experimental Run 1-15	540.8	0.0872	18.1	1.613
(4)	Experimental Run 1-19	541.3	0.0875	9.9	1.36
(5)	Experimental Run 1-22	552.4	0.0825	5.8	0.984

Figure V-1 shows the agreement between the numerical studies of Appendix H and the temperature profiles measured for the hydrogen pre-treatment runs. Also shown in contrast, is the computed surface temperature profile for the same set of system parameters but assuming perfect insulation at the back edge of the wedge. It is clear that the shape of the profile assuming an adiabatic boundary for the rear of the wedge is unacceptable.

The accuracy of the temperature measurements was about 0.1°F with a measured temperature change along the wedge surface of about 15°F for the experimental runs. This corresponds to a change in the dimensionless temperature of 0.03. The dashed curve shows the temperature profile predicted by numerical studies which assume the rear of the wedge is perfectly insulated. The broken curve shows numerical results assuming about 6% of the total heat is lost uniformly over the back of the wedge. Symbols follow the trend of the measured temperatures for the various experimental runs as indicated. The scatter among these points for each run is attributed to the variation in location below the surface along the wedge.

The values for Φ_o (the stagnation point temperature) extrapolated from the experimental measurements vary from 1.32 to 1.40 for the three runs shown, while Φ_o predicted by the numerical solution with heat loss is about 1.50.

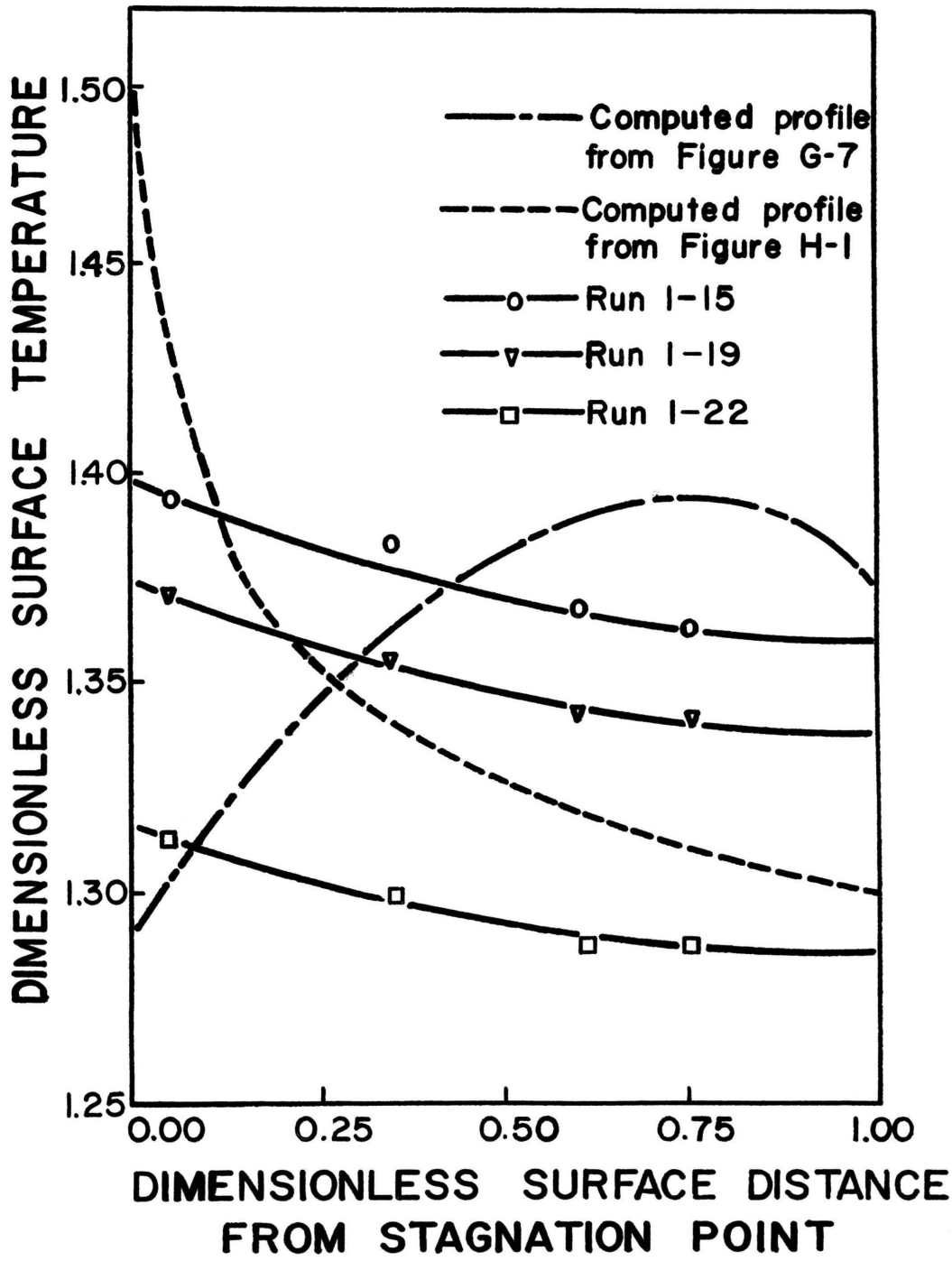

Figure V-1

Comparison Of The Computed Surface Temperature Profiles With The Measured Surface Temperature Profiles For Runs At Various Feed Rates With The Wedge Soaked In Hydrogen

By extrapolating the predicted distribution from the back of the wedge, forward to the stagnation point, the value of Φ_o is lowered to 1.37. This corresponds to increasing the value of the heat transfer coefficient assumed at the stagnation point. This gives a maximum temperature difference between the computed values and experimental values at any location of 30°F out of a total temperature rise from the bulk gas to the wedge of nearly 200°F. The numerical solution therefore agrees within 15 percent of the measured values for these runs.

The total moles of ethane produced experimentally is compared with the numerical studies in Table V-1. For a uniform velocity profile, the moles produced should be the same when the feed temperature, composition and feed flow are equal. Although the conditions do not match precisely, the measured conversion, in tests 1-15, 1-19, 1-22, is significantly higher than that suggested by the numerical model. This implies that the experimental transport coefficients are larger than those obtained from the boundary layer equations. Part of this effect might be attributed to the influence of the wall upon the velocity profile. The numerical studies, and their agreement with the measured temperature profiles, indicates that the reaction is surprisingly uniformly distributed along the wedge. Therefore, the behavior of the transport coefficients along the entire catalyst surface is very important in determining the total ethane produced. As the boundary layer develops along the

wedge, its interaction with the reactor wall would produce an increase in velocity of the outer edge of the boundary layer. This implies an increase in the transport coefficients, with a comparable increase in reaction. The main consideration is that in this modeled system, it is not only necessary that the temperature measurements agree with the computed distributions, but also the measured bulk conversion be used to provide an additional test of the numerical model.

B. Nitrogen Pretreatment

The only way the character of the computed temperature distributions of Appendices E, F, and G, with a maximum between the stagnation point and the back edge, could be realized experimentally was:

(i) the gas feed mixture of hydrogen and ethylene was diluted with nitrogen (see Run 1-10)

or

(ii) the catalyst was bathed in nitrogen for an extended period of time (greater than 24 hours) and then the reaction mixture was introduced at room temperature (see Runs 1-5, 6, 7, 11, 12, and 13).

It is quite likely that this situation would exist for two other cases which are:

(iii) systems involving a low activity catalyst, i.e., whenever the kinetic regime can be obtained for the given catalyst-reactant system

(iv) more generally for any system where the reaction is distributed over the full extent of the catalyst and the insulated condition is realized (less than 1% of the total heat generated is lost from the back of the wedge).

Regarding the nitrogen influenced cases mentioned in (i) and (ii), it is noteworthy that a company representative (36) indicated that nitrogen has no effect on the catalyst activity. This was in reference to the common use of this catalyst for converting carbon monoxide, carbon dioxide, and oxygen with hydrogen to methane and water where much higher operating temperatures (400 to 750°F) are required to give substantial conversion. For our reaction, the bulk temperature of necessity had to be maintained much lower (100°F or less) to keep the reaction from getting entirely too hot.

At these conditions, the nitrogen reduces the catalyst activity possibly by blanketing pore diffusion of the reactants, or adsorbing on some of the active sites (37), thus significantly reducing the reaction rate at the wedge tip and surface. This provides a more even distribution of

the reaction throughout the catalyst, reducing the conductive heat loss effect and therefore experimentally demonstrating a maximum temperature along the surface.

C. Nitrogen Diluted Feed

No rate expression is proposed for this case as a check between the experimental and computed reaction rates. However, Figure V-2 does show a comparison between the experimentally measured surface temperature distribution and those calculated for mild reaction conditions.

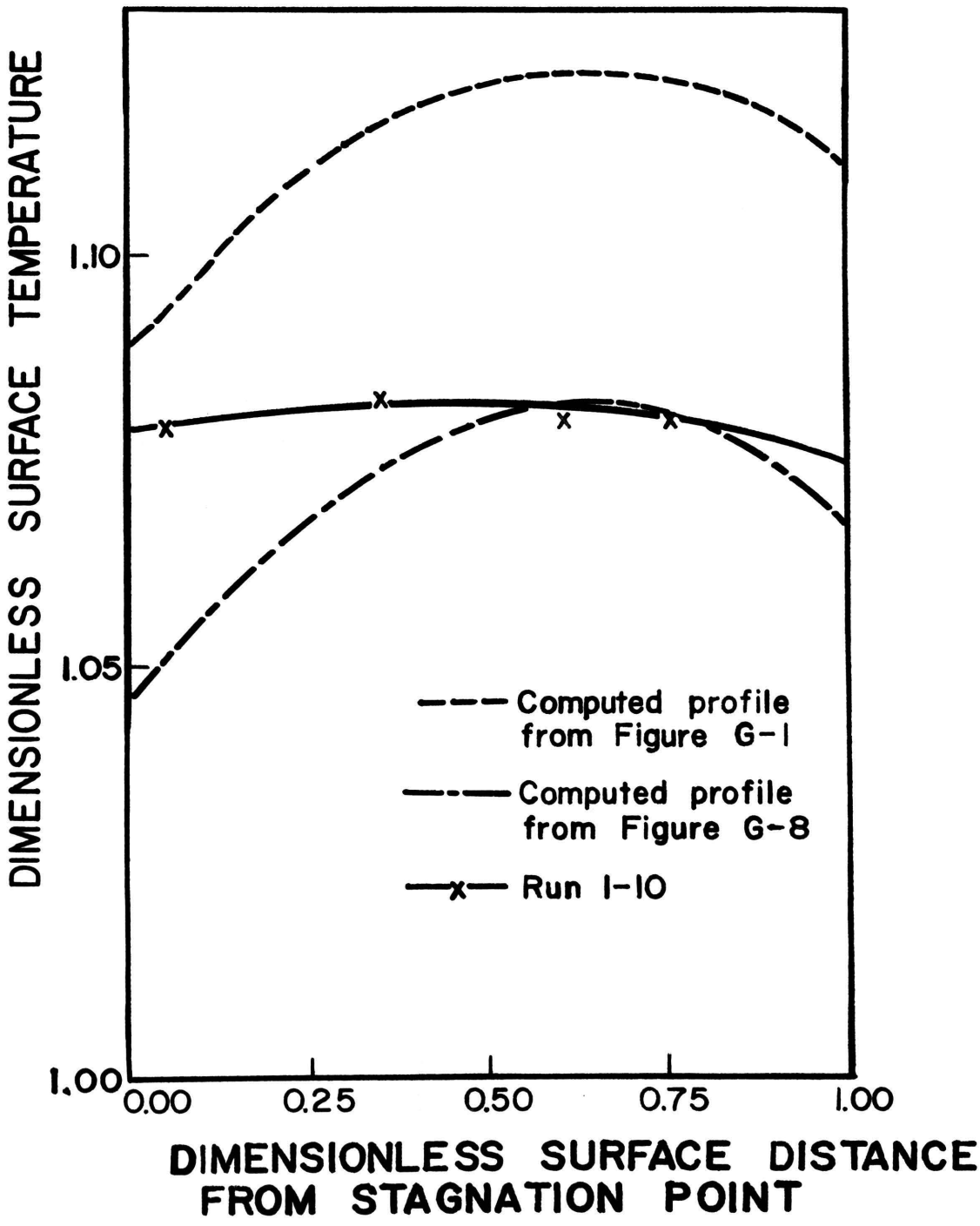

Figure V-2

Comparison Of The Computed Surface Temperature Profile With The Measured Surface Temperature Profile For Run 1-10 With Nitrogen Diluted Feed

VI. CONCLUSIONS

Based on the discussion of the system model and the experimental temperature and conversion measurements the following conclusions can be drawn:

1. Measurements of temperature within a hydrogen soaked porous catalyst wedge verify substantial temperature increases for diffusion controlled exothermic reactions. Reaction is distributed almost uniformly along the surface of the catalyst wedge even with measured surface temperature differences from T_1 to T_4 as high as 20°F. The temperature at the front of the wedge was 200°F higher than in the free stream, and the usual flat plate boundary conditions cannot apply.
2. The high activity exhibited by the wedge bathed in hydrogen could be reversibly reduced by bathing the catalyst wedge in nitrogen for extended time periods (greater than 24 hours). This nitrogen soaking changed the experimental conditions from those of diffusion controlled kinetics to those typically exhibited by systems in the kinetic regime.
3. The surface temperature distribution, with a maximum between the stagnation point and the back edge, as predicted by the numerical model has been experimentally verified using the hydrogenation of ethylene reaction on a supported nickel catalyst for the cases when

(i) The gas feed mixture of hydrogen and ethylene was diluted with nitrogen and

(ii) The catalyst was bathed in nitrogen for an extended period of time (greater than 24 hours) and then the reaction mixture was introduced at room temperature.

TABLE OF NOMENCLATURE

Symbol	Meaning
a	Constant in separation of variables solution to equations (B-5 i-iii)
A	Frequency factor in rate equation (sec^{-1})
A_c	Geometric area of catalyst particle which is not insulated (cm^2)
A_s	Cross-sectional area of the reactor (cm^2)
c	Total molar concentration ($gm\text{-}moles/cm^3$)
c_i	Molar concentration of component i ($gm\text{-}moles/cm^3$)
C_p	Molar specific heat ($cal/gm\text{-}mole\text{-}°K$)
d	Constant in separation of variables solution to equations (B-5 i-iii)
D	Effective molar diffusivity of the catalyst wedge (cm^2/sec)
DCHTC	Dimensionless heat transfer constant ($\equiv h^{\cdot}L/k_H$)
DCMTC	Dimensionless mass transfer constant ($= k_x^{\cdot}L/Dc$)
D_{ij}	Gaseous diffusion coefficient of component i in j (cm^2/sec)
e	Constant in separation of variables solution to equations (B-5 i-iii)
E	Reaction activation energy ($cal/gm\text{-}mole$)
f	Constant in separation of variables solution to equations (B-5 i-iii)
g	Constant in separation of variables solution to equations (B-5 i-iii)
$h^{\cdot}$	Heat transfer coefficient ($cal/cm^2\text{-}sec\text{-}°K$)
ΔH_i	Heat of reaction with respect to species i ($cal/gm\text{-}mole\text{-}°K$)
k	First order reaction rate constant (sec^{-1})

Symbol	Meaning
k_G	Gas phase thermal conductivity (cal/cm-sec-°K)
k_H	Effective thermal conductivity of the wedge (cal/cm-sec-°K)
$k_x^{\cdot}$	Mass transfer coefficient (gm-mole/cm^2-sec)
L	Base and height length of wedge cross-section (cm)
L_o	Overall wedge length (cm)
m	Defined as $\sigma/2-\sigma$, integers in solution to equation (B-8), finite difference index in equation (D-8)
n	Integers in solution to equation (B-7), finite difference index in equation (D-8)
N_i	Molar flux of component i (gm-moles/cm^2-sec)
Pr	Prandtl Number ($\equiv \mu C_p/k_G$)
q	Heat flux (cal/cm^2-sec)
Q_{CH}	Total rate of heat convection (cal/sec)
Q_{CM}	Total rate of mass convection (gm-moles/sec)
Q_{VH}	Total rate of heat generation (cal/sec)
Q_{VM}	Total rate of mass generation (gm-moles/sec)
R	Gas constant (cal/gm-mole-°K)
R_i	Volumetric rate of generation of species i (gm-moles/cm^3-sec)
R_V	Volumetric rate of heat generation (cal/cm^3-sec)
Sc	Schmidt Number ($\equiv \nu/D_{ij}$)
T	Absolute temperature (°K)
$\overline{T}$	Functional form of the time solution in the separation of variables equation (B-3)
ΔT_o	Difference between the stagnation point temperature and the bulk gas temperature (°K)

Symbol	Meaning
$U(x)$	Bulk phase velocity profile (cm/sec)
u	Velocity component in the boundary layer parallel to the wedge surface (cm/sec)
v	Velocity component in the boundary layer perpendicular to the wedge surface (cm/sec)
V_i	Volumetric feed rate of component i (cm^3/sec)
x	Coordinate distance within the wedge (cm)
χ	Functional form of one dimensional solution in the separation of variables equation (B-3)
X_i	Mole fraction of component i (dimensionless)
y	Coordinate distance within the wedge (cm)
γ	Functional form of one dimensional solution in the separation of variables equation (B-3)
Y_i	Percent conversion of component i
Y_i'	Percent conversion of component i per mole of total feed
z	Coordinate distance along the wedge length (cm)

Greek Symbols

θ	Time (sec)
Δ	Limit of appropriate parameter as it approaches zero
Ψ_i	Dimensionless mole fraction of component i ($\equiv X_i/X_{i_\infty}$)
Ψ_i^*	Dimensionless mole fraction solution to the separation of variables diffusion equation (B-3)
τ	Dimensionless time ($\equiv \theta k_\infty$)
ξ	Dimensionless distance ($\equiv x/L$)
ζ	Dimensionless distance ($\equiv y/L$)

Symbol	Meaning
Φ	Dimensionless temperature ($\equiv T/T_\infty$)
β	Dimensionless constant ($\equiv E/RT_\infty$)
α^2	Dimensionless constant ($\equiv D/k_\infty L^2$)
λ	Dimensionless constant ($\equiv -\Delta H_i Dc_{i_\infty}/k_H T_\infty$)
λ^2	Separation of variables parameter in Appendix B
μ	Absolute viscosity (gm/cm-sec)
μ^2	Separation of variables parameter in Appendix B
η	Thermal diffusivity of the gas phase ($= k_g/\rho C_p$)
Π	Dimensionless constant ($\equiv DcC_p/k_H$)
π'	First derivative of similarity parameter used in the solution of equations (D-3) and (D-4)
ρ	Fluid density (gm/cm^3)
ν	Kinematic viscosity ($\equiv \mu/\rho$) (cm^2/sec)
σ	Included wedge angle (radians)

Subscripts

A	Chemical reactant (ethylene)
B	Chemical reactant (hydrogen)
C	Reaction product (ethane)
I	Parameter refers to the insulating material used
i	General chemical component i
n	nth solution in separation of variables problem equations (B-5i - iii)
o	Indicates condition at the stagnation point
s	Surface condition of applicable parameter
t	Indicates initial condition ($t<0$)

Symbol	Meaning
x,y	Coordinate direction of applicable parameter
∞	Applicable parameter an infinite distance and/or conditions from the solid surface

Superscripts

Ψ_A^*	Diffusion equation solution to equation (B-3)
'	First derivative with respect to the specified variable
"	Second derivative with respect to the specified variable

BIBLIOGRAPHY

1. Zeldowitsch, J. B., Acta Physicochim, U.R.S.S., 1939, 10, 583.

2. Theile, E. W., "Relation Between Catalytic Activity and Size of Particle," Ind. Eng. Chem., 1939, 31, 916.

3. Prater, C. D., "The Temperature Produced by Heat of Reaction in the Interior of Porous Particles," Chem. Eng. Sci., 1958, 8, 284.

4. Wheeler, A., Catalysis Vol. II (Edited by P. H. Emmett) Reinhold Publishing Co. New York, 1955.

5. Schilson, R. E. and Amundson, N. R., "Intraparticle Diffusion and Conduction in Porous Catalysts. I. Single Reactions," Chem. Eng. Sci., 1961, 13, 226.

6. Weisz, P. B. and Hicks, J. S., "The Behavior of Porous Catalyst Particles in View of Internal Mass and Heat Diffusion Effects," Chem. Eng. Sci., 1962, 17, 265.

7. Petersen, E. E., "Non-Isothermal Chemical Reaction in Porous Catalysts," Chem. Eng. Sci., 1962, 17, 987.

8. Cunningham, R. A. and Carberry, J. J. and Smith, J. M., "Effectiveness Factors in a Nonisothermal Reaction System," A.I.Ch.E. Journal, 1965, 11, 636.

9. Miller, F. W., "Transport Phenomena and Chemical Reaction Inside a Single Catalyst Pellet," Ph.D. Dissertation, Rice University, 1964.

10. Jiracek, F. and Horak, J. and Pasek, J., "The Effects of Internal Mass Transfer of the Hydrogenation of Benzene Over Nickel-Alumina Catalyst," A.I.Ch.E. Journal, 1969, 15, 400.

11. Irving, J. P. and Butt, J. B., "An Experimental Study of the Effect of Intra-particle Temperature Gradients on Catalytic Activity," Chem. Eng. Sci., 1967, 22, 1859.

12. Bischoff, K. B., "Effectiveness Factors and Temperature Distributions for Catalyst Particles in Non-Uniform Environments," Chem. Eng. Sci., 1968, 23, 451.

13. Copelowitz, I. and Aris, R., "Communications on the Theory of Diffusion and Reaction--VI. The Effectiveness of Spherical Catalyst Particles in Steep External Gradients," Chem. Eng. Sci., 1970, 25, 885.

14. E. E. Petersen, J. C. Friedly and R. J. DeVogelaere, "The Rate of Chemical Reaction at the Surface of a Non-Porous Catalytic Sphere in Concentration and Temperature Gradients-I," Chem. Eng. Sci., 1964, 19, 683.

15. Mihail, R., "A Superposition Integral Equation for Catalytic External Surfaces," Chem. Eng. Sci., 1970, 25, 463.

16. Chambre, P. L., Appl. Scient. Res. 1956, A6, 97.

17. Chambre, P. L. and Acrivos, A., "On Chemical Surface Reactions in Laminar Boundary Layer Flows," J. Appl. Phys., 1956, 27, 1322.

18. Rosner, D. E., J. Aero/Space Sci., 1959, 26, 281.

19. Hougen, O. A. and Wilke, C. R., Trans. Am. Inst. Chem. Engrs., 1945, 41, 445.

20. Miller, J. W., Private Communication, January 15, 1970.

21. Miller, J. W., Private Communication, July 16, 1970.

22. Girdler Catalysts, "Girdler G-65 Methanation Catalyst," Technical Data Sheet G-65-0366.

23. Barber-Colman Company, "Series 621 Power Controller (Silicon Controlled Rectifier), Instruction Manual," F-12368-2, August 1965.

24. Barber-Colman Company, "Model 357A Digiset Null Balance Controller, Instruction Manual," F-12593-2, September 1965.

25. Leeds & Northrup Company, "7554 Type K-4 Potentiometer, Directions 177361 Issue 3,".

26. Leeds & Northrup Company,"9834 and 9834-1 Electronic D-C Null Detector, Directions 177121 Issue 5".

27. Lab-Line Instruments Inc., "Chromalyzer-100, Instruction Manual," April 1965.

28. Beckman Instruments Inc., "Beckman Instructions 1379-A," November 1965.

29. Disc Instruments, Inc., "Disc Chart Integrator - Model 236, Instruction Manual," 1965.

30. Hatfield, B., and Aris, R., "Communications on the Theory of Diffusion and Reaction - IV Combined Effects of Internal and External Diffusion in the Non-Isothermal Case," Chem. Eng. Sci., 1969, 24, 1213.

31. Hlavacek, V., and Kubicek, M., "Modeling of Chemical Reactors - XX Heat and Mass Transfer in Porous Catalyst: The Particle in a Non-Uniform External Field," Chem. Eng. Sci., 1970, 25, 1527.

32. Elzy, E., and Myers, G. A., "Engineering Calculations of Momentum, Heat and Mass Transfer Through Laminar Boundaries," Engineering Experiment Station, Oregon State University, Corvallis, Oregon, Bulletin No. 41, July 1968.

33. Elzy, E., and Myers, G. A., "Tables of Similar Solutions to the Equations of Momentum, Heat and Mass Transfer in Laminar Boundary Layer Flow," Engineering Experiment Station, Oregon State University, Corvallis, Oregon, Bulletin No. 40, February 1967.

34. Fulton, J. W., "Influence of Catalyst Particle Size on Reaction Kinetics: Hydrogenation of Ethylene on Nickel," Ph.D. Thesis, University of Oklahoma, (1964).

35. Fulton, J. W., and Crosser, O. K., "Influence of Catalyst Particle Size on Reaction Kinetics: Hydrogenation of Ethylene on Nickel," A.I.Ch.E. Journal, 1965, 11, 513.

36. Yen, Wen-Hwa, Private Communication, March 17, 1970.

37. Eischens, R. P., "Infrared Spectra of Chemisorbed Molecules," Accounts of Chemical Research, 1972, 5, 74.

38. Danckwerts, P. V., "Absorption by Simultaneous Diffusion and Chemical Reaction into Particles of Various Shapes and into Falling Drops," Trans. Faraday Soc., 47, 1014-1023 (1951).

39. Crank, I., "The Mathematics of Diffusion," Oxford University Press, 124-125 (1956).

40. Smith, J. M., and VanNess, H. C., "Introduction to Chemical Engineering Thermodynamics," McGraw-Hill Book Co. Inc., New York, 138, (1959).

41. Perry, J. F., "Chemical Engineers' Handbook," McGraw-Hill Book Co. Inc., New York, 3-197, (1963).

42. Perry, J. F., "Chemical Engineers' Handbook," McGraw-Hill Book Co. Inc., New York, 14-19, (1963).

43. Bird, R. B., Stewart, W. E., and Lightfoot, E. N., "Transport Phenomena," John Wiley and Sons Inc., New York, 247, (1960).

APPENDICES

APPENDIX A

THEORETICAL DEVELOPMENT OF THE MATERIAL AND ENERGY BALANCES APPLICABLE IN THE CATALYST WEDGE INTERIOR

FIGURE A-1 THE GENERAL MODEL

FIGURE A-2 CROSS-SECTIONAL VIEW AND COORDINATES FOR MODELED SYSTEM

THEORETICAL DEVELOPMENT OF THE MATERIAL AND ENERGY BALANCES APPLICABLE IN THE CATALYST WEDGE INTERIOR

The mathematical model used in this study describes a long right wedge of a porous catalyst material with length L_o. A gaseous reaction mixture is flowing perpendicular to the back edge of the wedge and impinging on the stagnation point. This situation is shown graphically in Figure A-1.

For the purpose of analysis and boundary description, this wedge may also be viewed as a catalyst box of square cross section as shown in Figure A-2. For convenience, rectangular coordinates are employed with the origin at the leading edge of the wedge.

In this case, the opposite side of this wedge should be its mirror image, using the center line as the axis of rotation.

Derivation of the Material Balance:

Let component A be a reactant species (ethylene). Then, generally,

Mass In - Mass Out + Mass Generated = Mass Accumulation,

or

$$N_{A_x} L_o \Delta y \Delta\theta \big|_{x,y} - N_{A_x} L_o \Delta y \Delta\theta \big|_{x+\Delta x,y} + N_{A_y} L_o \Delta x \Delta\theta \big|_{x,y}$$

$$- N_{A_y} L_o \Delta x \Delta\theta \big|_{x,y+\Delta y} - R_A (L_o \Delta x \Delta y \Delta\theta)$$

$$= c_A \Delta x \Delta y L_o \big|_{\theta+\Delta\theta} - c_A \Delta x \Delta y L_o \big|_{\theta} .$$

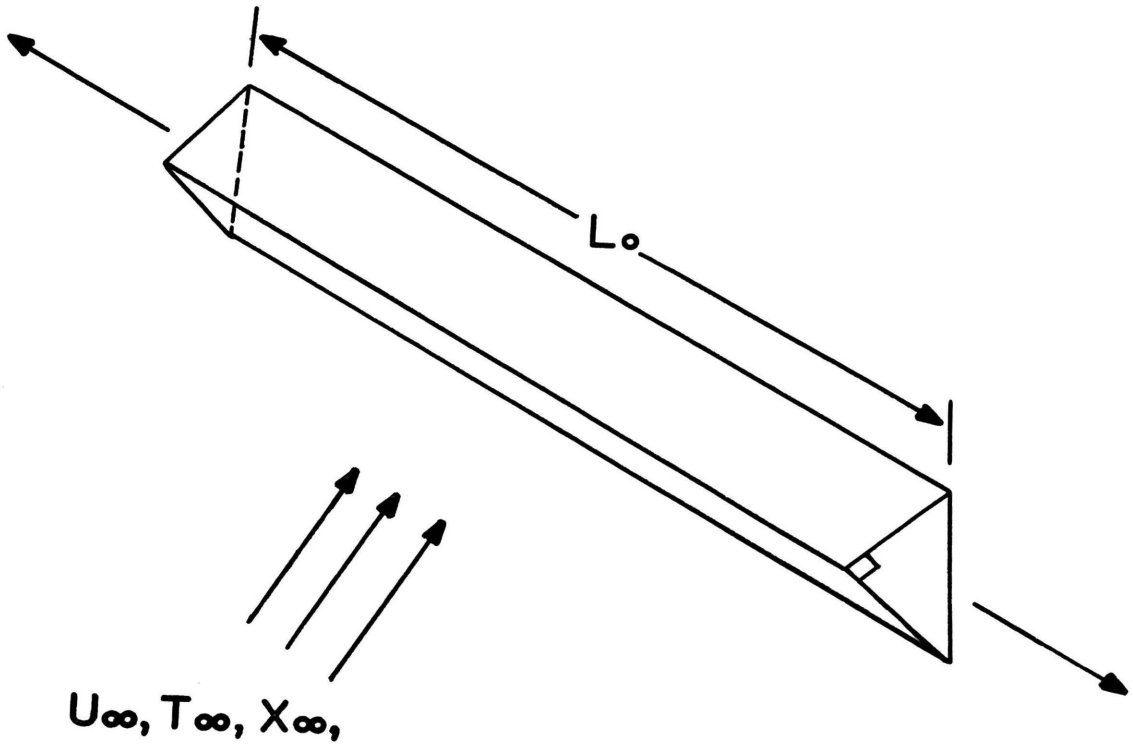

Figure A-1

The General Model

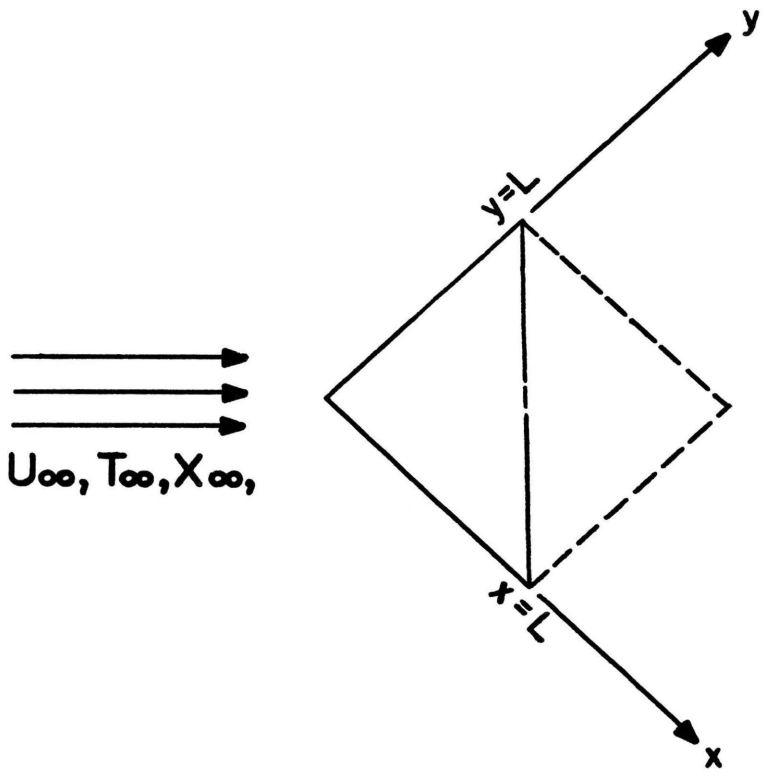

Figure A-2

Cross-Sectional View And
Coordinates For Modeled System

Dividing through by $L_o \Delta x \Delta y \Delta \theta$ and taking the limit as these quantities approach zero, gives

$$- \frac{\partial N_{A_x}}{\partial x} - \frac{\partial N_{A_y}}{\partial y} - R_A = \frac{\partial c_A}{\partial \theta} \quad . \tag{A-1}$$

This is the general material balance on reactant A. For a product the sign on R_A would change.

Now, neglecting bulk flow in the catalyst and assuming that c and D are constant throughout the wedge,

c = total molar concentration in catalyst

D = effective molecular diffusivity

X_i = mole fraction of component i

then

$$N_{i_x} = - cD \frac{\partial X_i}{\partial x} \quad . \tag{A-2}$$

Substituting this into Equation (A-1),

$$cD \frac{\partial^2 X_A}{\partial x^2} + cD \frac{\partial^2 X_A}{\partial y^2} - R_A = c \frac{\partial X_A}{\partial \theta}$$

Therefore,

$$\frac{\partial X_A}{\partial \theta} = D\left(\frac{\partial^2 X_A}{\partial x^2} + \frac{\partial^2 X_A}{\partial y^2}\right) - \frac{R_A}{c} \quad . \tag{A-3}$$

Now, defining the following dimensionless variables,

$$\Psi_A \equiv \frac{X_A}{X_A} \qquad\qquad \xi \equiv x/L$$

$$\tau \equiv \theta k_{\infty} \qquad\qquad \zeta \equiv y/L.$$

The definition of τ implies the reaction has been assumed to be first order with respect to species A. The ∞ on k implies the quantity is evaluated at the bulk gas conditions. So,

$$k_{\infty} X_{A_{\infty}} \frac{\partial \Psi_A}{\partial \tau} = D \frac{X_{A\infty}}{L^2} \left(\frac{\partial^2 \Psi_A}{\partial \xi^2} + \frac{\partial^2 \Psi_A}{\partial \zeta^2} \right) - \frac{R_A}{c} \qquad \text{(A-4)}$$

with

$$R_A \equiv kc_A = kcX_A = kcX_{A_{\infty}} \Psi_A. \qquad \text{(A-5)}$$

Assuming an Arrhenius rate constant form,

$$k = A\exp(-E/RT) \qquad \text{(A-6)}$$

and elimination of the frequency factor (A) in favor of the bulk temperature rate constant (k_{∞}) leads to:

$$k = k_{\infty} \exp\left(E/RT_{\infty}\left(1 - \frac{T_{\infty}}{T}\right)\right)$$

where

$$k_{\infty} = A\exp(-E/RT_{\infty}).$$

Defining

$$\Phi \equiv T/T_{\infty}$$

and

$$\beta \equiv E/RT_{\infty}$$

gives:

$$k = k_{\infty}\exp(\beta(1 - 1/\Phi)). \tag{A-7}$$

Substituting (A-7) into (A-5) and then into (A-4) gives:

$$k\ \frac{\partial \Psi_A}{\partial \tau} = \frac{D}{L^2}\left(\frac{\partial^2 \Psi_A}{\partial \xi^2} + \frac{\partial^2 \Psi_A}{\partial \zeta^2}\right) - k_{\infty}\exp(\beta(1 - 1/\Phi))\Psi_A. \tag{A-8}$$

Letting $\alpha^2 = \frac{D}{k_{\infty}L^2}$ yields:

$$\frac{\partial \Psi_A}{\partial \tau} = \alpha^2\left(\frac{\partial^2 \Psi_A}{\partial \xi^2} + \frac{\partial^2 \Psi_A}{\partial \zeta^2}\right) - \exp[\beta(1 - 1/\Phi)]\ \Psi_A \tag{A-9}$$

which is the unsteady-state material balance for the wedge.

Derivation of the Energy Balance:

Generally,

Energy In - Energy Out + Energy Generated = Energy Accumulation.

Then:

$$q_x L_o \Delta y \Delta\theta\big|_{x,y} - q_x L_o \Delta y \Delta\theta\big|_{x+\Delta x,y} + q_y L_o \Delta x \Delta\theta\big|_{x,y}$$
$$- q_y L_o \Delta x \Delta\theta\big|_{x,y+\Delta y} + R_V(\Delta x \Delta y L_o \Delta\theta).$$
$$= c(\Delta x \Delta y L_o) C_p T\big|_{\theta+\Delta\theta} - c(\Delta x \Delta y L_o) C_p T\big|_{\theta}.$$

Dividing through by $L_o \Delta x \Delta y \Delta\theta$ and taking the limit as these quantities approach zero, we obtain

$$-\frac{\partial q_x}{\partial x} - \frac{\partial q_y}{\partial y} + R_V = cC_p \frac{\partial T}{\partial \theta} \tag{A-10}$$

This is the general energy balance. The sign on R_V is positive for an exothermic reaction and negative for an endothermic reaction.

Assuming Fourier's Low of Heat Conduction is followed and k_H is constant, then

$$q_x = -k_H \frac{\partial T}{\partial X} . \qquad \text{(A-11)}$$

Substituting (A-11) into (A-10),

$$k_H \left(\frac{\partial^2 T}{\partial x^2} + \frac{\partial^2 T}{\partial y^2}\right) + R_V = cC_p \frac{\partial T}{\partial \theta} \qquad \text{(A-12)}$$

Considering the reaction being studied is exothermic, R_V may be rewritten as

$$R_V = (-\Delta H_A) R_A$$

where $(-\Delta H_A)$ is the negative heat of reaction per mole of species A. Employing the previously defined dimensionless variables, equation (A-12) is transformed as follows:

$$\frac{k_H T_\infty}{L^2}\left(\frac{\partial^2 \Phi}{\partial \xi^2} + \frac{\partial^2 \Phi}{\partial \zeta^2}\right) + (-\Delta H_A) R_A = T_\infty k_\infty cC_p \frac{\partial \theta}{\partial \tau} . \qquad \text{(A-13)}$$

Substituting for R_A and dividing by T k c gives

$$C_p \frac{\partial \Phi}{\partial \tau} = \frac{k_H}{k_\infty cL^2}\left(\frac{\partial^2 \Phi}{\partial \xi^2} + \frac{\partial^2 \Phi}{\partial \zeta^2}\right) + \frac{(-\Delta H_A) X_{A\infty}}{T_\infty} \exp[\beta (1 - 1/\Phi)] \Psi_A .$$

Multiplying through by $\frac{Dc}{k_H}$ and defining

$$\Pi \equiv \frac{Dc C_p}{k_H}$$

and

$$\lambda \equiv \frac{(-\Delta H_A) Dc_{A\infty}}{k_H T_\infty}$$

gives

$$\Pi \frac{\partial \theta}{\partial \tau} = \alpha^2 \left(\frac{\partial^2 \Phi}{\partial \xi^2} + \frac{\partial^2 \Phi}{\partial \zeta^2}\right) + \lambda \exp\left[\beta\left(1 - 1/\Phi\right)\right] \Psi_A \qquad \text{(A-14)}$$

which is the unsteady-state energy balance.

Equations (A-9) and (A-14) apply to the interior of the catalyst particle. Solutions to these equations for various boundary conditions to be considered are discussed and analyzed elsewhere.

APPENDIX B

A COMPARISON OF THE NUMERICAL AND ANALYTICAL SOLUTIONS FOR AN ISOTHERMAL FIRST ORDER REACTION IN A CATALYST WEDGE WITH THE SURFACE-SATURATION BOUNDARY CONDITIONS

FIGURE B-1 THE ANALYTICAL SOLUTION FOR Ψ_A WITH AN ISOTHERMAL FIRST ORDER REACTION IN A CATALYST WEDGE WITH THE SURFACE SATURATION CONDITION

FIGURE B-2 THE NUMERICAL SOLUTION FOR Ψ_A WITH AN ISOTHERMAL FIRST ORDER REACTION IN A CATALYST WEDGE WITH THE SURFACE SATURATION CONDITION

A COMPARISON OF THE NUMERICAL AND ANALYTICAL SOLUTIONS FOR AN ISOTHERMAL FIRST ORDER REACTION IN A CATALYST WEDGE WITH THE SURFACE-SATURATION BOUNDARY CONDITION

Here the particle is in an isothermal state with the Surface-Saturation Condition. That is, the surface is at equilibrium at all times with the surroundings which are assumed to be of constant composition, so that the mole fraction at the interface has a constant value X_{A_s}.

Therefore, the prevailing situation is that the energy balance equation is extraneous and the only equation which needs to be solved is the material balance. Due to the linear form the equation thus takes it may be solved analytically as well as numerically.

i) Analytic Solution:

The method of solution is the standard technique of separation of variables.

In this case, equation (A-9) reduced to

$$\frac{\partial \Psi_A}{\partial \tau} = \alpha^2 \left(\frac{\partial^2 \Psi_A}{\partial \xi^2} + \frac{\partial^2 \Psi_A}{\partial \zeta^2}\right) - \Psi_A \qquad \text{(B-1)}$$

Since $\Phi = 1$ (isothermal), the initial and boundary conditions are:

$$\begin{aligned} \Psi_A(\xi,\zeta,0) &= \Psi_{A_t} \quad t<0 \\ \Psi_A(0,\zeta,\tau) &= \Psi_{A_s} \\ \Psi_A(1,\zeta,\tau) &= \Psi_{A_s} \end{aligned} \qquad \text{(B-2)}$$

$$\Psi_A(\xi,0,\tau) = \Psi_{A_s}$$

$$\Psi_A(\xi,1,\tau) = \Psi_{A_s}$$

The solution technique was originally derived by Danckwerts (38) and may also be found in Crank (39). It requires solution of the pure diffusion equation,

$$\frac{\partial \Psi_A^*}{\partial \tau} = \alpha^2 \left(\frac{\partial^2 \Psi_A^*}{\partial \xi^2} + \frac{\partial^2 \Psi_A^*}{\partial \zeta^2}\right) \qquad \text{(B-3)}$$

subject to the original boundary conditions (B-2). Assuming a solution of the form

$$\Psi_A^*(\xi,\zeta,\tau) - \Psi_{A_s} = X(\xi)Y(\zeta)T(\tau) \qquad \text{(B-4)}$$

and substituting this into the differential equation (B-3), we obtain

$$XYT' = \alpha^2 (X''YT + XY''T)$$

Separating variables,

$$\frac{T'}{T} = \alpha^2 \left(\frac{X''}{X} + \frac{Y''}{Y}\right)$$

or

$$\frac{Y''}{Y} = \frac{1}{\alpha^2}\left(\frac{T'}{T} - \frac{X''}{X}\right)$$

and letting

$$\frac{Y''}{Y} = \lambda^2$$

implies

$$\frac{X''}{X} = \frac{1}{\alpha^2}\frac{T'}{T} - \lambda^2.$$

Now letting

$$\frac{Y''}{X} = \mu^2$$

then

$$\frac{1}{\alpha^2}\frac{T'}{T} - \lambda^2 = \mu^2 \text{ where } \mu \neq f(\lambda).$$

Solution now requires solving the following set of equations.

$$\begin{array}{lll} Y'' - \lambda^2 Y = 0 & Y(0) = 0 & Y(1) = 0 \text{(i)} \\ X'' - \mu^2 X = 0 & X(0) = 0 & X(1) = 0 \text{(ii)} \\ T' - (\lambda^2 + \mu^2)\alpha^2 T = 0 & T(0) = \Psi_{A_t} & t<0 \quad \text{(iii)} \end{array} \qquad \text{(B-5)}$$

Solving (B-5iii),

$$T' - (\lambda^2 + \mu^2)\alpha^2 T = 0$$

implies

$$T_n = a\exp[\alpha^2(\lambda^2 + \mu^2)\tau]. \qquad \text{(B-6)}$$

Now try $\lambda^2 < 0$ in (B-5i),

$$Y_n = d\sin\lambda\zeta + e\cos\lambda\zeta$$

$$Y(0) = 0$$

implies $e = 0$

$Y(1) = 0$ implies

$\lambda = n\pi$

and

$$Y_n = d\sin n\pi\zeta . \tag{B-7}$$

Now trying $\mu^2 < 0$ in equation (B-5ii) implies

$X_n = f\sin\mu\xi + g\cos\mu\xi$

$X(0) = 0$ implies $g = 0$

$X(1) = 0$ implies $\mu = m\pi$

and

$$X_n = f\sin m\pi\xi . \tag{B-8}$$

The formal solution is,

$$\Psi_A^*(\xi, \zeta, \tau) - \Psi_{A_s} = \sum_{m=1}^{\infty} \sum_{n=1}^{\infty} X_n(\xi) Y_n(\zeta) T_n(\tau) . \tag{B-9}$$

Substituting (B-6), (B-7) and (B-8) in equation (B-9) yields,

$$\Psi_A^*(\xi, \zeta, \tau) - \Psi_{A_s} = \sum_{m=1}^{\infty} \sum_{n=1}^{\infty} A_{mn} \sin m\pi\xi \sin n\pi\zeta \exp[-\pi^2 \alpha^2 (m^2 + n^2)\tau] . \tag{B-10}$$

for $\tau = 0$,

$$\Psi_{A_t} - \Psi_{A_s} = \sum_{m=1}^{\infty} \sum_{n=1}^{\infty} A_{mn} \sin m\pi\xi \sin n\pi\zeta$$

or

$$\Psi_{A_t} - \Psi_{A_s} = \sum_{m=1}^{\infty} \left(\sum_{n=1}^{\infty} A_{mn} \sin n\pi\zeta \right) \sin m\pi\xi \qquad \text{(B-11)}$$

Now, for each fixed ζ, this is the Fourier sine representation of the function $\Psi_{A_t} - \Psi_{A_s}$ of the variable ξ, provided that the coefficients of the term $\sin m\pi\xi$ are those in the Fourier sine series, i.e.,

$$\sum_{n=1}^{\infty} A_{mn} \sin n\pi\zeta = \frac{2}{1} \int_0^1 (\Psi_{A_t} - \Psi_{A_s}) \sin m\pi\delta \, d\delta$$

$$= 2 \frac{(\Psi_{A_t} - \Psi_{A_s})}{m\pi} \int_0^{m\pi} \sin\theta \, d\theta$$

$$= \frac{2(\Psi_{A_t} - \Psi_{A_s})}{m\pi} (-\cos\theta) \Big|_0^{m\pi}$$

$$= \frac{2(\Psi_{A_t} - \Psi_{A_s})}{m\pi} [-(\cos m\pi - 1)]$$

$$= \frac{4(\Psi_{A_t} - \Psi_{A_s})}{(2m - 1)\pi} \qquad \text{(B-12)}$$

then,

$$A_{mn} = \frac{2}{1} \int_0^1 \frac{4(\Psi_{A_t} - \Psi_{A_s})}{(2m - 1)\pi} \sin n\pi\eta \, d\eta$$

$$A_{mn} = \frac{8(\Psi_{A_t} - \Psi_{A_s})}{(2m - 1)\pi \cdot n\pi} \int_0^{n\pi} \sin\eta \cdot d\eta \cdot$$

$$A_{mn} = \frac{8(\Psi_{A_t} - \Psi_{A_s})}{(2m - 1)n\pi^2} (-\cos\eta \cdot) \Big|_0^{n\pi}$$

$$A_{mn} = \frac{16(\Psi_{A_t} - \Psi_{A_s})}{\pi^2(2m - 1)(2n - 1)} \cdot \tag{B-13}$$

Finally,

$$\Psi_A{}^*(\xi, \zeta, \tau) - \Psi_{A_s} = \frac{16(\Psi_{A_t} - \Psi_{A_s})}{\pi^2} \sum_{m=1}^{\infty} \sum_{n=1}^{\infty} \frac{\sin(2m - 1)\pi\xi}{(2m-1)} \cdot \tag{B-14}$$

$$\frac{\sin(2n - 1)\pi\zeta}{(2n - 1)} \exp[-\pi^2\alpha^2\{(2m - 1)^2 + (2n - 1)^2\}\tau] .$$

Dividing both sides of equation (B-14) by Ψ_{A_s} gives

$$\frac{\Psi_A{}^*}{\Psi_{A_s}} = 1 - \frac{16(\Psi_{A_t} - \Psi_{A_s})}{\pi^2\Psi_{A_s}} \sum_{m=1}^{\infty} \sum_{n=1}^{\infty} \frac{\sin(2m - 1)\pi\xi}{2m - 1} \frac{\sin(2n - 1)\pi\zeta}{2n - 1} \tag{B-15}$$

$$\exp[-\pi^2\alpha^2\{(2m - 1)^2 + (2n - 1)^2\}\tau]$$

which is the solution for the pure diffusion problem. Applying Danckwerts' theory (38), the solution to the problem with first order reaction then becomes,

$$\frac{\Psi_A(\xi, \zeta, \tau)}{\Psi_{A_s}} = 1 - \frac{16(\Psi_{A_t} - \Psi_{A_s})}{\pi^2\Psi_{A_s}} \sum_{m=1}^{\infty} \sum_{n=1}^{\infty} \frac{\sin(2m-1)\pi\xi}{2m-1} \frac{\sin(2n-1)\pi\zeta}{2n-1} \tag{B-16}$$

$$\cdot \frac{1+\pi^2\alpha^2\{(2m-1)^2+(2n-1)^2\}\exp[-\tau(1+\pi^2\alpha^2\{(2m-1)^2+(2n-1)^2\})]}{1+\pi^2\alpha^2\{(2m-1) +(2n-1)^2\}}$$

For the steady-state solution the time dependent portion of (B-16) may be set equal to zero yielding:

$$\frac{\Psi_A(\xi,\zeta)}{\Psi_{A_s}} = 1 - \frac{16(\Psi_{A_t}-\Psi_{A_s})}{\pi^2\Psi_{A_s}} \sum_{m=1}^{\infty}\sum_{n=1}^{\infty} \frac{\sin(2m-1)\pi\xi}{2m-1} \frac{\sin(2n-1)\pi\zeta}{2n-1}$$

$$\cdot \frac{1}{1+\pi^2\alpha^2\{(2m-1)^2+(2n-1)^2\}} \cdot \qquad \text{(B-17)}$$

Values for this infinite series were computed using a digital computer and are given in Figure B-1 for $\Psi_{A_t} = 0.0$ and $\Psi_{A_s} = 1.0$.

ii) Numerical Solution:

The method of solution employed was the relaxation technique. The equation which was solved was exactly the one given by (B-1) with boundary conditions identical to (B-2).

The steady-state situation was considered ($\frac{\partial \Psi_A}{\partial \tau} = 0$), so the initial condition of (B-2) was not needed.

Thus the equation solved was

$$\frac{\partial^2\Psi_A}{\partial\xi^2} + \frac{\partial^2\Psi_A}{\partial\zeta^2} - \frac{\Psi_A}{\alpha^2} - 0. \qquad \text{(B-18)}$$

Using the central difference formula for the derivative, this equation becomes:

$$\frac{\Psi_A|_{\xi+\Delta\xi,\zeta} - 2\Psi_A|_{\xi,\zeta} + \Psi_A|_{\xi-\Delta\xi,\zeta}}{(\Delta\xi)^2} + \frac{\Psi_A|_{\xi,\zeta+\Delta\zeta} - 2\Psi_A|_{\xi,\zeta} + \Psi_A|_{\xi,\zeta-\Delta\zeta}}{(\Delta\zeta)^2}$$

$$- \frac{\Psi_A|_{\xi,\zeta}}{\alpha^2} = 0. \qquad \text{(B-19)}$$

Now, letting $\Delta\xi = \Delta\zeta$,

$$\Psi_A|_{\xi+\Delta\xi,\zeta} + \Psi_A|_{\xi-\Delta\xi,\zeta} + \Psi_A|_{\xi,\zeta+\Delta\zeta} + \Psi_A|_{\xi,\zeta-\Delta\zeta} - 4\,\Psi_A|_{\xi,\zeta} - \frac{\Delta\xi^2}{\alpha^2}\,\Psi_A|_{\xi,\zeta} = 0. \tag{B-20}$$

This equation was solved using the computer, with the results being shown in Figure B-2. As it can be seen, the finite difference solution compares quite favorably with the analytical solution which is given in Figure B-1.

The arrow to the left on Figure B-1 and all figures succeeding indicates the reactant flow direction. The lower half of the wedge is not shown as the values are the mirror image of the upper half which is shown.

$\Psi_{A_o} = 1.0$

$\alpha^2 = 0.0781$

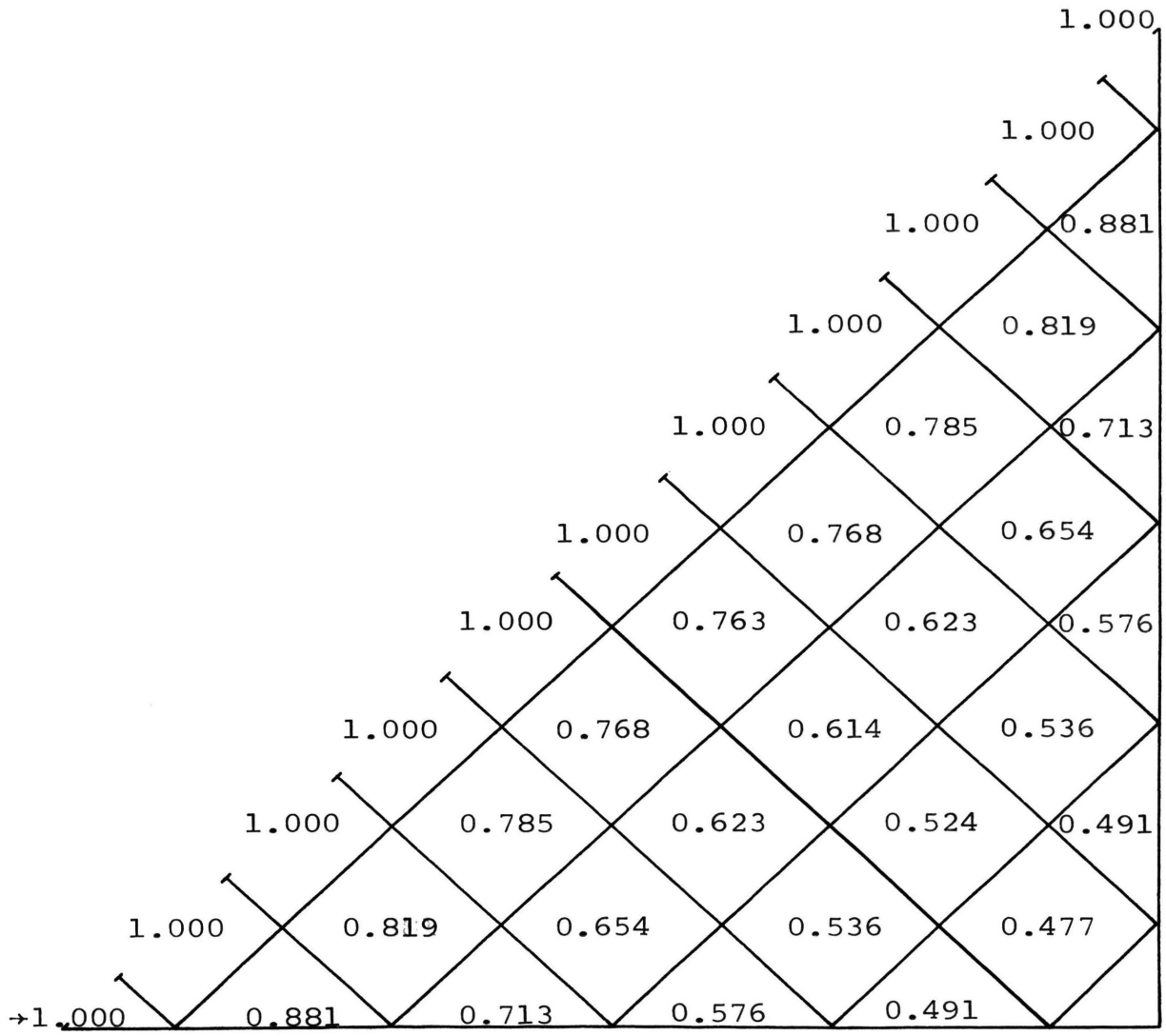

Figure B-1

The Analytical Solution For Ψ_A With
An Isothermal First Order Reaction In A
Catalyst Wedge With The Surface Saturation Condition

$\Psi_{A_o} = 1.0$

$\alpha^2 = 0.0781$

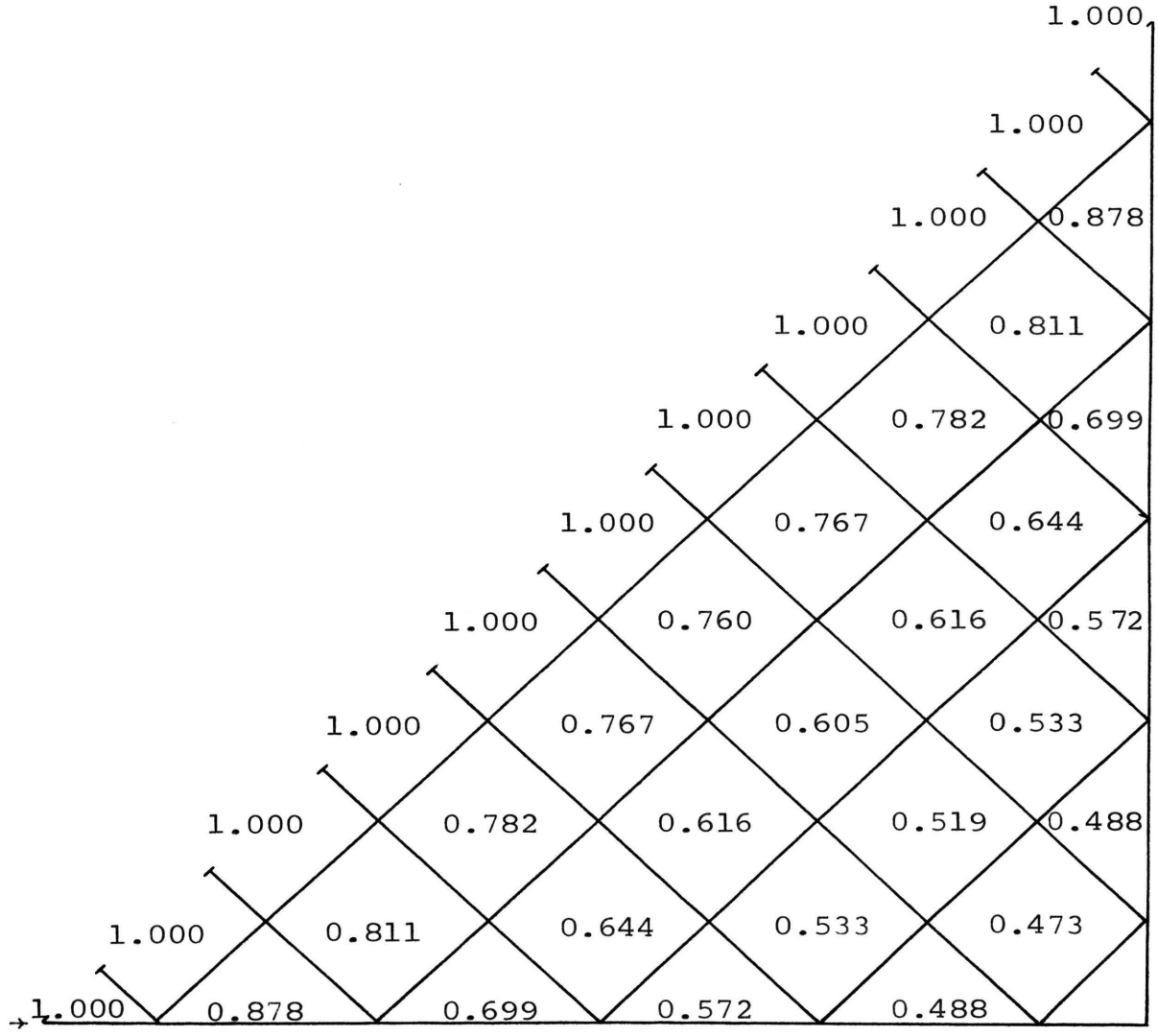

Figure B-2

The Numerical Solution For Ψ_A With
An Isothermal First Order Reaction In
A Catalyst Wedge With The Surface Saturation Condition

APPENDIX C

SOLUTION FOR THE CASE OF NON-ISOTHERMAL FIRST ORDER REACTION IN A CATALYST WEDGE WITH SURFACE SATURATION OF BOTH CONCENTRATION AND TEMPERATURE

FIGURE C-1 DIMENSIONLESS MOLE FRACTION (Ψ_A) PROFILE FOR THE CASE OF NON-ISOTHERMAL FIRST ORDER REACTION WITH $\Psi_{A_s} = 1.0$ AND $\Phi_s = 1.0$ ($\alpha^2 = 0.0781$, $\beta = 2.4700$, $\lambda = 0.3560$)

FIGURE C-2 DIMENSIONLESS TEMPERATURE (Φ) PROFILE FOR THE CASE OF NON-ISOTHERMAL FIRST ORDER REACTION WITH $\Psi_{A_s} = 1.0$ AND $\Phi_s = 1.0$ ($\alpha^2 = 0.0781$, $\beta = 2.4700$, $\lambda = 0.3560$)

SOLUTION FOR THE CASE OF NON-ISOTHERMAL FIRST ORDER REACTION IN A CATALYST WEDGE WITH SURFACE SATURATION OF BOTH CONCENTRATION AND TEMPERATURE

In this case the particle is in a non-isothermal state with the Surface-Saturation Condition applying to both the mole fraction and temperature. The steady-state problem was the only one considered.

The applicable equations and boundary conditions are:

$$\alpha^2\left(\frac{\partial^2\Psi_A}{\partial\xi^2}+\frac{\partial^2\Psi_A}{\partial\zeta^2}\right)-\exp\left[\beta\left(1-1/\Phi\right)\right]\Psi_A=0 \quad \text{(i)}$$

$$\Psi_A(0,\zeta)=\Psi_{A_s} \quad \text{(ii)} \qquad \Psi_A(\xi,0)=\Psi_{A_s} \quad \text{(iv)} \qquad \text{(C-1)}$$

$$\Psi_A(1,\zeta)=\Psi_{A_s} \quad \text{(iii)} \qquad \Psi_A(\xi,1)=\Psi_{A_s} \quad \text{(v)}$$

and

$$\alpha^2\left(\frac{\partial^2\Phi}{\partial\xi^2}+\frac{\partial^2\Phi}{\partial\zeta^2}\right)+\lambda\exp\left[\beta\left(1-1/\Phi\right)\right]\Psi_A=0 \quad \text{(i)}$$

$$\Phi(0,\zeta)=\Phi_s \quad \text{(ii)} \qquad \Phi(\xi,0)=\Phi_s \quad \text{(iv)} \qquad \text{(C-2)}$$

$$\Phi(1,\zeta)=\Phi_s \quad \text{(iii)} \qquad \Phi(\xi,1)=\Phi_s \quad \text{(v)}$$

Following a development presented by Prater (3), these two equations can be reduced to the solution of only one of the equations with the other dependent variable directly calculable. The results are as follows:

$$(T-T_s)=\frac{(-\Delta H_i)D}{k_H}\left(C_{i_s}-C_i\right) \qquad \text{(C-3)}$$

Converting this to dimensionless variables:

$$(\Phi - 1) = \frac{(-\Delta H_A) Dc_{A_s}}{k_H T_s} (1 - \Psi_A) \qquad \text{(C-4)}$$

defining $\lambda = \frac{(-\Delta H_A) Dc_{A_s}}{k_H T_s}$ then

$$(\Phi - 1) = \lambda (1 - \Psi_A) . \qquad \text{(C-5)}$$

This equation can then be solved for Φ, substituted into the material balance (C-1i) and solved.

Following this procedure gives:

$$\alpha^2 \left(\frac{\partial^2 \Psi_A}{\partial \xi^2} + \frac{\partial^2 \Psi_A}{\partial \zeta^2}\right) - \exp\left[\beta \left(1 - \frac{1}{1 + \lambda (1 - \Psi_A)}\right)\right] \Psi_A = 0$$

or,

$$\alpha^2 \left(\frac{\partial^2 \Psi_A}{\partial \xi^2} + \frac{\partial^2 \Psi_A}{\partial \zeta^2}\right) - \exp\left[\beta\lambda (1 - \Psi_A)/\{1 + \lambda (1 - \Psi_A)\}\right] \Psi_A = 0 \qquad \text{(C-6)}$$

with the boundary conditions of (C-1ii) - (C-1v).

Putting the equation into finite difference form,

$$\Psi_A|_{\xi + \Delta\xi, \zeta} + \Psi_A|_{\xi - \Delta\xi, \zeta} + \Psi_A|_{\xi, \zeta + \Delta\zeta} + \Psi_A|_{\xi, \zeta - \Delta\zeta} - 4\Psi_A|_{\xi, \zeta} \qquad \text{(C-7)}$$

$$- \frac{\Delta\xi^2}{\alpha^2} \exp\left[\beta\lambda (1 - \Psi_A|_{\xi, \zeta})/\{1 + \lambda (1 - \Psi_A|_{\xi, \zeta})\}\right] \Psi_A|_{\xi, \zeta} = 0$$

Equation (C-7) was solved using the digital computer with the results shown in Figure C-1 for $\Psi_{A_s} = 1.0$, $\Phi_s = 1.0$. These values were then substituted in equation (C-5) and solved for Φ. The values for $\Phi(\xi,\zeta)$ are given in Figure C-2.

$\alpha^2 = 0.0781$

$\beta = 2.4700$

$\lambda = 0.3560$

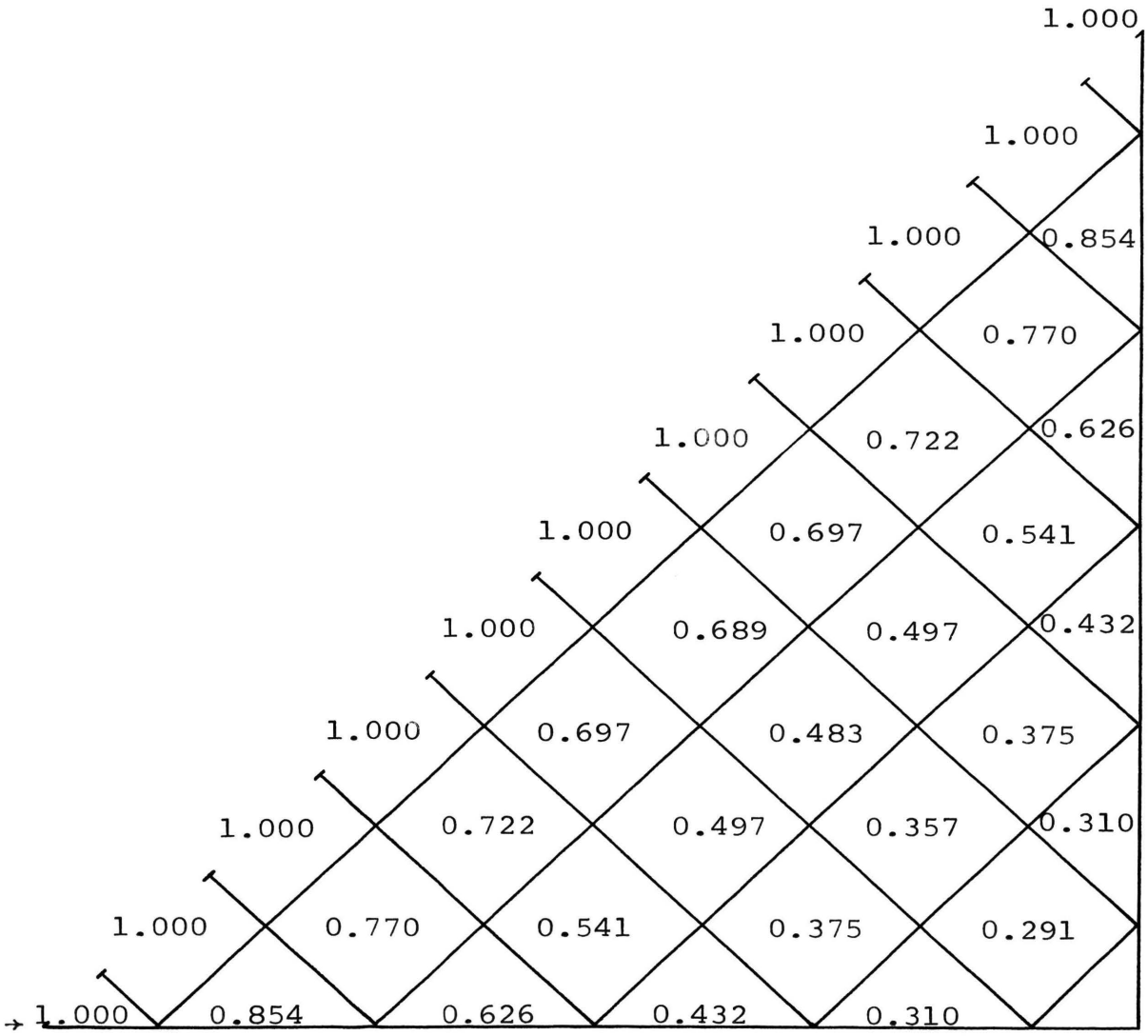

Figure C-1

Dimensionless Mole Fraction (Ψ_A) Profile For The Case Of Non-Isothermal First Order Reaction With $\Psi_{A_s} = 1.0$ and $\Phi_s = 1.0$.

$\alpha^2 = 0.0781$

$\beta = 2.4700$

$\lambda = 0.3560$

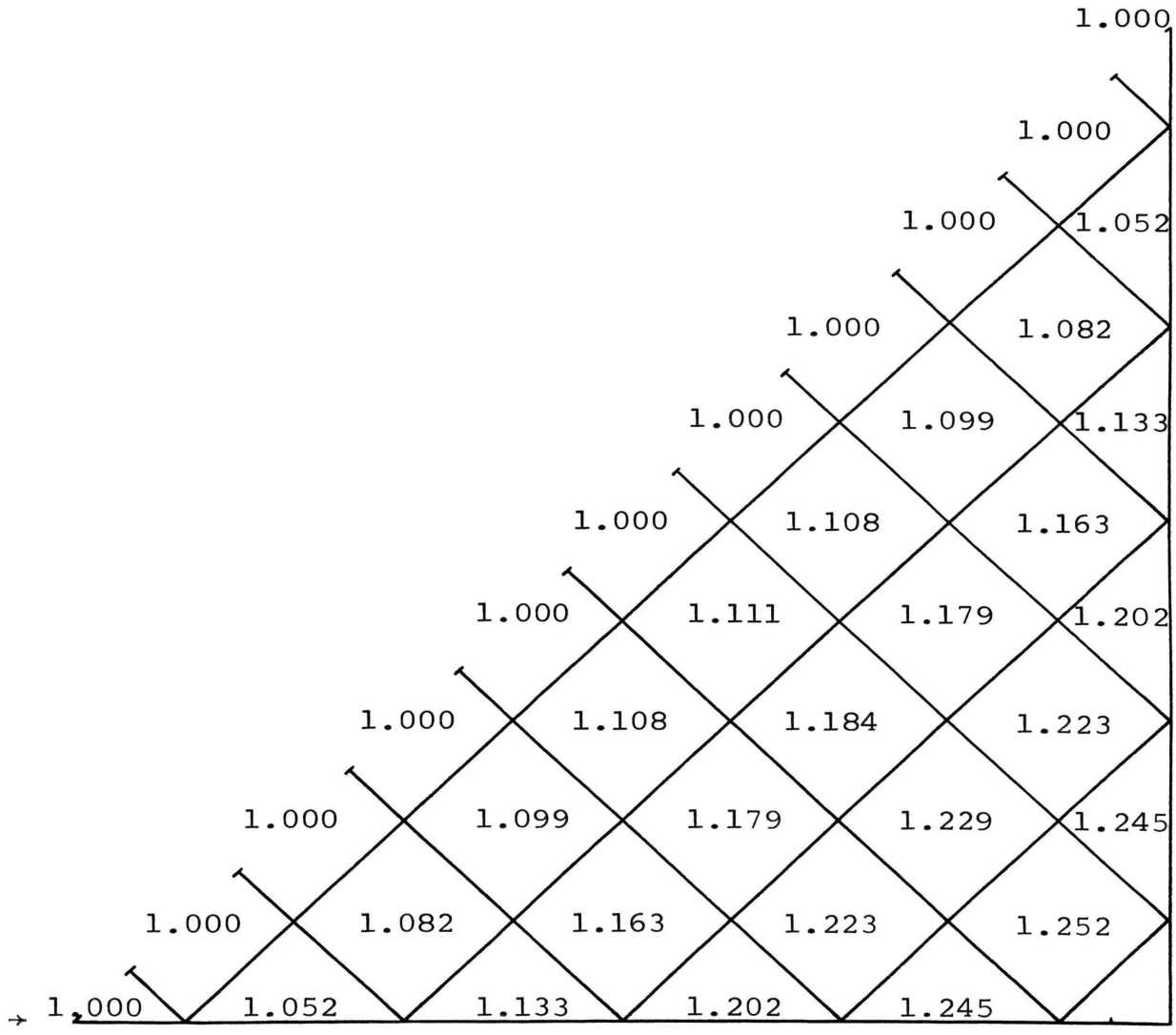

Figure C-2

Dimensionless Temperature (Φ) Profile
For The Case Of Non-Isothermal First
Order Reaction With $\Psi_{A_s} = 1.0$ and $\Phi_s = 1.0$

APPENDIX D

DEVELOPMENT OF BOUNDARY CONDITIONS TO INCORPORATE BOUNDARY LAYER CONSIDERATIONS INTO THE MODEL SOLUTION

FIGURE D-1 BOUNDARY CONFIGURATION USED FOR FINITE DIFFERENCE CALCULATIONS

DEVELOPMENT OF BOUNDARY CONDITIONS TO INCORPORATE BOUNDARY LAYER CONSIDERATIONS INTO THE MODEL SOLUTION

In order to incorporate boundary layer considerations into the solution of the wedge problem, expressions for heat and mass transfer coefficients were required. These expressions were obtained by solving the following set of boundary layer equations.

Equation of continuity of mass:

$$\frac{\partial u}{\partial x} + \frac{\partial v}{\partial y} = 0 \qquad \text{(D-1)}$$

Equation of motion:

$$u \frac{\partial u}{\partial x} + v \frac{\partial u}{\partial y} = - 1/\rho \frac{dP}{dx} + \nu \frac{\partial^2 u}{\partial y^2} \qquad \text{(D-2)}$$

Equation of energy:

$$u \frac{\partial T}{\partial x} + v \frac{\partial T}{\partial y} = \frac{\partial^2 T}{\partial y^2} \qquad \text{(D-3)}$$

Equation of continuity of species:

$$u \frac{\partial X_A}{\partial x} + v \frac{\partial X_A}{\partial y} = D_{AB} \frac{\partial^2 X_A}{\partial y^2} \qquad \text{(D-4)}$$

Subject to the following boundary conditions:

at $y = 0$: $u(x,y) = 0$ (i) (D-5)

$v = v_s(x)$ (ii)

$T = T_s$ (iii)

$X_A = X_{A_s}$ (iv)

and as $y \to \infty$:

$$u = U(x) \qquad \text{(v)}$$

$$T = T_\infty \qquad \text{(vi)}$$

$$X_A = X_{A_\infty} \qquad \text{(vii)}$$

Viscous dissipation, radiation, chemical reaction within the fluid phase, and the Soret effect have been neglected.

The mass and heat transfer coefficients were then defined by equating their definitions to the surface flux. This has been done by Elzy and Myers (22) with the following results

$$k_x^{\cdot} = \frac{cU(x)\pi'}{Sc} \left(\frac{m+1}{2} \frac{\nu}{U(x)x}\right)^{1/2} \qquad \text{(D-6)}$$

$$h^{\cdot} = \frac{\rho C_p U(x)\pi'}{Pr} \left(\frac{m+1}{2} \frac{\nu}{U(x)x}\right)^{1/2} \qquad \text{(D-7)}$$

where

$U(x)$ = Velocity profile at the edge of boundary layer given by $U_\infty x^m$

U_∞ = Free stream velocity

π = Similarity solution to equations (D-3) and (D-4)

π' = First derivative of similarity solution to equations (D-3) and (D-4)

c = Total molar density

Sc = Schmidt number (ν / D_{ij})

D_{ij} = Gaseous diffusion coefficient

$m = \sigma/2-\sigma$

σ = Included wedge angle in radians

ρ = Total mass density

ν = Kinematic viscosity (μ/ρ)

μ = Absolute viscosity

Pr = Prandtl Number ($\mu C_p/k_G$)

C_p = Specific heat

k_G = Gas thermal conductivity

The values of π and π' are tabulated by Elzy and Myers (23).

These relationships were used for $k_x^{\cdot}$ and $h^{\cdot}$ in the boundary equations which are derived in the following. Figure D-1 shows the boundary configuration used in the finite difference computations.

MATERIAL BALANCE BOUNDARY EQUATION

The material balance boundary equation may be derived in finite difference form as follows:

Along the x = 0 boundary, with m being the index for the x coordinate and n the index for the y coordinate, at steady state

INPUT - OUTPUT + GENERATION = 0

$$\left(-cD\,\frac{X_A|_{m,n} - X_A|_{m,n-1}}{\Delta y}\right)\frac{\Delta x}{2} - \left(-cD\,\frac{X_A|_{m,n+1} - X_A|_{m,n}}{\Delta y}\right)\frac{\Delta x}{2}$$

$$- \left(-cD\,\frac{X_A|_{m+1,n} - X_A|_{m,n}}{\Delta x}\right)\Delta y + k_x^{\cdot}\Delta y\left(X_{A_\infty} - X_A|_{m,n}\right) \qquad \text{(D-8)}$$

$$-A\exp\left(-E/RT|_{m,n}\right)cX_A|_{m,n}\left(\Delta y\,\Delta x/2\right) = 0.$$

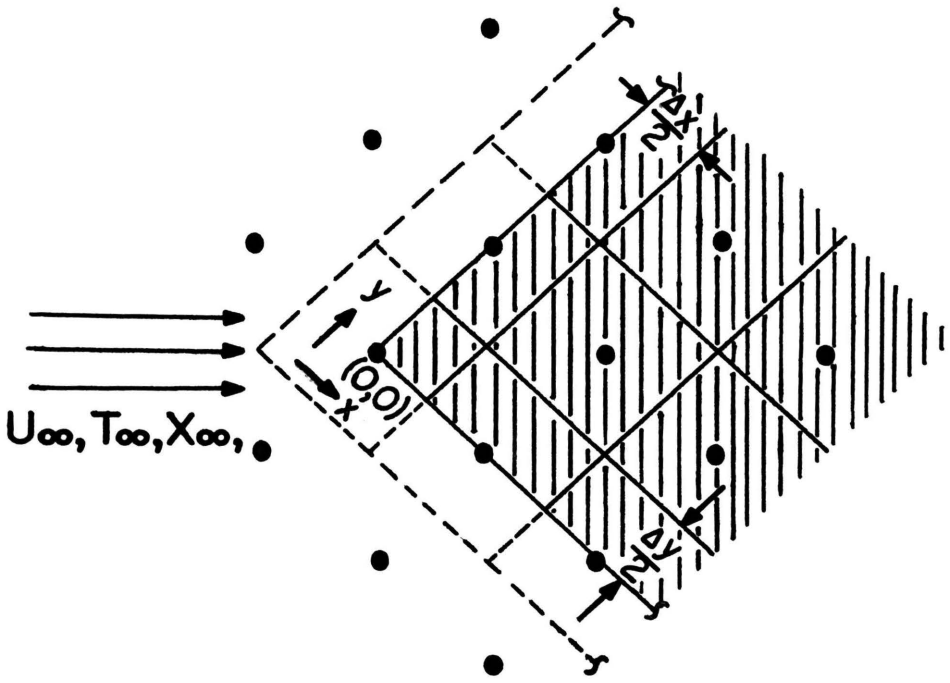

Figure D-1

Boundary Configuration Used For
Finite Difference Calculations

Putting this into dimensionless form, and letting $\Delta x = \Delta y$

$$-cD\,\frac{\Psi_A|_{m,n} - \Psi_A|_{m,n-1}}{2} + cD\,\frac{\Psi_A|_{m,n+1} - \Psi_A|_{m,n}}{2}$$

$$+(cD\,[\Psi_A|_{m+1,n} - \Psi_A|_{m,n}]) + k_x^{\cdot}L\,\Delta\xi(1.0 - \Psi_A|_{m,n})$$

$$-k_\infty \exp[\beta\,(1 - 1/\Phi|_{m,n})]\,c\,\Psi_A|_{m,n} L^2 \frac{2(\Delta\xi)^2}{2} = 0.$$

or

$$\frac{\Psi_A|_{m,n-1}}{2} + \frac{\Psi_A|_{m,n+1}}{2} + \Psi_A|_{m+1,n} - 2\Psi_A|_{m,n} + \frac{k_x^{\cdot}L}{Dc}\,\Delta\xi(1.0 - \Psi_A|_{m,n}) \tag{D-9}$$

$$\frac{k_\infty L^2}{D}\,\frac{\Delta\xi^2}{2}\exp[\beta(1 - 1/\Phi|_{m,n})]\Psi_A|_{m,n} = 0.$$

Defining $DCMTC \equiv \frac{k_x^{\cdot}L}{Dc}$, then

$$\frac{\Psi_A|_{m,n-1}}{2} + \frac{\Psi_A|_{m,n+1}}{2} + \Psi_A|_{m+1,n} - 2\Psi_A|_{m,n} + DCMTC\,\Delta\xi(1.0 - \Psi_A|_{m,n}) \tag{D-10}$$

$$-\frac{\Delta\xi^2}{2\alpha}\exp[\beta(1 - 1/\Phi|_{m,n})]\,\Psi_A|_{m,n} = 0$$

which may be expressed in differential form as:

$$\frac{\partial \Psi_A}{\partial \xi}\Big|_{\xi=0} = DCMTC(\Psi_A - 1.0). \tag{D-11}$$

ENERGY BALANCE BOUNDARY EQUATION

Along the x = o boundary,

$$-k_H\left(\frac{T|_{m,n}-T|_{m,n-1}}{\Delta y}\right)\frac{\Delta x}{2} + k_H\left(\frac{T|_{m,n+1}-T|_{m,n}}{\Delta y}\right)\frac{\Delta x}{2}$$

$$+k_H\left(\frac{T|_{m+1,n}-T|_{m,n}}{\Delta x}\right)\Delta y - h^{\cdot}\Delta y\,(T|_{m,n}-T_\infty) \qquad \text{(D-12)}$$

$$+(-\Delta H_A)A\exp(-E/RT|_{m,n})\,cX_A|_{m,n}\left(\Delta y\frac{\Delta x}{2}\right) = 0.$$

Putting this into dimensionless form and letting $\Delta x = \Delta y$,

$$-k_hT_\infty\frac{\Phi|_{m,n}-\Phi|_{m,n-1}}{2} + k_hT_\infty\frac{\Phi|_{m,n+1}-\Phi|_{m,n}}{2}$$

$$+ k_HT_\infty(\Phi|_{m+1,n}-\Phi|_{m,n}) - h^{\cdot}T_\infty L\Delta\xi\,(\Phi|_{m,n}-1.0)$$

$$+ (-\Delta H_A)k_\infty\exp[\beta(1 - 1/\Phi|_{m,n})]\,cX_{A\infty}\Psi_A|_{m,n}L^2\left(\frac{\Delta\xi^2}{2}\right) = 0$$

or

$$\frac{\Phi|_{m,n-1}}{2} + \frac{\Phi|_{m,n+1}}{2} + \Phi|_{m+1,n} - 2\Phi|_{m,n} - \frac{h^{\cdot}L}{k_H}\Delta\xi\,(\Phi|_{m,n}-1.0) \qquad \text{(D-13)}$$

$$+\frac{(-\Delta H)k_\infty cX_{A\infty}L^2}{k_HT_\infty}\left(\frac{\Delta\xi}{2}\right)^2\exp[\beta(1 - 1/\Phi|_{m,n})]\Psi_A|_{m,n} = 0.$$

Multiplying the last term by D/D and defining $DCHTC = \frac{h^{\cdot}L}{k_H}$ we have,

$$\frac{\Phi|_{m,n-1}}{2} + \frac{\Phi|_{m,n+1}}{2} + \Phi|_{m+1,n} - 2\Phi|_{m,n} - DCHTC\Delta\xi(\Phi_{m,n} - 1.0) \tag{D-14}$$

$$+ \frac{\lambda}{\alpha 2}\frac{(\Delta\xi)^2}{2}\exp[\beta(1 - 1/\Phi|_{m,n})]\Psi_A|_{m,n} = 0$$

which may be expressed in differential form as:

$$\left.\frac{\partial\Phi}{\partial\xi}\right|_{\xi=0} = DCHTC(\Phi - 1.0). \tag{D-15}$$

In addition to the conditions that the flux of mass and heat arriving at the surface through the solid phase must respectively equal the flux of mass and heat arriving at the surface through the gas phase, there are two other conditions which must hold when steady-state conditions exist. These are that the volumetric rate of mass and heat generation within the solid are also equal to the conductive and convective fluxes at the catalyst wedge surface.

These conditions are mathematically derived as follows:

INTEGRAL CONDITIONS WITH RESPECT TO MASS

The volumetric rate of mass generation within the wedge is expressed as:

$$Q_{VM} = \iiint_V R_A dV \tag{D-16}$$

with R_A being as given in Equation (A-5) as

$$R_A = kc_{A_\infty}\Psi_A$$

and

$$k = k_{\infty}\exp[\beta(1 - 1/\Phi)].$$

This yields

$$Q_{VM} = \iiint_V k_{\infty}\exp[\beta(1 - 1/\Phi)]c_{A_{\infty}}\Psi_A dxdydz \qquad (D\text{-}17)$$

Replacing the integration by a summation for use in computer calculation gives:

$$Q_{VM} = \sum\sum\sum_V k_{\infty}\exp[\beta(1 - 1/\Phi)]\, c_{A_{\infty}}\Psi_A \Delta x \Delta y \Delta z \qquad (D\text{-}18)$$

Φ and Ψ_A are assumed to be independent of z so the expression can be rewritten as:

$$Q_{VM} = k_{\infty} c_{A_{\infty}} L_o \sum\sum\exp[\beta(1 - 1/\Phi)]\, \Psi_A \Delta x \Delta Y \qquad (D\text{-}19)$$

Putting this into dimensionless forms and noting that $\alpha^2 = \frac{D}{k_{\infty}L^2}$ gives

$$Q_{VM} = \frac{Dc_{A_{\infty}}L_o}{\alpha^2}\sum\sum\exp[\beta(1 - 1/\Phi)]\, \Psi_A \Delta\xi \Delta\zeta. \qquad (D\text{-}20)$$

If $\Delta\xi = \Delta\zeta$, then

$$Q_{VM} = \frac{Dc_{A_{\infty}}L_o}{\alpha^2}\sum\sum\exp[\beta(1 - 1/\Phi)]\Psi_A \Delta\xi^2. \qquad (D\text{-}21)$$

The total rate at which ethylene (component A) is transferred to the catalyst surface by convection is expressed by

$$Q_{CM} = \iint_A N_A dA \qquad (D\text{-}22)$$

where

$$N_A = k_x^{\cdot}(X_{A_\infty} - X_{A_O}) \tag{D-23}$$

or in dimensionless terms,

$$N_A = k_x^{\cdot}(1.0 - \Psi_A)X_{A_\infty}. \tag{D-24}$$

Then

$$Q_{CM} = X_{A_\infty}\iint_A k_x^{\cdot}(1.0 - \Psi_A)dxdz \tag{D-25}$$

Ψ_A is not a function of z, nor is $k_x^{\cdot}$ so

$$Q_{CM} = X_{A_\infty} L_O \int k_x^{\cdot}(1.0 - \Psi_A)dx \tag{D-26}$$

or for use in finite difference form

$$Q_{CM} = X_{A_\infty} L_O \Sigma k_x^{\cdot}(1.0 - \Psi_A)\Delta x. \tag{D-27}$$

Putting this into dimensionless form and noting that

$DCMTC = \frac{k_x^{\cdot} L}{Dc}$, then

$$Q_{CM} = C_{A_\infty} L_O D \Sigma DCMTC(1.0 - \Psi_A)\Delta\xi. \tag{D-28}$$

At steady-state,

$$Q_{CM} = Q_{VM}$$

or

$$Q_{CM} - Q_{CM} = 0. \tag{D-29}$$

Therefore, the terms

$$\Sigma\Sigma \frac{\Delta\xi^2}{\alpha^2} \exp[\beta(1 - 1/\Phi)]\Psi_A - \Sigma DCMTC(1.0 - \Psi_A)\Delta\xi \qquad (D-30)$$

must sum to zero at steady-state conditions.

INTEGRAL CONDITIONS WITH RESPECT TO ENERGY

The volumetric rate of heat generation within the catalyst wedge can be expressed as

$$Q_{VH} = Q_{VM}(-\Delta H) = \iiint_V \frac{(-\Delta H)Dc_{A\infty}}{\alpha^2} \exp[\beta(1 - 1/\Phi)]\Psi_A d\xi\, d\zeta dz. \qquad (D-31)$$

Noting that the integrand is independent of z and multiplying the top and bottom of equation (D-31) by $T_\infty k_H$ gives

$$Q_{VH} = \frac{L_o T_\infty k_H \lambda}{\alpha^2} \iint \exp[\beta(1 - 1/\Phi)]\Psi_A d\xi d\zeta. \qquad (D-32)$$

Replacing the integration by finite summations yields:

$$Q_{VH} = \frac{L_o T_\infty k_H \lambda}{\alpha^2} \Sigma\Sigma \exp[\beta(1 - 1/\Phi)]\Psi_A \Delta\xi\Delta\zeta \qquad (D-33)$$

If $\Delta\xi = \Delta\zeta$ then

$$Q_{VH} = \frac{L_o T_\infty k_H \lambda}{\alpha^2} \Sigma\Sigma \exp[\beta(1 - 1/\Phi)]\Psi_A \Delta\xi^2. \qquad (D-34)$$

The total amount of heat transferred away from the catalyst surface by convection is given by

$$Q_{CH} = \iint_A q_{CH} dA \qquad (D-35)$$

where

$$q_{CH} = h^{\cdot}(T_s - T_\infty). \tag{D-36}$$

Putting this expression into dimensionless form gives

$$Q_{CH} = T_\infty \iint_A h^{\cdot}(\Phi - 1.0)dxdz. \tag{D-37}$$

However, Φ is not a function of z, nor is $h^{\cdot}$ so

$$Q_{CH} = T_\infty L_o \int h^{\cdot}(\Phi - 1.0)dx. \tag{D-38}$$

In finite form equation (D-38) becomes

$$Q_{CH} = T_\infty L_o \Sigma h^{\cdot}(\Phi - 1.0)\Delta x \tag{D-39}$$

and noting that DCHTC = $\frac{h^{\cdot}L}{k_H}$ yields

$$Q_{CH} = T_\infty L_o k_H \Sigma DCHTC(\Phi - 1.0)\Delta\xi. \tag{D-40}$$

At steady-state,

$$Q_{CH} = Q_{VH}$$

or

$$Q_{VH} - Q_{CH} = 0. \tag{D-41}$$

Therefore, the terms

$$\Sigma\Sigma \frac{\lambda\Delta\xi^2}{\alpha^2} \exp[\beta(1-1/\Phi)]\,\Psi_A - \Sigma DCHTC(\Phi-1.0)\Delta\xi \tag{D-42}$$

must sum to zero at steady-state.

APPENDIX E

SOLUTION FOR THE CASE OF NON-ISOTHERMAL FIRST ORDER REACTION IN A CATALYST WEDGE WITH CONSTANT HEAT AND MASS TRANSFER COEFFICIENTS AT THE BOUNDARY

Figure E-1 Computer Dimensionless Temperature (1.000) and Mole Fraction (1.000) Profiles Inside the Catalyst Wedge (α^2 = 0.1222, β = 2.47, λ = 0.356, DCMTC = 22.88, DCHTC = 22.88)

Figure E-2 Computer Dimensionless Temperature (1.000) and Mole Fraction (1.000) Profiles Inside the Catalyst Wedge (α^2 = 0.1222, β = 2.47, λ = 0.356, DCMTC = 22.88, DCHTC = 14.88)

Figure E-3 Computer Dimensionless Temperature (1.000) and Mole Fraction (1.000) Profiles Inside the Catalyst Wedge (α^2 = 0.1222, β = 2.47, λ = 0.356, DCMTC = 22.88, DCHTC = 6.88)

SOLUTION FOR THE CASE OF NON-ISOTHERMAL FIRST ORDER REACTION IN A CATALYST WEDGE WITH CONSTANT HEAT AND MASS TRANSFER COEFFICIENTS AT THE BOUNDARY

The steady-state mathematical description of the system solved here is given by equations (C-1i) and (C-2i) and boundary conditions as given by:

$$\alpha^2 \frac{\partial^2 \Psi_A}{\partial \xi^2} + \frac{\partial^2 \Psi_A}{\partial \zeta^2} - \exp\left[\beta(1 - 1/\Phi)\right] \Psi_A = 0 \qquad \text{(C-1i)}$$

with

$$\frac{\partial \Psi_A(\xi,0)}{\partial \zeta} = \text{DCMTC}\left[\Psi_A(\xi,0) - 1.0\right] \qquad \text{(E-1i)}$$

$$\frac{\partial \Psi_A(\xi,1)}{\partial \zeta} = \text{DCMTC}\left[\Psi_A(\xi,1) - 1.0\right] \qquad \text{(E-1ii)}$$

$$\frac{\partial \Psi_A(0,\zeta)}{\partial \xi} = \text{DCMTC}\left[\Psi_A(0,\zeta) - 1.0\right] \qquad \text{(E-1iii)}$$

$$\frac{\partial \Psi_A(1,\zeta)}{\partial \xi} = \text{DCMTC}\left[\Psi_A(1,\zeta) - 1.0\right] \qquad \text{(E-1iv)}$$

$$\Psi_A(0,0) = 1.0 \qquad \text{(E-1v)}$$

$$\Psi_A(1,1) = 1.0 \qquad \text{(E-1vi)}$$

and

$$\alpha^2 \left(\frac{\partial^2 \Phi}{\partial \xi^2} + \frac{\partial^2 \Phi}{\partial \zeta^2}\right) + \lambda \exp\left[\beta\,(1 - 1/\Phi)\right] \Psi_A = 0 \qquad \text{(C-2i)}$$

with

$$\frac{\partial\Phi(\xi,0)}{\partial\zeta} = \text{DCHTC}\,[\Phi(\xi,0) - 1.0] \qquad \text{(E-2i)}$$

$$\frac{\partial\Phi(\xi,1)}{\partial\zeta} = \text{DCHTC}\,[\Phi(\xi,1) - 1.0] \qquad \text{(E-2ii)}$$

$$\frac{\partial\Phi(0,\zeta)}{\partial\xi} = \text{DCHTC}\,[\Phi(0,\zeta) - 1.0] \qquad \text{(E-2iii)}$$

$$\frac{\partial\Phi(1,\zeta)}{\partial\xi} = \text{DCHTC}\,[\Phi(1,\zeta) - 1.0] \qquad \text{(E-2iv)}$$

$$\Phi(0,0) = 1.0 \qquad \text{(E-2v)}$$

$$\Phi(1,1) = 1.0 \qquad \text{(E-2vi)}$$

These equations and boundary conditions were put in finite difference form as demonstrated by equations (C-7), (D-10), and (D-14) and solved using the digital computer with DCHTC and DCMTC having constant values over the entire surface of the particle.

Solutions to these equations for dimensionless temperature and mole fraction are presented in Figures E-1 through E-3 for three values of DCHTC.

These solutions are for a very mild reaction state in contrast to conditions during the experiments. However, the effect of changes in DCHTC on the temperature and mole fraction profiles can be seen.

The dimensionless temperature (Φ) and mole fraction (Ψ_A) values for the wedge profiles are presented as

$$\frac{\text{Dimensionless Temperature } (\Phi)}{\text{Dimensionless Mole Fraction } (\Psi_A)}$$

in Appendix E and those succeeding.

$\alpha^2 = 0.1222$

$\beta = 2.47$

$\lambda = 0.356$

DCMTC = 22.88

DCHTC = 22.88

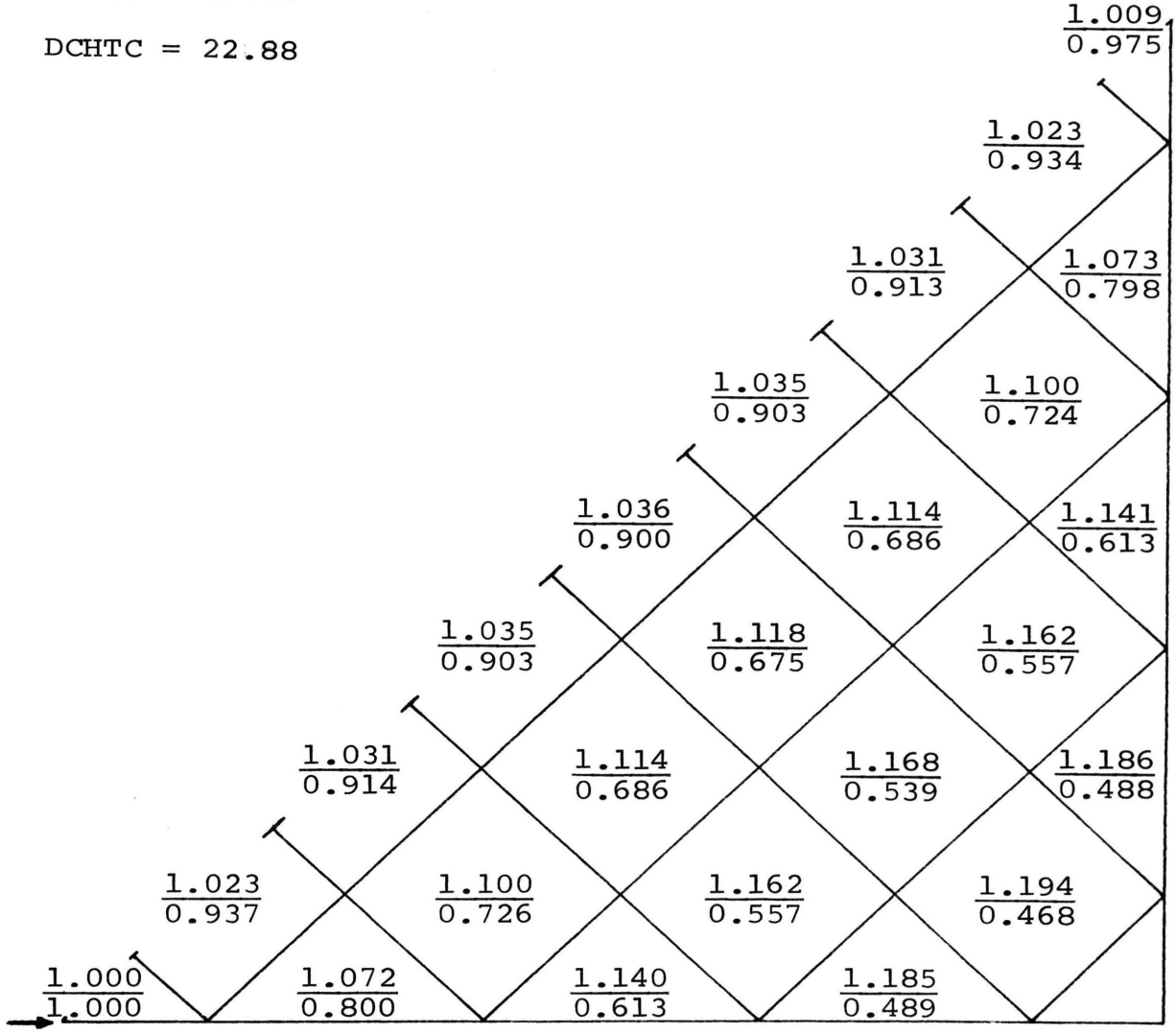

Figure E-1

Computer Dimensionless Temperature (1.000) and Mole Fraction (1.000) Profiles Inside the Catalyst Wedge

$\alpha^2 = 0.1222$

$\beta = 2.47$

$\lambda = 0.356$

DCMTC = 22.88

DCHTC = 14.88

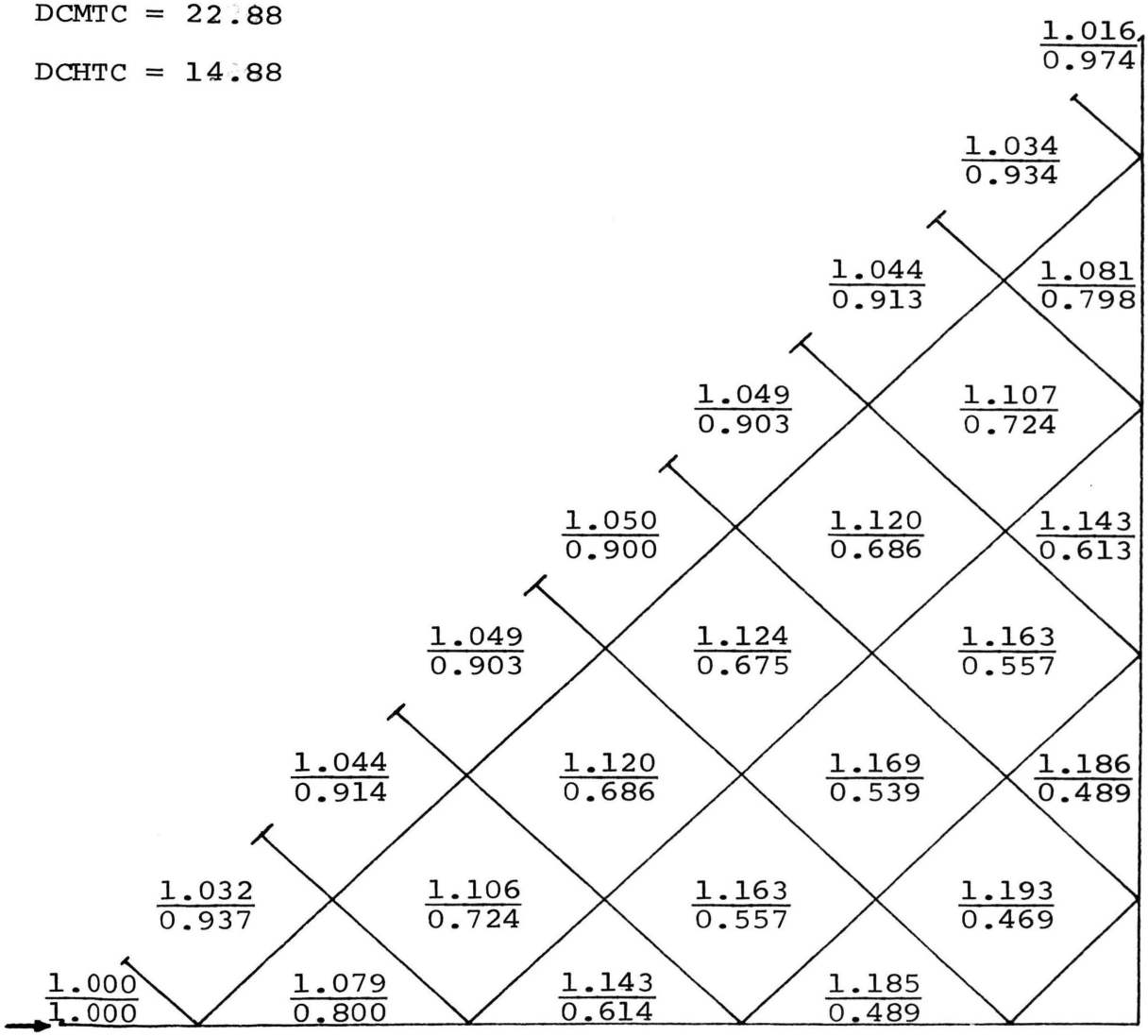

Figure E-2

Computer Dimensionless Temperature (1.000) and Mole Fraction (1.000) Profiles Inside the Catalyst Wedge

$\alpha^2 = 0.1222$

$\beta = 2.47$

$\lambda = 0.356$

DCMTC = 22.88

DCHTC = 6.88

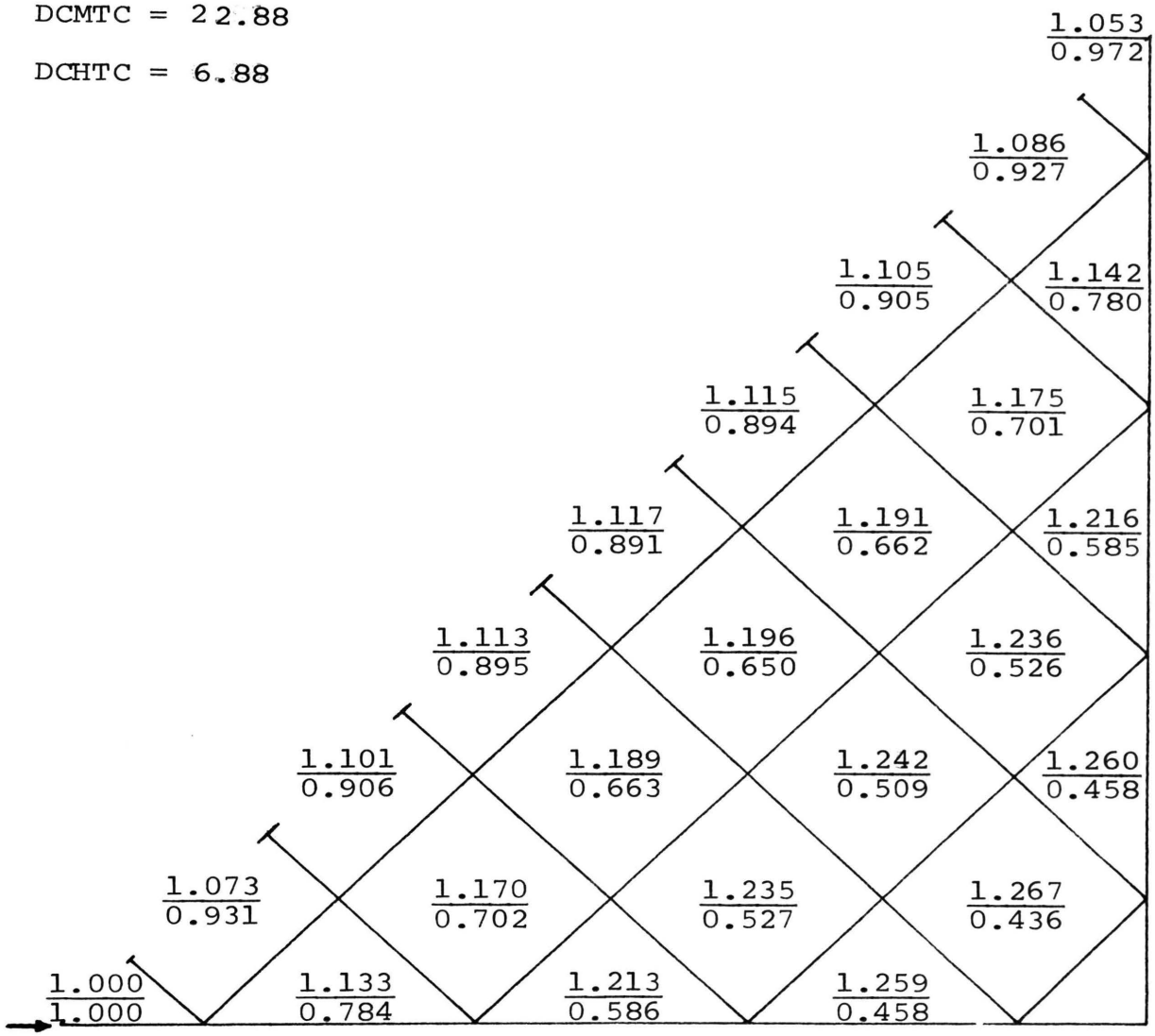

Figure E-3

Computer Dimensionless Temperature (1.000) and
Mole Fraction (1.000) Profiles
Inside the Catalyst Wedge

APPENDIX F

SOLUTION FOR THE CASE OF NON-ISOTHERMAL FIRST ORDER REACTION IN A CATALYST WEDGE WITH VARIABLE HEAT AND MASS TRANSFER COEFFICIENTS AT THE BOUNDARY, (Φ_o = 1.0 and Ψ_{A_o} = 1.0 I.E., INFINITE HEAT AND MASS TRANSFER COEFFICIENTS AT THE STAGNATION POINT)

Figure F-1 Computer Dimensionless Temperature (1.000) and Mole Fraction (1.000) Profiles Inside the Catalyst Wedge (α^2 = 0.1222, β = 2.47, λ = 0.356, DCMTC = $11.44\xi^{-1/3}$, DCHTC = $11.44\xi^{-1/3}$)

Figure F-2 Computer Dimensionless Temperature (1.000) and Mole Fraction (1.000) Profiles Inside the Catalyst Wedge (α^2 = 0.1222, β = 2.47, λ = 0.356, DCMTC = $19.44\xi^{-1/3}$, DCHTC = $11.44\xi^{-1/3}$)

SOLUTION FOR THE CASE OF NON-ISOTHERMAL FIRST ORDER REACTION IN A CATALYST WEDGE WITH VARIABLE HEAT AND MASS TRANSFER COEFFICIENTS AT THE BOUNDARY, (Φ_o = 1.0 and Ψ_{A_o} = 1.0 I.E., INFINITE HEAT AND MASS TRANSFER COEFFICIENTS AT THE STAGNATION POINT)

This problem required the solution of the same set of equations as those given in Appendix E but here DCMTC and DCHTC were not constants, but functions of the distance from the stagnation point as given below. These expressions were obtained by combining the definitions of DCMTC and DCHTC and the relationships given in Appendix D for $k_x^{\cdot}$ and $h^{\cdot}$, thus with DCMTC defined by

$$DCMTC \equiv \frac{k_x^{\cdot} L}{Dc} \qquad (D\text{-}9i)$$

and

$$k_x^{\cdot} = \frac{cU(x)\pi'}{Sc} \left(\frac{m+1}{2} \frac{\nu}{U(x)x}\right)^{1/2} \qquad (D\text{-}6)$$

then

$$DCMTC = \frac{LU(x)\,\pi'}{DSc} \left(\frac{m+1}{2} \frac{\nu}{U(x)x}\right)^{1/2} \qquad (F\text{-}1)$$

if the bulk gas concentration equals the bulk concentration in the wedge. Also, with DCHTC defined by

$$DCHTC = \frac{h^{\cdot} L}{k_H} \qquad (D\text{-}13i)$$

and

$$h^{\cdot} = \frac{\rho C_p U(x) \pi'}{Pr} \left(\frac{m+1}{2} \frac{\nu}{U(x) x} \right)^{1/2} \qquad \text{(D-7)}$$

then

$$DCHTC = \frac{L \rho C_p U(\xi) \pi'}{Pr} \left(\frac{m+1}{2} \frac{\nu}{U(\xi) \xi L} \right)^{1/2} \qquad \text{(F-2)}$$

These relations were substituted into the boundary conditions (E-1i)-(E-1vi) and (E-2i)-(E-2vi) and used to solve equations (C-1i) and C-2i).

The results are given in Figures F-1 and F-2 for two values of DCMTC.

$\alpha^2 = 0.1222$

$\beta = 2.47$

$\lambda = 0.356$

DCMTC = $11.44\xi^{-1/3}$

DCHTC = $11.44\xi^{-1/3}$

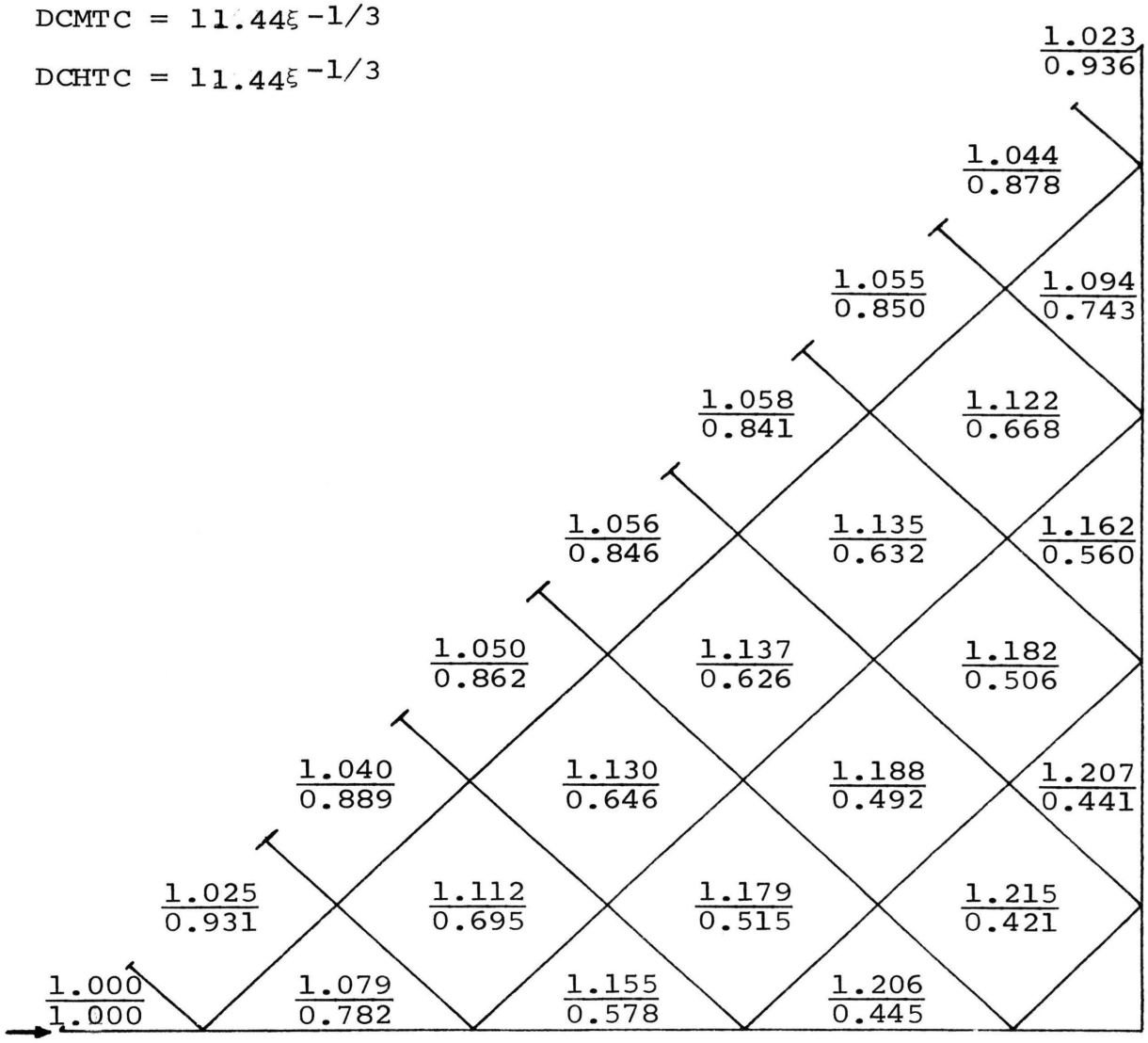

Figure F-1

Computer Dimensionless Temperature (1.000) and
Mole Fraction (1.000) Profiles
Inside the Catalyst Wedge

$\alpha^2 = 0.1222$

$\beta = 2.47$

$\lambda = 0.356$

$DCMTC = 19.44\xi^{-1/3}$

$DCHTC = 11.44\xi^{-1/3}$

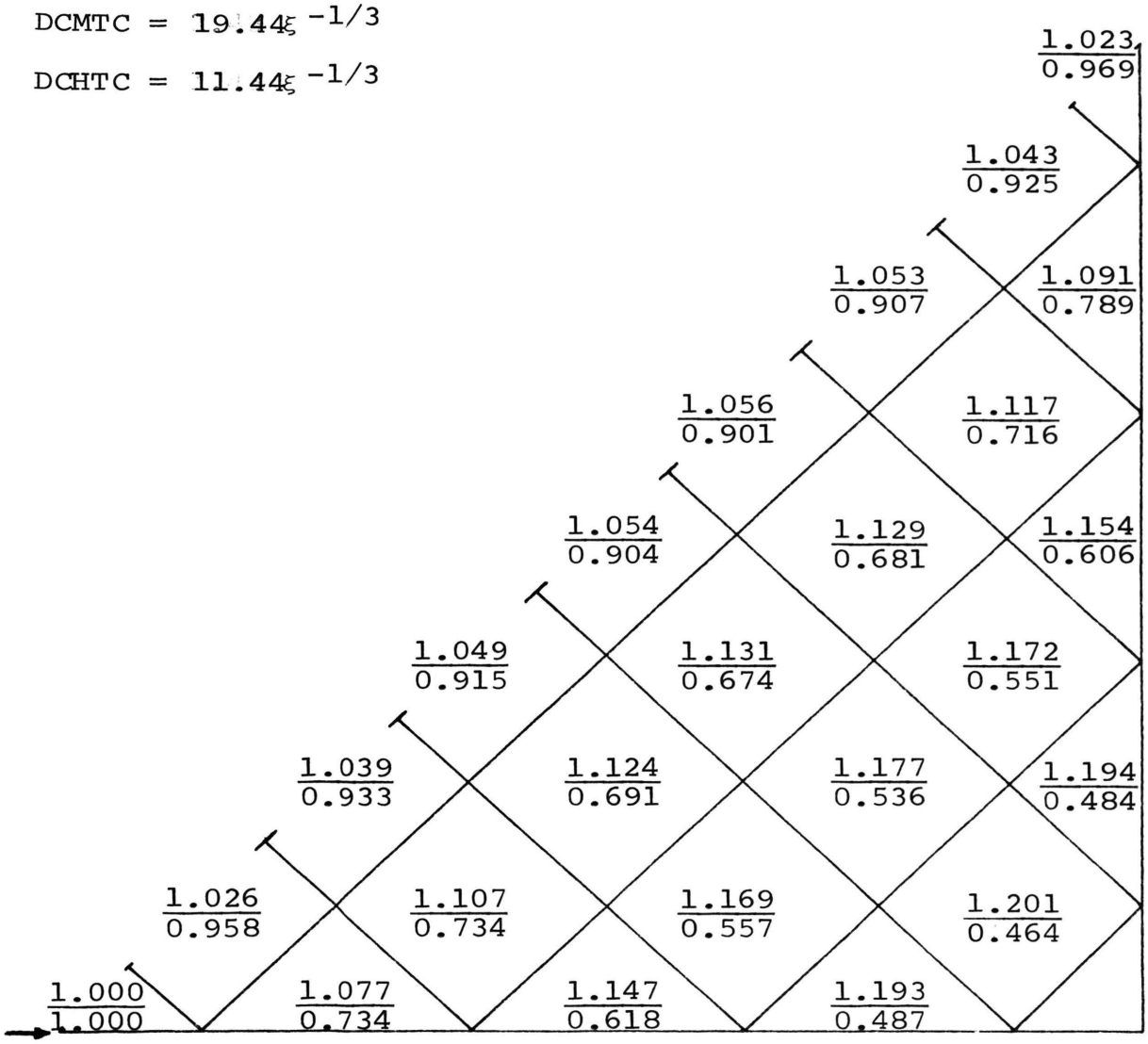

Figure F-2

Computer Dimensionless Temperature (1.000) and
Mole Fraction (1.000) Profiles
Inside the Catalyst Wedge

APPENDIX G

SOLUTION FOR THE CASE OF NON-ISOTHERMAL FIRST ORDER REACTION IN A CATALYST WEDGE WITH VARIABLE HEAT AND MASS TRANSFER COEFFICIENTS AT THE BOUNDARY. (FINITE HEAT AND MASS TRANSFER COEFFICIENTS AT THE STAGNATION POINT)

Figure G-1 Computer Dimensionless Temperature (1.089) and Mole Fraction (0.959) Profiles Inside the Catalyst Wedge ($\alpha^2 = 0.1011$, $\beta = 3.29$, $\lambda = 0.0443$, DCMTC = $14.01\xi^{-1/3}$, DCHTC = $0.628\xi^{-1/3}$)

Figure G-2 Computer Dimensionless Temperature (1.337) and Mole Fraction (0.981) Profiles Inside the Catalyst Wedge ($\alpha^2 = 0.1011$, $\beta = 3.29$, $\lambda = 0.0443$, DCMTC = $14.01\xi^{-1/3}$, DCHTC = $0.24\xi^{-1/3}$)

Figure G-3 Computer Dimensionless Temperature (1.047) and Mole Fraction (0.909) Profiles Inside the Catalyst Wedge ($\alpha^2 = 0.0077$, $\beta = 3.29$, $\lambda = 0.0443$, DCMTC = $27.68\xi^{-1/3}$, DCHTC = $3.68\xi^{-1/3}$)

Figure G-4 Computer Dimensionless Temperature (1.327) and Mole Fraction (0.863) Profiles Inside the Catalyst Wedge ($\alpha^2 = 0.0077$, $\beta = 3.29$, $\lambda = 0.0443$, DCMTC = $27.68\xi^{-1/3}$, DCHTC = $1.17\xi^{-1/3}$)

Figure G-5 Computer Dimensionless Temperature (1.137) and Mole Fraction (0.946) Profiles Inside the Catalyst Wedge ($\alpha^2 = 0.0202$, $\beta = 3.29$, $\lambda = 0.0443$, DCMTC = $27.68\xi^{-1/3}$, DCHTC = $1.17\xi^{-1/3}$)

Figure G-6 Computer Dimensionless Temperature (1.231) and Mole Fraction (0.909) Profiles Inside the Catalyst Wedge ($\alpha^2 = 0.0108$, $\beta = 3.29$, $\lambda = 0.0443$, DCMTC = $27.68\xi^{-1/3}$, DCHTC = $1.17\xi^{-1/3}$)

Figure G-7 Computer Dimensionless Temperature (1.281) and Mole Fraction (0.909) Profiles Inside the Catalyst Wedge ($\alpha^2 = 0.0092$, $\beta = 3.29$, $\lambda = 0.0443$, DCMTC = $27.68\xi^{-1/3}$, DCHTC = $1.17\xi^{-1/3}$)

Figure G-8 Computer Dimensionless Temperature (1.046) and Mole Fraction (0.940) Profiles Inside the Catalyst Wedge ($\alpha^2 = 0.5047$, $\beta = 3.29$, $\lambda = 0.221$, DCMTC = $2.77\xi^{-1/3}$, DCHTC = $1.17\xi^{-1/3}$)

SOLUTION FOR THE CASE OF NON-ISOTHERMAL FIRST ORDER REACTION IN A CATALYST WEDGE WITH VARIABLE HEAT AND MASS TRANSFER COEFFICIENTS AT THE BOUNDARY. (FINITE HEAT AND MASS TRANSFER COEFFICIENTS AT THE STAGNATION POINT)

In the steady-state this problem again required solution of the equations as given in Appendix E, however, the boundary conditions of (E-1v), (E-1vi), (E-2v) and (E-2vi) had to be replaced by the conditions as given in equations (D-30) and (D-42).

The problem is therefore formulated as follows:

$$\alpha^2 \frac{\partial^2 \Psi_A}{\partial \xi^2} + \frac{\partial^2 \Psi_A}{\partial \zeta^2} - \exp[\beta(1 - 1/\Phi)]\Psi_A = 0 \qquad \text{(C-1i)}$$

with

$$\frac{\partial \Psi_A(\xi,0)}{\partial \zeta} = \text{DCMTC}[\Psi_A(\xi,0) - 1.0] \qquad \text{(E-1i)}$$

$$\frac{\partial \Psi_A(\xi,1)}{\partial \zeta} = \text{DCMTC}[\Psi_A(\xi,1) - 1.0] \qquad \text{(E-1ii)}$$

$$\frac{\partial \Psi_A(0,\zeta)}{\partial \xi} = \text{DCMTC}[\Psi_A(0,\zeta) - 1.0] \qquad \text{(E-1iii)}$$

$$\frac{\partial \Psi_A(1,\zeta)}{\partial \xi} = \text{DCMTC}[\Psi_A(1,\zeta) - 1.0] \qquad \text{(E-1iv)}$$

$$\iint_V \frac{1}{\alpha^2} \exp[\beta(1 - 1/\Phi)]\, \Psi_A d\xi\, d\zeta = \int_A \text{DCMTC}[\Psi_A - 1.0]\, d\xi \qquad \text{(D-30)}$$

and

$$\alpha^2\left(\frac{\partial^2\Phi}{\partial\xi^2} + \frac{\partial^2\Phi}{\partial\zeta^2}\right) + \lambda\exp\left[\beta(1 - 1/\Phi)\right]\Psi_A = 0 \qquad \text{(C-2i)}$$

with

$$\frac{\partial\Phi(\xi,0)}{\partial\zeta} = \text{DCHTC}\left[\Phi(\xi,0) - 1.0\right] \qquad \text{(E-2i)}$$

$$\frac{\partial\Phi(\xi,1)}{\partial\zeta} = \text{DCHTC}\left[\Phi(\xi,1) - 1.0\right] \qquad \text{(E-2ii)}$$

$$\frac{\partial\Phi(0,\zeta)}{\partial\xi} = \text{DCHTC}\left[\Phi(0,\zeta) - 1.0\right] \qquad \text{(E-2iii)}$$

$$\frac{\partial\Phi(1,\zeta)}{\partial\xi} = \text{DCHTC}\left[\Phi(1,\zeta) - 1.0\right] \qquad \text{(E-2iv)}$$

$$\iint_V \frac{\lambda}{\alpha^2}\exp\left[\beta(1 - 1/\Phi)\right]\Psi_A d\xi d\zeta = \int_A \text{DCHTC}\left[\Phi - 1.0\right]d\xi \qquad \text{(D-42)}$$

This problem was solved for various values of α^2, λ, DCHTC, and DCMTC. Solutions are given in Figures G-1 through G-8.

$\alpha^2 = 0.1011$

$\beta = 3.29$

$\lambda = 0.0443$

$DCMTC = 14.01\xi^{-1/3}$

$DCHTC = 0.628\xi^{-1/3}$

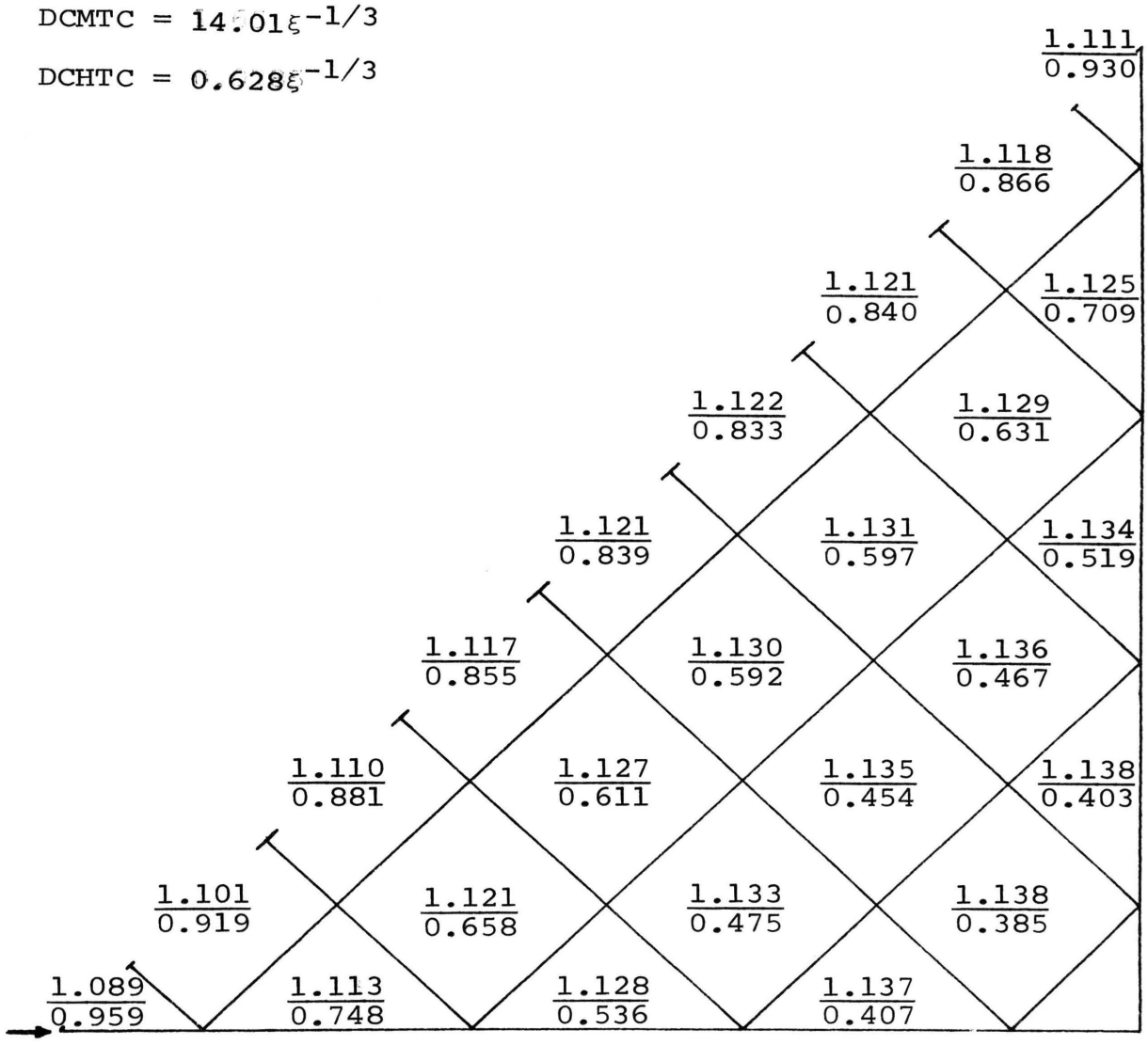

Figure G-1

Computer Dimensionless Temperature (1.089) and Mole Fraction (0.959) Profiles Inside the Catalyst Wedge

$\alpha^2 = 0.1011$

$\beta = 3.29$

$\lambda = 0.0443$

$DCMTC = 14.01\xi^{-1/3}$

$DCHTC = 0.24\xi^{-1/3}$

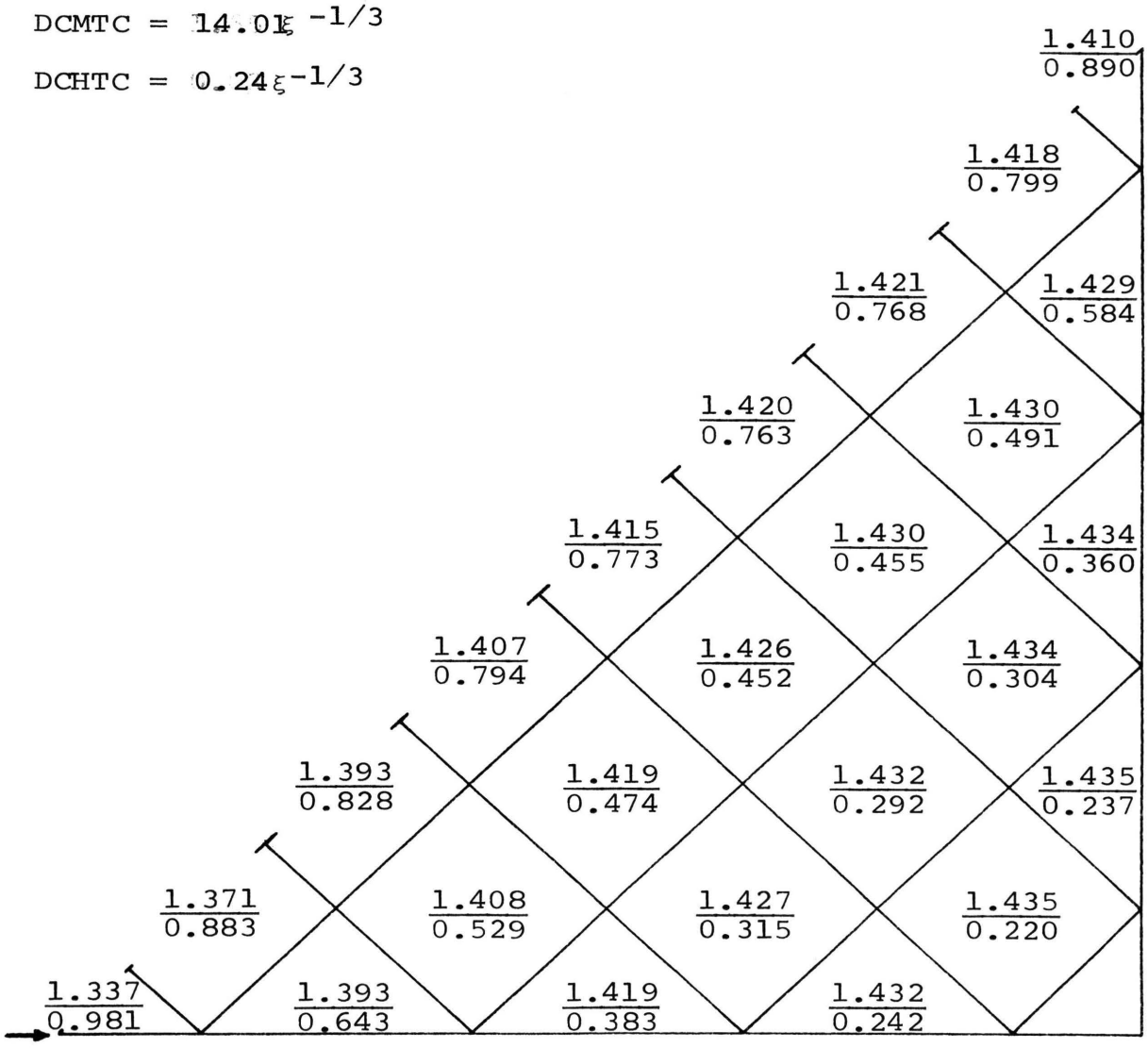

Figure G-2

Computer Dimensionless Temperature (1.337) and
Mole Fraction (0.981) Profiles
Inside the Catalyst Wedge

$\alpha^2 = 0.0077$

$\beta = 3.29$

$\lambda = 0.0443$

$DCMTC = 27.68\xi^{-1/3}$

$DCHTC = 3.68\xi^{-1/3}$

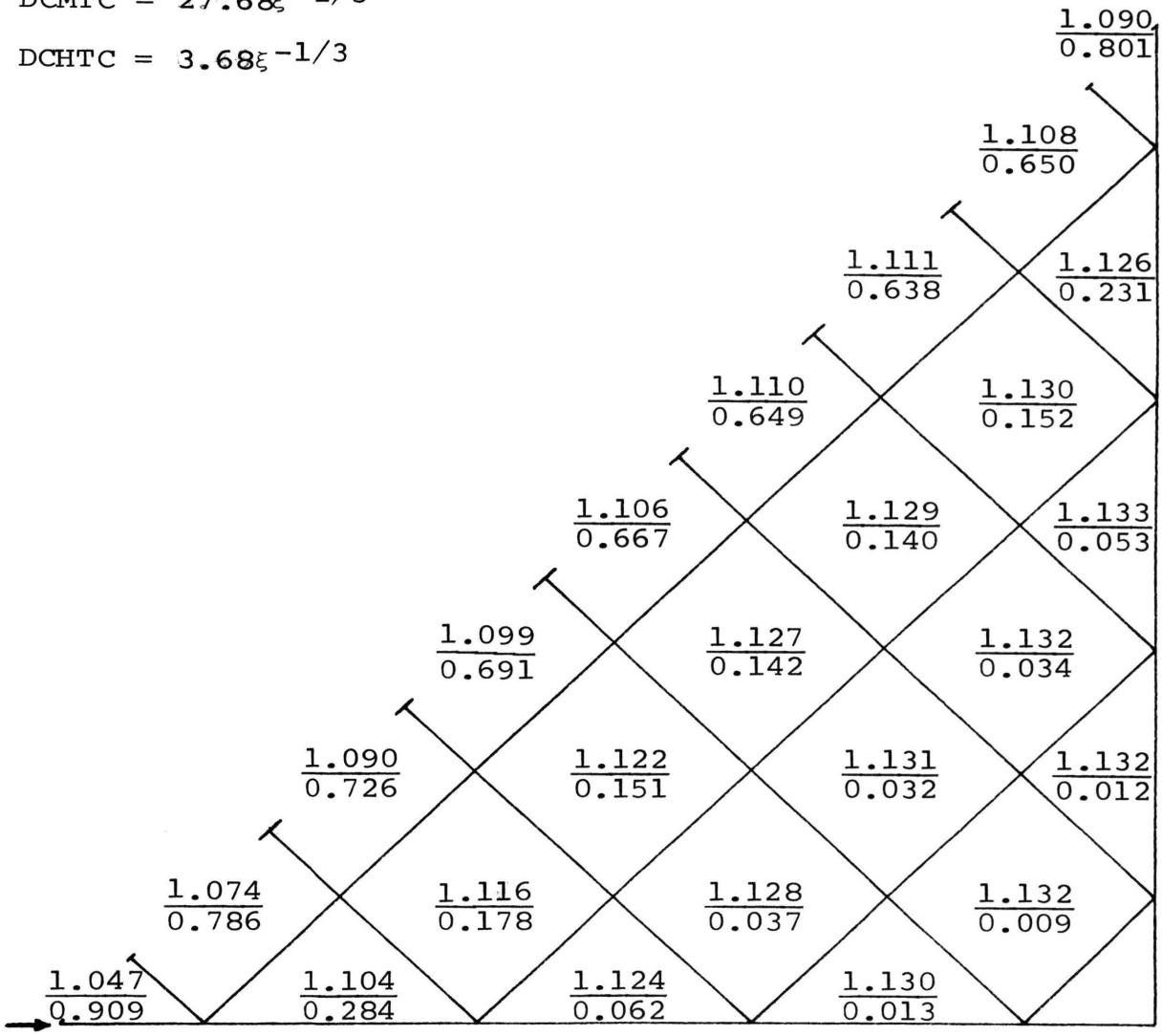

Figure G-3

Computer Dimensionless Temperature (1.047) and
Mole Fraction (0.909) Profiles
Inside the Catalyst Wedge

$\alpha^2 = 0.0077$

$\beta = 3.29$

$\lambda = 0.0443$

$DCMTC = 27.68\xi^{-1/3}$

$DCHTC = 1.17\xi^{-1/3}$

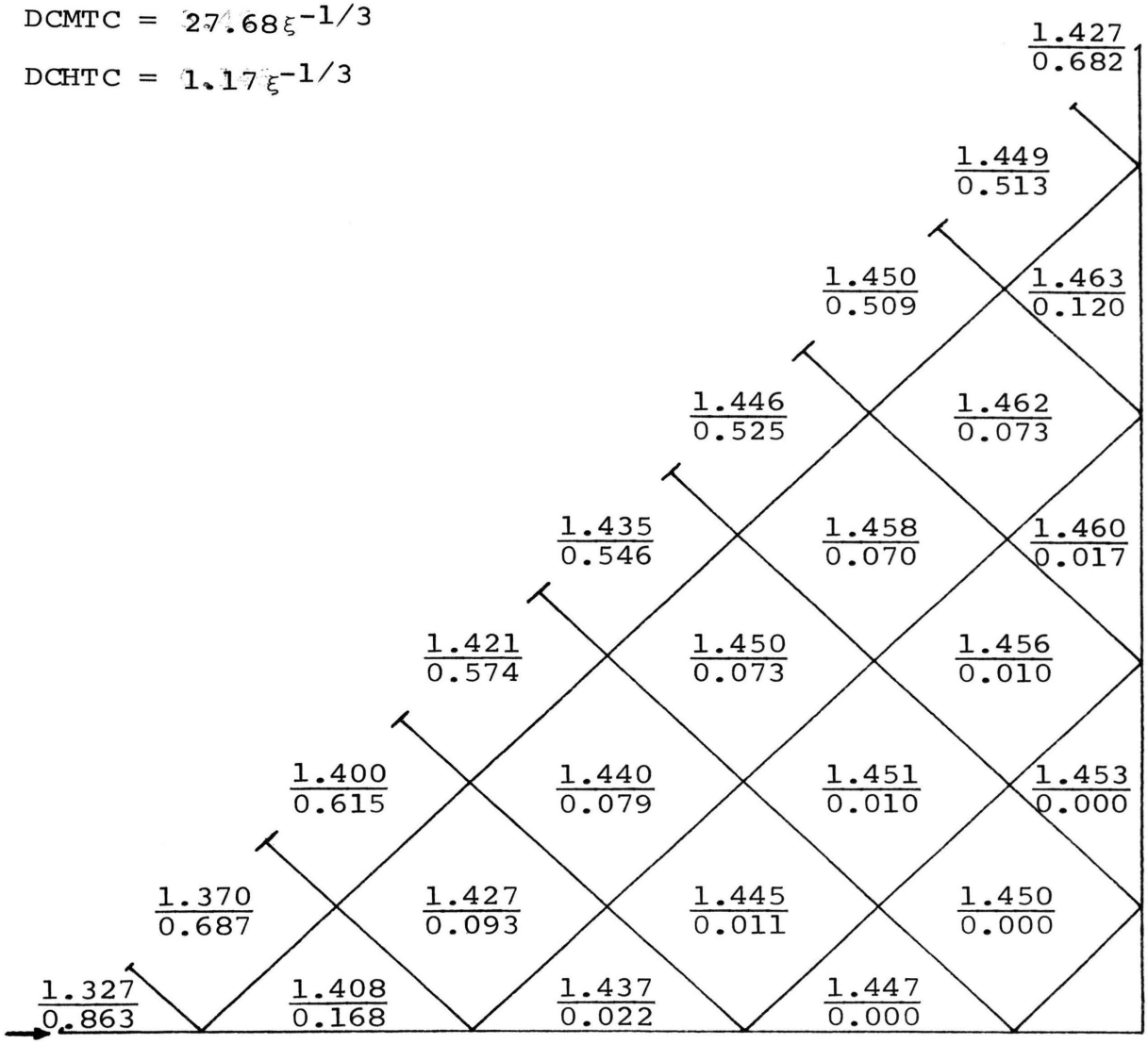

Figure G-4

Computer Dimensionless Temperature (1.327) and
Mole Fraction (0.863) Profiles
Inside the Catalyst Wedge

$\alpha^2 = 0.0202$

$\beta = 3.49$

$\lambda = 0.0443$

$DCMTC = 27.68\,\xi^{-1/3}$

$DCHTC = 1.17\,\xi^{-1/3}$

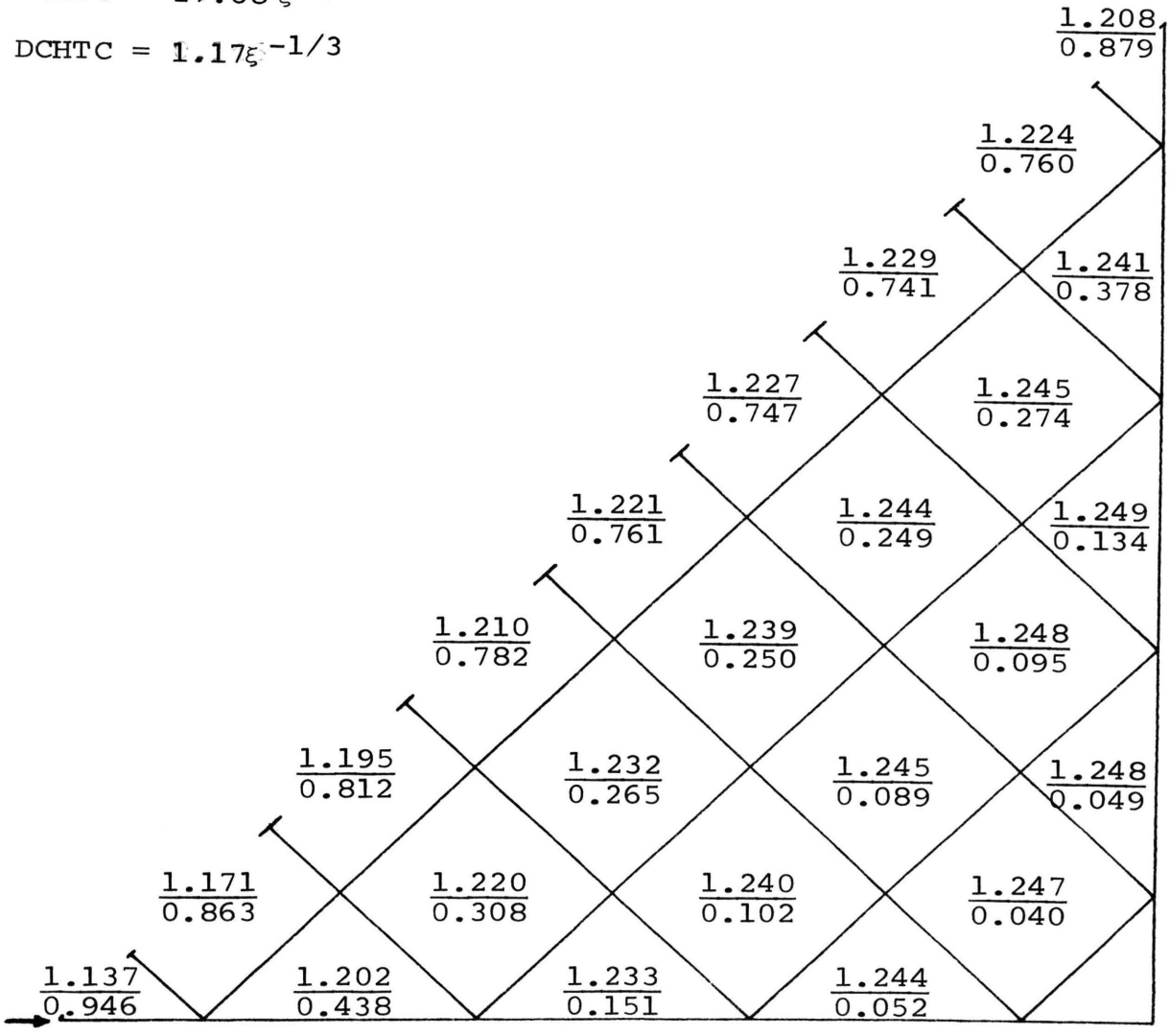

Figure G-5

Computer Dimensionless Temperature (1.137) and
Mole Fraction (0.946) Profiles
Inside the Catalyst Wedge

$\alpha^2 = 0.0108$

$\beta = 3.29$

$\lambda = 0.0443$

$DCMTC = 27.68\xi^{-1/3}$

$DCHTC = 1.17\xi^{-1/3}$

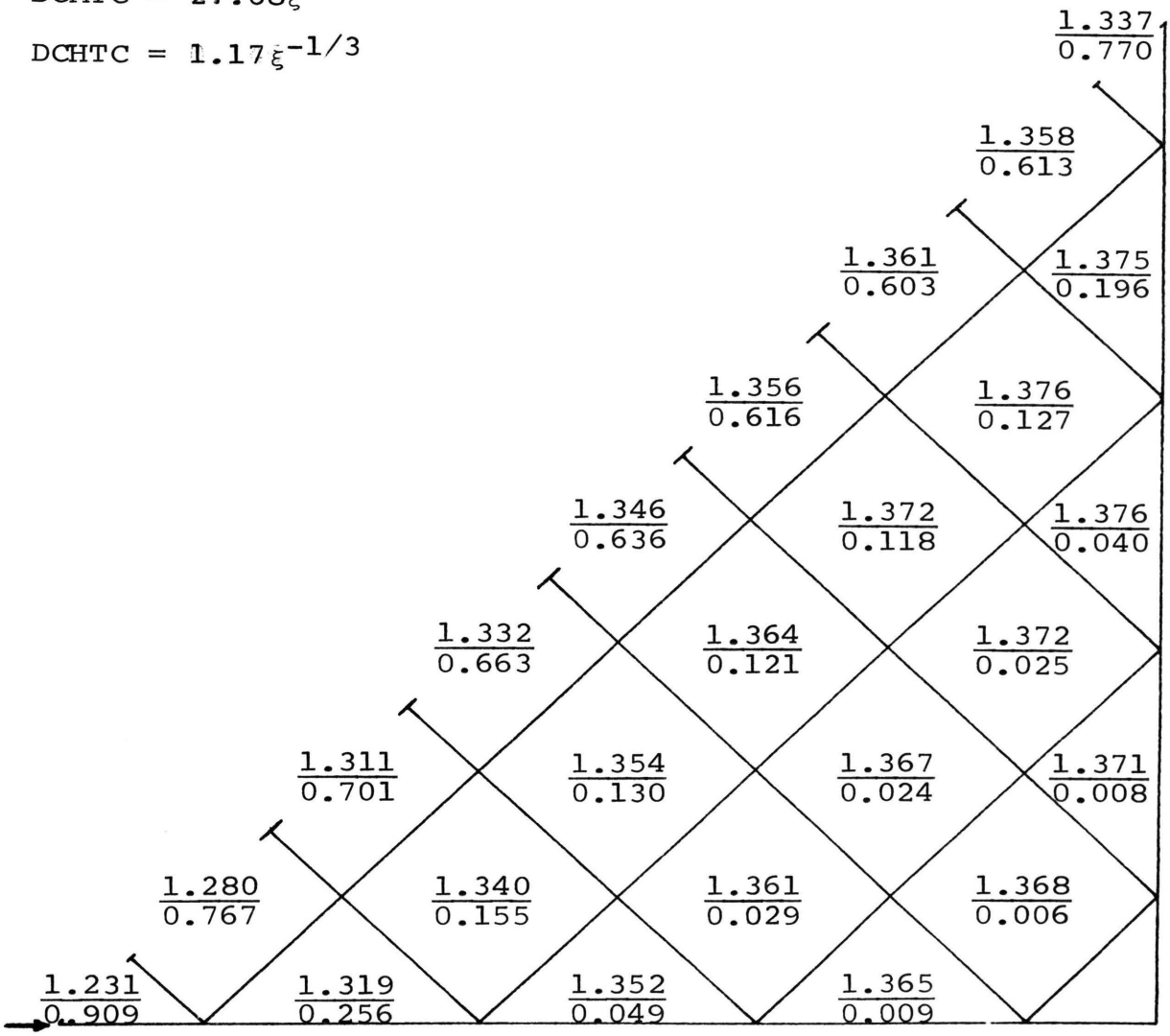

Figure G-6

Computer Dimensionless Temperature (1.231) and Mole Fraction (0.909) Profiles Inside the Catalyst Wedge

$\alpha^2 = 0.0092$

$\beta = 3.29$

$\lambda = 0.0443$

$DCMTC = 27.68\xi^{-1/3}$

$DCHTC = 1.17\xi^{-1/3}$

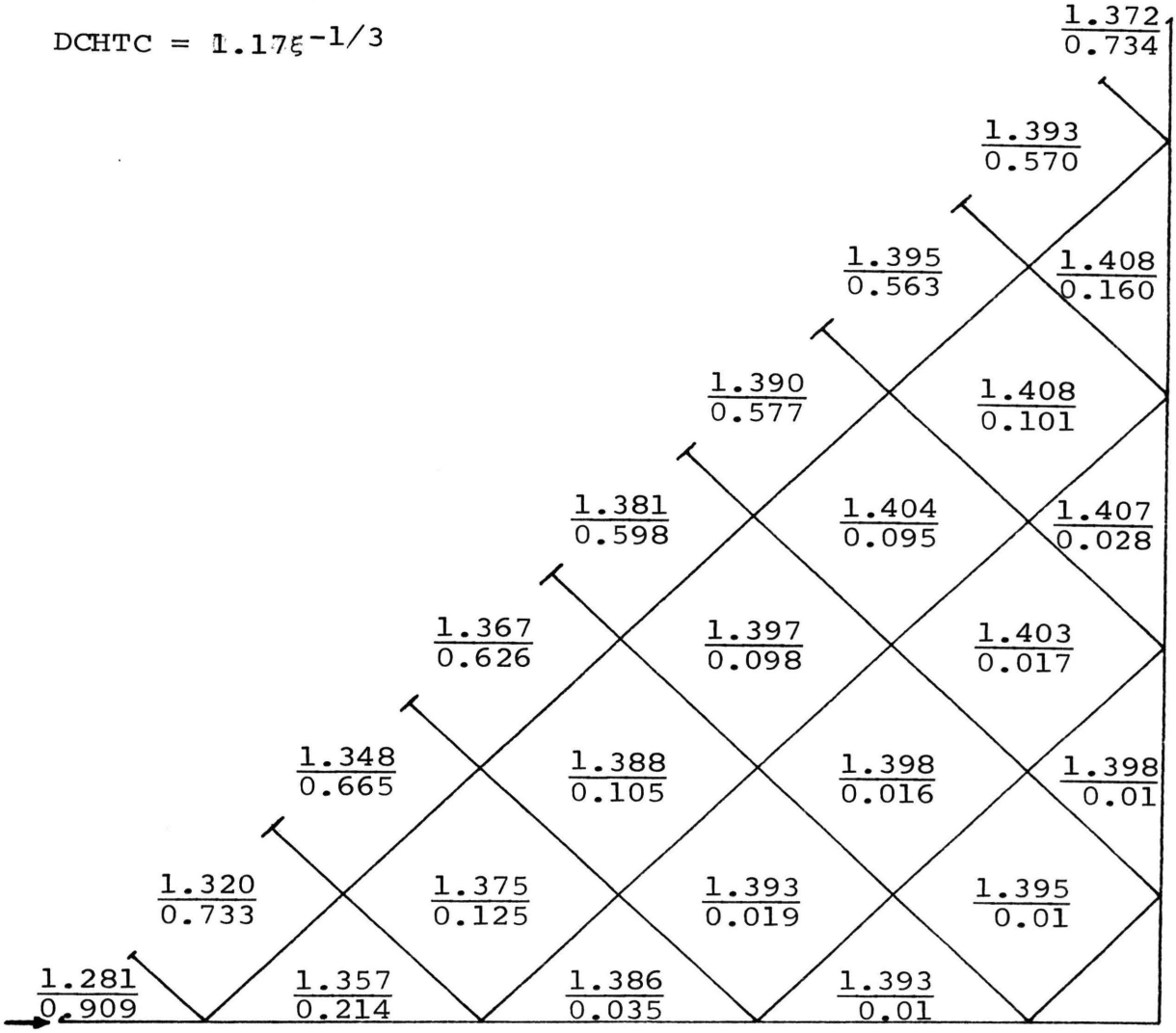

Figure G-7

Computer Dimensionless Temperature (1.281) and Mole Fraction (0.909) Profiles Inside the Catalyst Wedge

$\alpha^2 = 0.5047$

$\beta = 3.29$

$\lambda = 0.221$

$DCMTC = 2.77\xi^{-1/3}$

$DCHTC = 1.17\xi^{-1/3}$

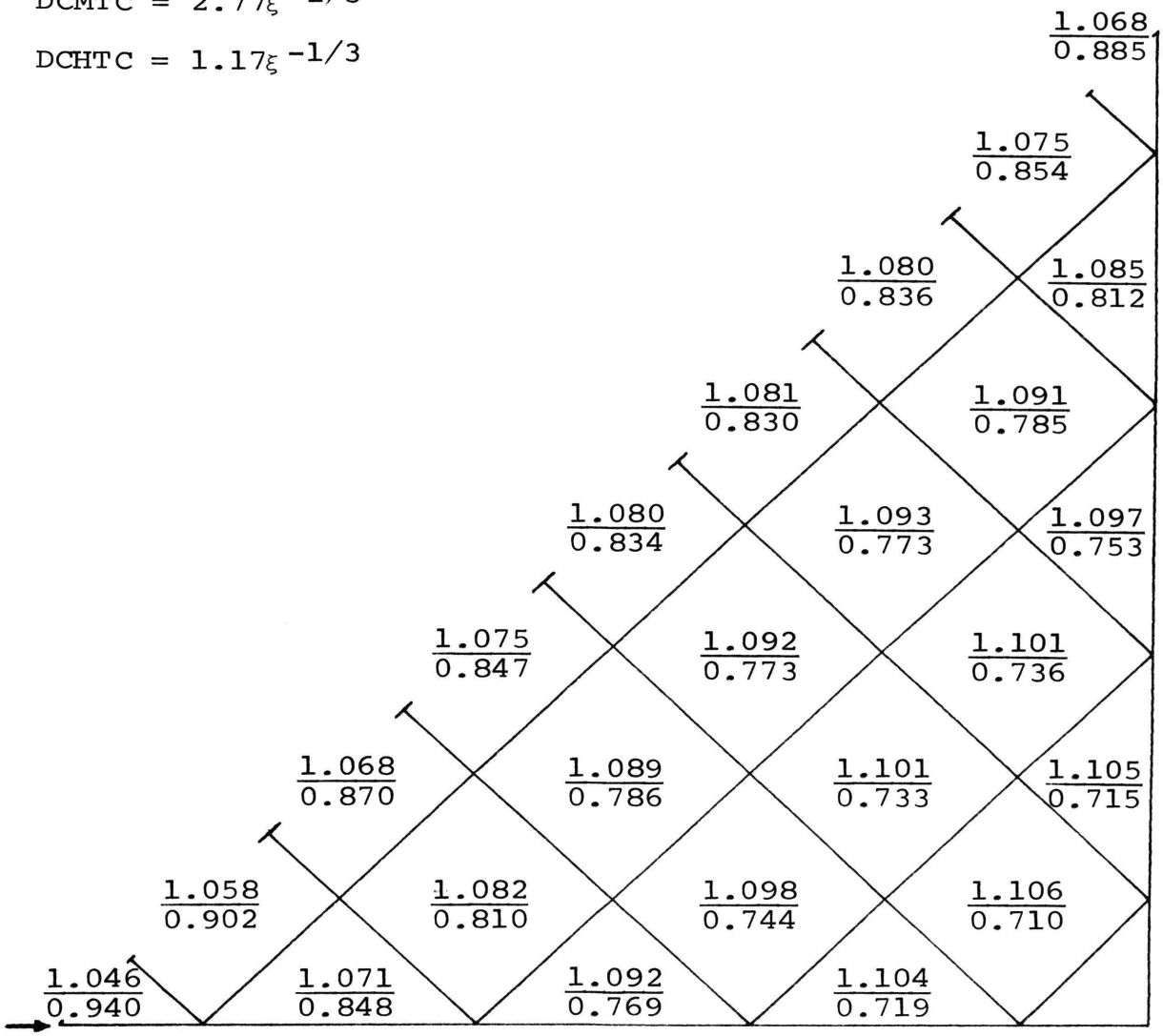

Figure G-8

Computer Dimensionless Temperature (1.046) and
Mole Fraction (0.940) Profiles
Inside the Catalyst Wedge

APPENDIX H

SOLUTION FOR THE CASE OF NON-ISOTHERMAL FIRST ORDER REACTION IN A CATALYST WEDGE WITH VARIABLE HEAT AND MASS TRANSFER COEFFICIENTS AT THE BOUNDARY (FINITE HEAT AND MASS TRANSFER COEFFICIENTS AT THE STAGNATION POINT WITH HEAT LOSS FROM THE BACK EDGE OF THE WEDGE)

Figure H-1 Computer Dimensionless Temperature (1.501) and Mole Fraction (0.855) Profiles Inside the Catalyst Wedge ($\alpha^2 = 0.0092$, $\beta = 3.29$, $\lambda = 0.0443$, DCMTC = $27.68\xi^{-1/3}$, DCHTC = $1.17\xi^{-1/3}$)

Figure H-2 Computer Dimensionless Temperature (1.866) and Mole Fraction (0.757) Profiles Inside the Catalyst Wedge ($\alpha^2 = 0.0092$, $\beta = 3.29$, $\lambda = 0.0443$, DCMTC = $27.68\xi^{-1/3}$, DCHTC = $1.17\xi^{-1/3}$)

Figure H-3 Computer Dimensionless Temperature (2.426) and Mole Fraction (0.460) Profiles Inside the Catalyst Wedge ($\alpha^2 = 0.0030$, $\beta = 3.29$, $\lambda = 0.0043$, DCMTC = $27.68\xi^{-1/3}$, DCHTC = $1.17\xi^{-1/3}$)

Figure H-4 Computer Dimensionless Temperature (1.711) and Mole Fraction (0.700) Profiles Inside the Catalyst Wedge ($\alpha^2 = 0.0045$, $\beta = 3.29$, $\lambda = 0.0443$, DCMTC = $27.68\xi^{-1/3}$, DCHTC = $1.17\xi^{-1/3}$)

SOLUTION FOR THE CASE OF NON-ISOTHERMAL FIRST ORDER REACTION IN A CATALYST WEDGE WITH VARIABLE HEAT AND MASS TRANSFER COEFFICIENTS AT THE BOUNDARY (FINITE HEAT AND MASS TRANSFER COEFFICIENTS AT THE STAGNATION POINT WITH HEAT LOSS FROM THE BACK EDGE OF THE WEDGE)

In this case the problem to be solved is identical as that of Appendix G, but heat is allowed to be lost from the back edge of the wedge. This is accomplished by forcing the temperature at the back edge to some pre-assigned value and then allowing the solution to relax to the steady state values.

Cases were solved in Figures H-1 through H-4 for various values of α^2 and values of Φ at the back edge.

$\alpha^2 = 0.0092$

$\beta = 3.29$

$\lambda = 0.0443$

$DCMTC = 27.68\,\xi^{-1/3}$

$DCHTC = 1.17\,\xi^{-1/3}$

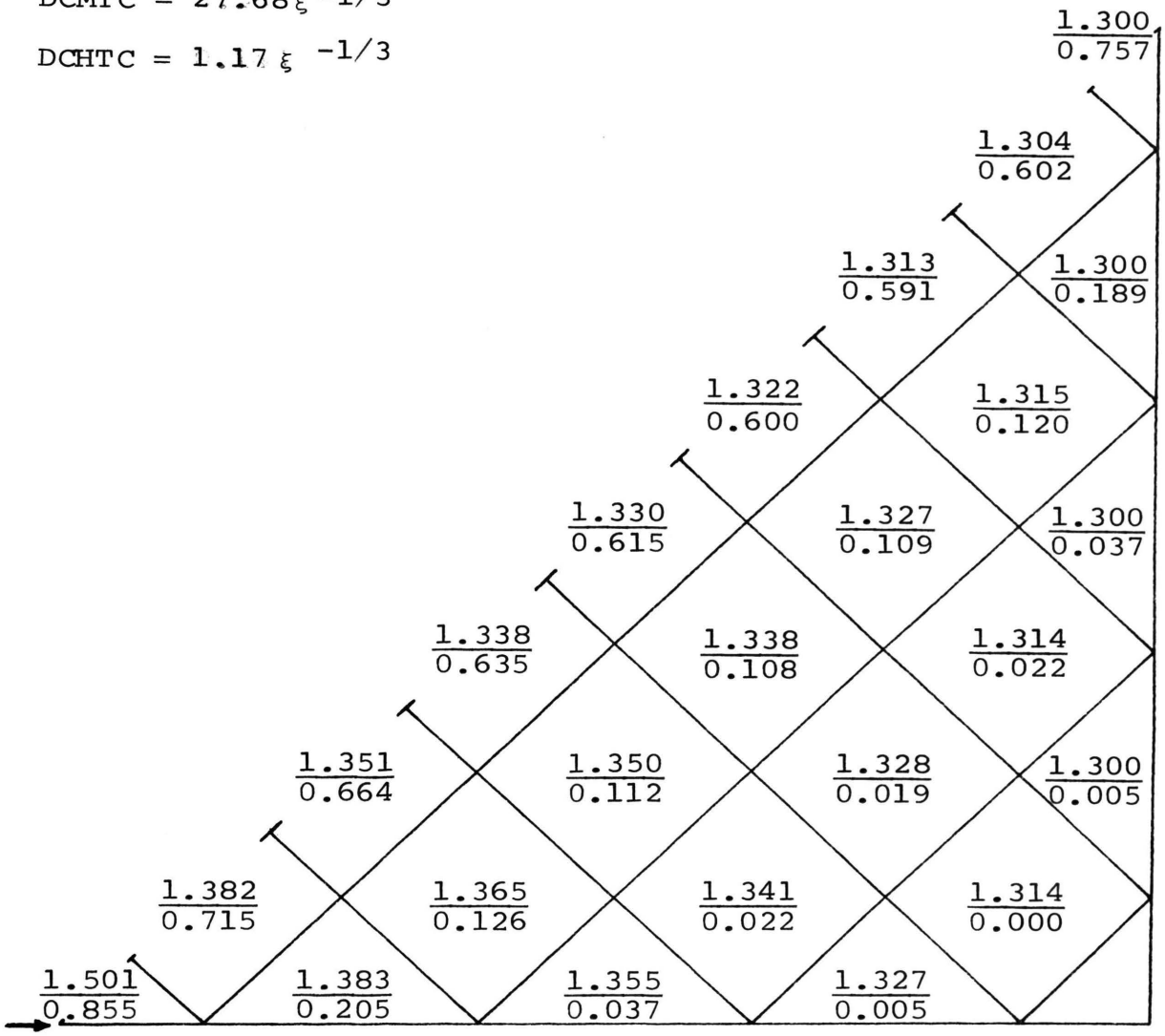

Figure H-1

Computer Dimensionless Temperature (1.501) and Mole Fraction (0.855) Profiles Inside the Catalyst Wedge

$\alpha^2 = 0.0092$

$\beta = 3.29$

$\lambda = 0.0443$

$DCMTC = 27.68\,\xi^{-1/3}$

$DCHTC = 1.176\,\xi^{-1/3}$

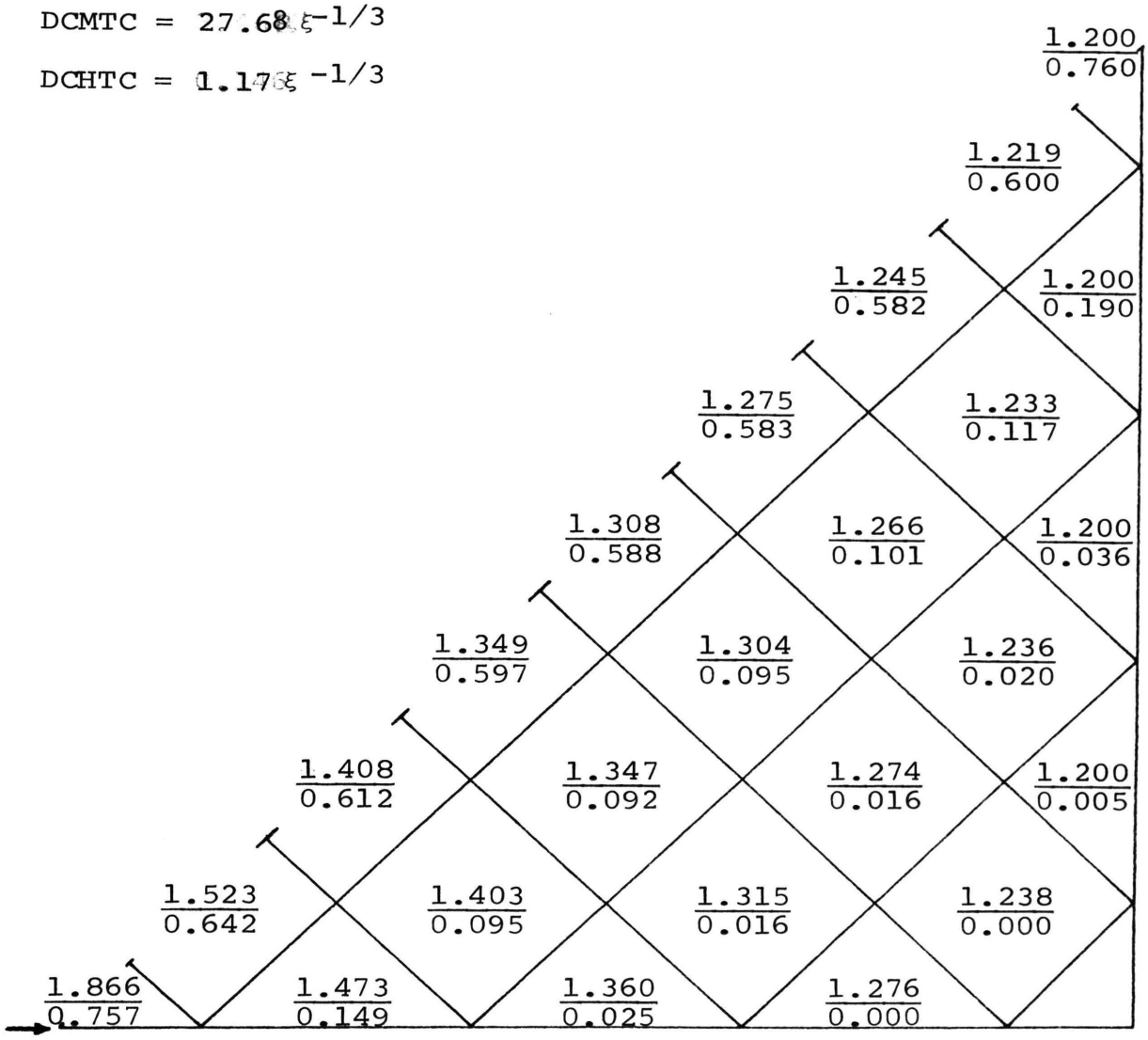

Figure H-2

Computer Dimensionless Temperature (1.866) and
Mole Fraction (0.757) Profiles
Inside the Catalyst Wedge

$\alpha^2 = 0.0030$

$\beta = 3.29$

$\lambda = 0.0443$

$DCMTC = 27.68\xi^{-1/3}$

$DCHTC = 1.17\xi^{-1/3}$

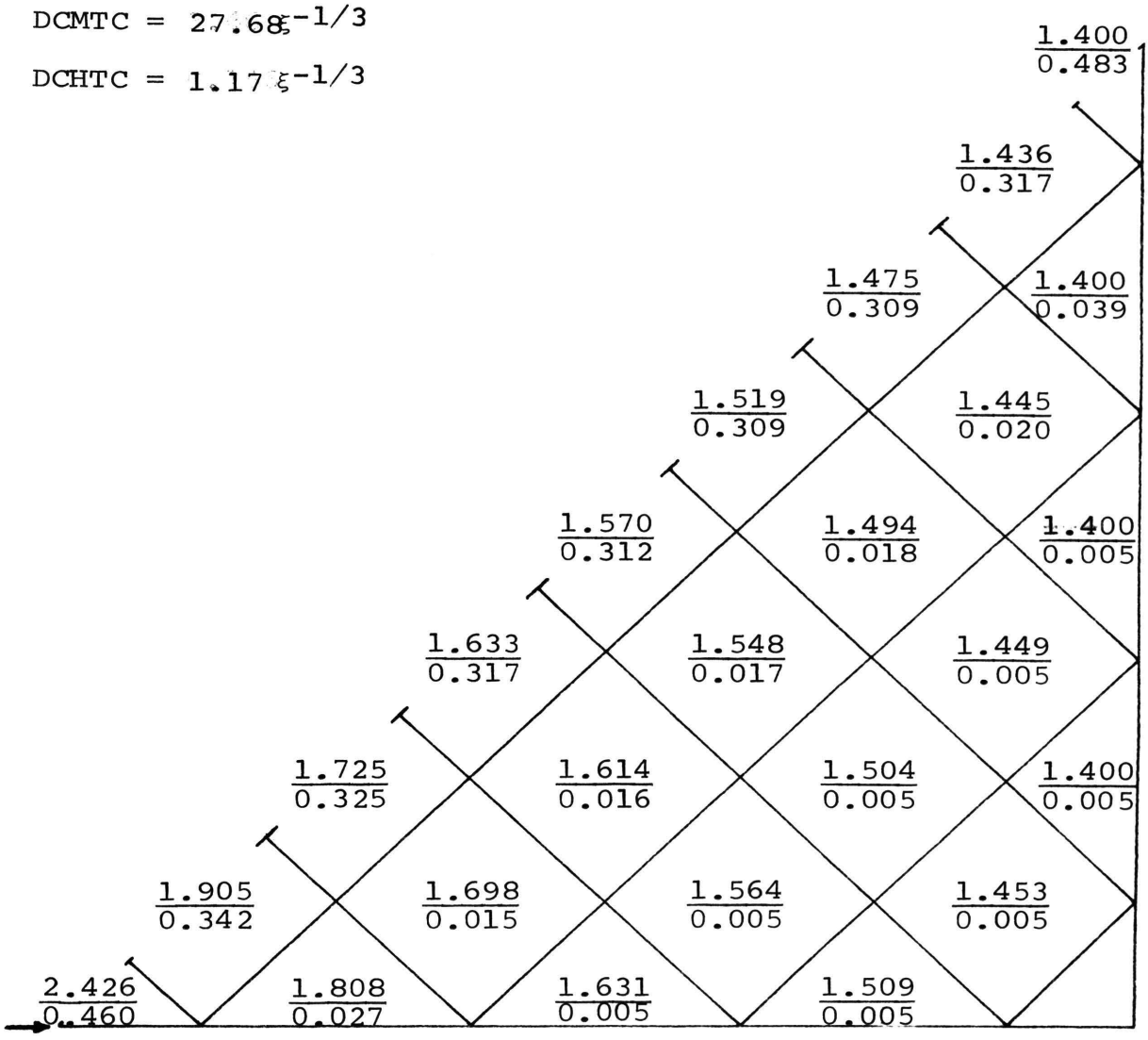

Figure H-3

Computer Dimensionless Temperature (2.426) and
Mole Fraction (0.460) Profiles
Inside the Catalyst Wedge

$\alpha^2 = 0.0045$

$\beta = 3.29$

$\lambda = 0.0443$

$DCMTC = 27.68\xi^{-1/3}$

$DCHTC = 1.17\xi^{-1/3}$

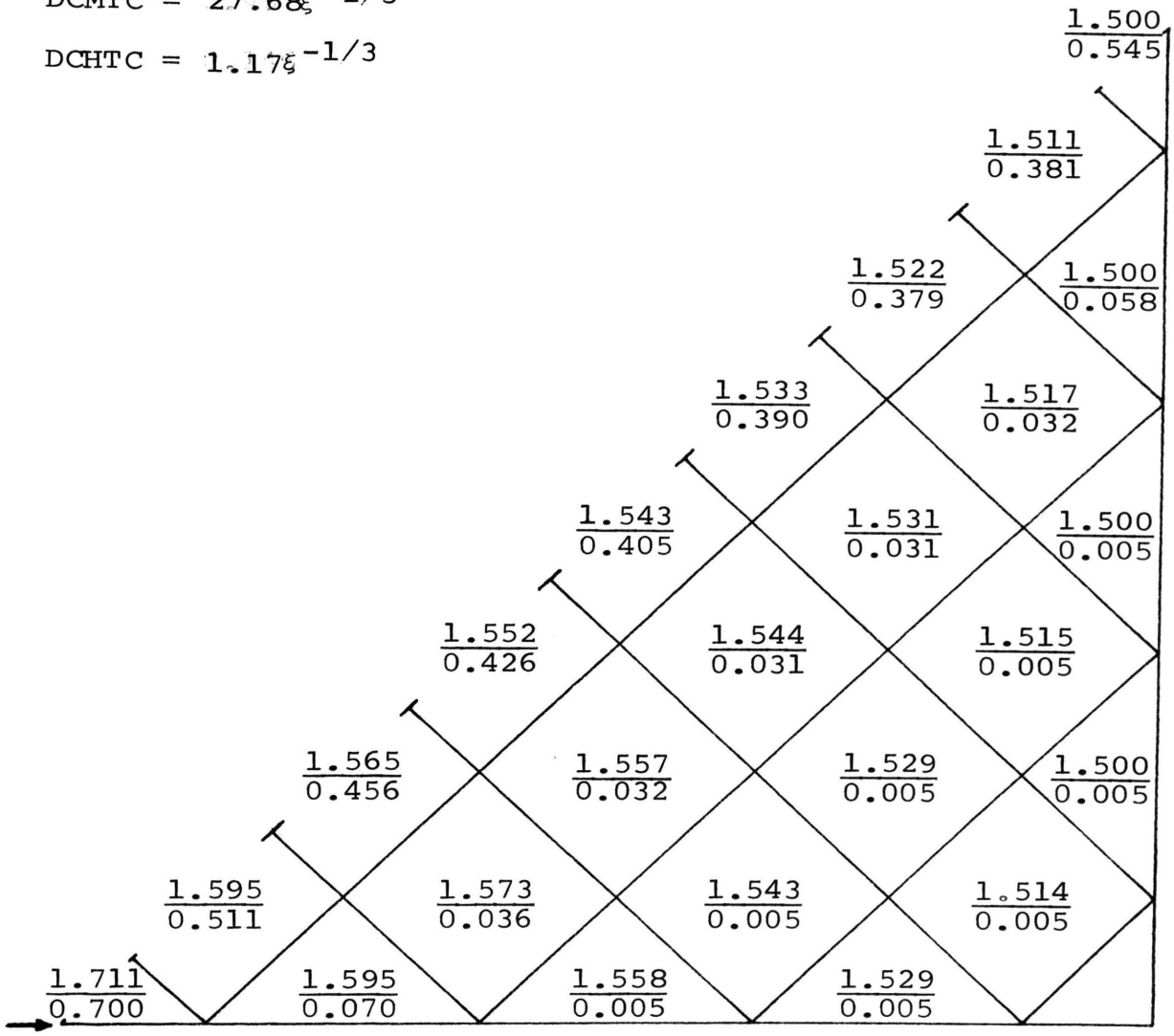

Figure H-4

Computer Dimensionless Temperature (1.711) and Mole Fraction (0.700) Profiles Inside the Catalyst Wedge

APPENDIX I

EXPERIMENTAL DATA

TABLE I-1 COMPOSITION AND CONVERSION DATA FOR EXPERIMENTAL RUNS

TABLE I-2 TEMPERATURE MEASUREMENT (°F) DATA FOR THE EXPERIMENTAL RUNS

TABLE I-1

COMPOSITION AND CONVERSION DATA
FOR EXPERIMENTAL RUNS

Run No.	$V_{A_{IN}}$ (SCFH)	$V_{B_{IN}}$ (SCFH)	$V_{T_{IN}}$ (SCFH)	$X_{A_{IN}}$	$X_{B_{IN}}$	$X_{A_{OUT}}$	$X_{B_{OUT}}$	$X_{C_{OUT}}$	$Y_{A_{BULK}}$	$Y_{A_{BL}}$	Y_A'
1-1	0.255	8.40	8.655	0.0295	0.9705	0.0237	0.9704	0.0059	19.92	51.05	0.5865
1-2	0.152	8.10	8.252	0.0184	0.9816	0.0164	0.9815	0.0021	11.35	-	0.2096
1-3	0.512	8.76	9.262	0.0553	0.9447	0.0474	0.9443	0.0084	15.00	48.95	0.8291
1-4	0.512	4.58	5.092	0.1005	0.8995	0.0775	0.8970	0.0256	24.87	54.10	2.4961
1-5	1.64	14.75	16.39	0.1000	0.9000				1.00	1.00	
1-6	1.57	11.85	13.55	0.1159	0.8841				1.00	1.00	
1-7	1.53	7.70	9.23	0.1658	0.8342				1.00	1.00	
1-8	0.66	14.35	15.01	0.0440	0.9560	0.0406	0.9559	0.0036	8.08	41.38	0.3557
1-9	0.63	14.00	14.63	0.0431	0.9569	0.0383	0.9567	0.0050	11.51	46.88	0.4955
1-10*	0.583	7.95	19.62	0.0297	0.4052				6.27	43.61	
1-11	0.63	15.38	16.01	0.0394	0.9606				1.00	1.24	
1-12	1.57	16.30	17.87	0.0879	0.9121				1.00	1.13	
1-13	1.58	15.30	16.88	0.0936	0.9064				1.00	1.62	
1-14	1.425	14.95	16.375	0.0870	0.9130	0.0776	0.9121	0.0104	11.79	53.92	1.0264
1-15	1.420	14.86	16.280	0.0872	0.9128	0.0782	0.9119	0.0099	11.22	53.91	0.9783
1-16	0.17	10.47	10.64	0.0160	0.9840	0.0149	0.9840	0.0011	6.94	30.01	0.1109
1-17	1.395	14.41	15.805	0.0883	0.9117	0.0786	0.9108	0.0106	11.87	54.42	1.0489
1-18	0.790	8.08	8.870	0.0891	0.9109						
1-19	0.775	8.08	8.855	0.0875	0.9125	0.0736	0.0111	0.0153	17.19	53.53	1.5040
1-20	0.415	4.68	5.095	0.0816	0.9184	0.0627	0.9169	0.0204	24.57	53.56	2.0011
1-21	0.263	4.45	4.713	0.0558	0.9442	0.0432	0.9435	0.0133	23.56	49.78	1.3145
1-22	0.426	4.74	5.166	0.0825	0.9175	0.0642	0.9159	0.0199	23.69	52.48	1.9531
1-23	0.490	9.33	9.820	0.0499	0.9501	0.0435	0.9500	0.0066	13.14	46.20	0.6557
1-24	0.725	14.10	14.825	0.0489	0.9511	0.0443	0.9509	0.0048	9.82	47.28	0.4807

*$V_{N_{2IN}}$ = 11.09 SCFH $X_{N_{2IN}}$ = 0.5652

TABLE I-2

TEMPERATURE MEASUREMENT (°F) DATA
FOR THE EXPERIMENTAL RUNS

Run No.	ΔT_1	T_∞ Bulk Temp of Feed	T_1	T_2	T_3	T_4	T_5
1-1	80.0	179.0	259.0	258.6	257.8	258.1	256.5
1-2	28.0	75.2	103.2	102.6	101.3	100.6	101.1
1-3	139.0	78.0	217.0	211.5	205.4	204.0	205.3
1-4	245.1	96.1	341.2	330.5	322.9	321.0	321.5
1-5	2.8	75.8	78.6	79.2	79.2	79.0	79.6
1-6	3.4	76.2	79.6	80.0	80.0	79.8	80.4
1-7	4.2	76.9	81.1	81.6	81.5	81.2	82.3
1-8	74.4	79.2	153.6	152.6	148.6	147.9	148.8
1-9	95.0	120.8	215.8	212.8	208.8	207.9	208.4
1-10	44.6	102.5	147.1	148.5	147.2	147.3	146.8
1-11	1.3	78.2	79.5	79.9	79.8	79.6	80.2
1-12	3.2	78.4	81.6	82.4	82.4	81.9	83.3
1-13	15.2	99.1	114.3	116.0	116.6	115.9	115.2
1-14	216.9	98.6	315.5	310.9	302.4	300.2	299.3
1-15	211.8	80.7	292.5	287.8	279.5	277.3	277.3
1-16	21.6	75.3	96.9	96.3	95.6	95.3	95.5
1-17	213.6	81.5	295.1	289.8	281.1	279.5	279.7
1-18	200.9	81.2	282.1	273.9	267.3	266.0	267.0
1-19	201.1	81.3	282.4	274.1	267.4	265.7	266.5
1-20	171.5	90.6	262.1	255.1	249.7	248.9	249.4
1-21	109.8	92.5	202.3	198.1	194.2	193.4	194.4
1-22	173.1	92.4	265.5	258.7	252.7	251.8	252.4
1-23	96.1	80.1	176.2	173.1	169.0	168.0	169.2
1-24	88.7	78.2	166.9	164.8	160.5	159.6	160.5

APPENDIX J

SAMPLE CALCULATIONS

SAMPLE CALCULATIONS

(1) Dimensionless Parameter: $\alpha^2 \equiv \frac{D}{k_\infty L^2}$

Using the rate expression of reference (34), then

$$R_A = \frac{r_m}{a_m} \cdot \frac{1}{v_m}$$

$$R_V = R_A(-\Delta H_A)$$

where

r_m = rate of reaction per unit weight of catalyst

$\frac{\text{gm moles}}{\text{hr-gm catalyst}}$

a_m = external surface area of the catalyst particle per unit weight $\frac{\text{cm}^2}{\text{gm catalyst}}$

v_m = volume of catalyst per unit external surface area

$(\frac{\text{cm}^3}{\text{cm}^2})$.

For an ideal gas,

$$P_i = X_i P_T$$

therefore,

$$R_A = \frac{1}{v_m} A' X_A X_B P_t^2 e^{-E/RT}$$

$$R_A = [\frac{1}{v_m} A' P_t^2 X_A X_B] \Psi_A e^{-E/RT}$$

The modeled rate in Appendix A was

$$R_A = kc_A = kcX_{A_\infty}\Psi_A$$

therefore,

$$kc = \frac{1}{v_m}A'P_t^2X_Be^{-E/RT}$$

or

$$k = \frac{A'P_t^2X_B}{v_mc}e^{-E/RT}.$$

For an ideal gas,

$$c = P_T/RT$$

and

$$k_\infty = \frac{A'P_tX_BRT_\infty}{v_m}\ e^{-E/RT_\infty}.$$

$$v_m = \frac{1/2bhL_o}{LL_o} = \frac{1/2(1/4)(1/4)}{\sqrt{(1/4)^2 + (1/4)^2}}$$

$$= \frac{1/32}{\sqrt{2}/4} = \frac{1}{8\sqrt{2}}\ \frac{in^3}{in^3} \times \frac{(2.54cm^3)}{in^3} \times \frac{in^2}{(2.54cm^2)}$$

$$= \frac{2.54}{8\sqrt{2}} = .224\ \frac{cm^3}{cm^2}$$

with

$$A' = 1.18\ \frac{g\text{-moles}}{hr\text{-}cm^2\text{-}atm^2}$$

$P_t = 1$ atm

$X_B = 0.9$

$T_\infty = 300°K$

$E = 1{,}960$ cal/g-mole

$$k_\infty = \frac{(1.18)(1)(0.09)(82.05)(300)}{0.224} e^{-(1960)/(1.987)(300)}$$

$$k_\infty = 1.165 \times 10^5 e^{-3.29} = 1.165 \times 10^5 (.0378)$$

$$k_\infty = 4.41 \times 10^3 hr^{-1}$$

$L = .899$ cm

$D = 0.1\ cm^2/sec = 360\ cm^2/hr$

$$\alpha^2 = \frac{360}{(4.41 \times 10^3)(0.899)^2}$$

$$\alpha^2 = 0.101$$

(2) Activation Energy Parameter: $\beta \equiv E/RT_\infty$

$$\beta = (1960)/(1.987)(300)$$

$$\beta = 3.29$$

(3) Energy Balance Parameter: $\lambda = (-\Delta H_A) D c_{A_\infty} / k_H T_\infty$

$k_H = 1.0 \times 10^{-3}$ cal/sec-°C-cm (Reference 20)

$T_\infty = 300°K$

$D = 0.1\ cm^2/sec$

$\Delta H_i = H_{C_2H_6} - H_{C_2H_4} - H_{H_2}$

$= -20,236 - (12,496) - 0$

$\Delta H_i = -32,732$ cal/g-mole Reference (40)

estimate of c_{A_∞}

$X_{A_\infty} = 0.10$

$c_{A_\infty} = X_{A_\infty} c$

$c = n/v = P/RT$

$$c_{A_\infty} = \frac{X_{A_\infty} P}{RT} = \frac{(0.1)(1\ atm)}{(82.05\ \frac{atm\text{-}cc}{g\text{-}mole°K})(300°K)}$$

$c_{A_\infty} = 4.07 \times 10^{-6}$ g-moles/cc

$$\lambda = \frac{(32,732)(0.1)(4.07 \times 10^{-6})}{(1.0 \times 10^{-3})(300)} = 0.0443$$

(4) Dimensionless Mass Transfer Coefficient: DCMTC = $k_x^{\cdot} L/Dc$

From Equation (D-6),

$$\frac{k_x^{\cdot}}{c} = \frac{\pi'}{Sc}\left(\frac{m+1}{2}\frac{\nu\, U(x)}{x}\right)^{1/2} = \frac{\pi'}{Sc}\left(\frac{m+1}{2}\frac{\nu U_1}{L^{2/3}\xi^{2/3}}\right)^{1/2}$$

where

$U(x) = U_\infty x^m$

with $U_\infty = 40$ and $m = 1/3$.

With $\nu = 0.473$ cm^2/sec (Reference 41) and $D_{AB} = 0.98$ cm^2/sec (Reference 42) then assuming $v_s = 0$, π' obtained from (23) is 0.404.

$$\frac{k_x^{\cdot}}{c} = \frac{(0.404)}{0.483}\left(\frac{1/3 + 1}{2}\,\frac{(0.473)(40)}{(0.899)^{2/3}}\right)^{1/2}\xi^{-1/3}$$

$$\frac{k_x^{\cdot}}{c} = 3.08\xi^{-1/3}$$

$$DCMTC = (3.08\xi^{-1/3})\,\frac{0.899}{0.1} = 27.69\xi^{-1/3}$$

(5) Dimensionless Heat Transfer Coefficient: $DCHTC = h^{\cdot}L/k_H$

Dividing equation (D-7) by (D-6) yields

$$\frac{h^{\cdot}}{k_x^{\cdot}} = \frac{k_G}{cD_{AB}}$$

$$k_G = 4227^{\backslash -7} \qquad \text{Reference (43)}$$

$$h^{\cdot} = \frac{k_x^{\cdot}k_G}{cD_{AB}} = (3.08\xi^{-1/3})\,\frac{4227^{\backslash -7}}{(0.98)}$$

$$h^{\cdot} = 1.33^{\backslash -3}\xi^{-1/3}$$

$$DCHTC = (1.33^{\backslash -3}\xi^{-1/3})\frac{0.899}{0.001} = 1.19\xi^{-1/3}$$

(6) Estimation of the dimensionless surface(s) mole fraction (Ψ_{A_s}) of ethylene with finite heat and mass transfer coefficients over the surface.

At steady state

$$Q_{CH_A} = Q_{CM_A}(-\Delta H_A)$$

or

$$k_x^{\cdot} X_{A_\infty}(1.0 - \Psi_{A_s}) = \frac{h^{\cdot} T_\infty}{(-\Delta H_A)} (\Phi_s - 1.0).$$

Therefore

$$\Psi_{A_s} = 1.0 - \frac{h^{\cdot}}{k_x^{\cdot}} \frac{T_\infty}{X_{A_\infty}(-\Delta H_A)} (\Phi_s - 1.0)$$

but dividing equation (D-7) by equation (D-6) gives

$$\frac{h^{\cdot}}{k_x^{\cdot}} \quad \frac{k_G}{cD_{AB}}$$

so

$$\Psi_{A_s} = 1.0 - \frac{k_G T_\infty}{D_{AB}(-\Delta H_A) c_{A_\infty}} (\Phi_s - 1.0).$$

Letting T_∞ = 540°F = °K

T = 740°F = °K

and all other values are typically presented previously, then

$$\Psi_{A_s} = 1.0 - \frac{(4227^{\backslash -7})(300)}{(0.98)(3.27^{\backslash 4})(4.07^{\backslash -6})} (1.37 - 1.0).$$

$$\Psi_{A_s} = 1.0 - \frac{(4.227)(3.0)10^{-2}}{(0.98)(4.07)(3.27)10^{-2}} (0.37)$$

$$\Psi_{A_s} = 1.0 - (0.971)(0.37)$$

$$\Psi_{A_s} = 1.0 - 0.359$$

$$\Psi_{A_s} = 0.641$$

(7) Estimation of heat loss from the back edge of the wedge at high reaction rates which lead to large temperature differences between the catalyst wedge and the gas

$$Q_{LOST} = K_I A_I \frac{\Delta T_I}{\Delta x_I}$$

$$k_I = 10^{-4} \text{ cal/cm-sec-°C}$$

$$A_I = (1/2)(3/4)x(2.54)^2 = (0.375)(6.45) = 2.42 \text{ cm}^2$$

$$x_I = (1/8)(2.54) = 0.318 \text{ cm}$$

At high temperature difference between the gas and the catalyst wedge the ΔT_I is estimated for Run 1-14 as follows:

$$\Delta T_I = T_5 - T_{GC} = 299.3 - 157.9 = 141.4°F = 78.5°C$$

$$Q_{LOST} = (10^{-4})(3600)(2.42)78/0.318$$

$$Q_{LOST} = (0.36)(2.42)(78/0.318)$$

$$Q_{LOST} = 240 \text{ cal/hr}$$

Total heat generated in Run 1-14 is

$$Q_{GEN} = (1.425)(0.79)(3.2 \times 10^4)(0.1179)$$

$$Q_{GEN} = (1.425)(0.79)(3.2 \times 10^4)(0.1179) = 4246 \text{ cal/hr}$$

The percent lost is then

$$\% \text{ Lost} = \frac{240 \times 100}{4246} = 5.65$$

(8) Calculation of inlet mole fractions: $X_{A_{IN}}$, $X_{B_{IN}}$

$$X_{A_{IN}} = V_{A_{IN}}/V_T$$

$$X_{B_{IN}} = V_{B_{IN}}/V_T$$

For Run 1-15,

$$X_{A_{IN}} = 1.420/16.28$$

$$X_{A_{IN}} = 0.0872$$

$$X_{B_{IN}} = 14.86/16.28$$

$$X_{B_{IN}} = 0.9128$$

(9) Calculation of outlet mole fractions: $X_{A_{OUT}}$, $X_{B_{OUT}}$, $X_{C_{OUT}}$

$$X_{A_{OUT}} = V_{A_{IN}} (1 - Y_{C_{BULK}} / [V_{B_{IN}} + V_{A_{IN}}(1 - Y_{C_{BULK}})]$$

$$X_{C_{OUT}} = V_{A_{IN}} Y_{C_{BULK}} / [V_{B_{IN}} + V_{A_{IN}} (1 - Y_{C_{BULK}})]$$

$$X_{B_{OUT}} = 1 - X_{A_{OUT}} - X_{C_{OUT}}$$

For Run 1-15,

$$X_{A_{OUT}} = 1.42(1 - 0.1122) / [14.86 + 1.42\ (1 - 0.1122)]$$

$$X_{A_{OUT}} = 0.0782$$

$$X_{C_{OUT}} = 1.42\ (0.1122) / [14.86 + 1.42\ (1 - 0.1122)]$$

$$X_{C_{OUT}} = 0.00988$$

$$X_{B_{OUT}} = 1.0 - 0.0782 - 0.0099$$

$$X_{B_{OUT}} = 0.9119$$

(10) Percent conversion of ethylene (A) per mole of total feed: Y'_A

From reference (8)

$$Y'_A = \frac{X_{C_{OUT}}}{1 + X_{C_{OUT}}} \times 100$$

For Run 1-15,

$$Y'_A = \frac{0.00988}{1 + 0.00988} \times 100$$

$$Y'_A = 0.9783$$

VITA

Joseph Michael Schardl, Jr. was born on October 24, 1944 in Pine Bluff, Arkansas. He received his primary and secondary education in St. Louis, Missouri. In September 1962 he entered the University of Kansas City, Kansas City, Missouri. He transferred to the University of Missouri in September 1963 from where he received a Bachelor of Science degree in Chemical Engineering in June 1966. He was enrolled in the Graduate School at the University of Missouri at Rolla in September 1966 and received his Master of Science degree in Chemical Engineering in June 1968. He remained at UMR until October 1970 working toward the Doctor of Philosophy Degree in Chemical Engineering at which time he went to work for USS Chemicals, a Division of US Steel Corporation in Haverhill, Ohio as a Process Development Engineer. Presently he is Senior Market Analyst in the Plastic Department USS Chemicals, Pittsburgh, Pennsylvania.